Metabolic engineering of *Escherichia coli* for the production of coenzyme Q10

Corinne Cluis

A Thesis

In the Department

of

Biology

Presented in Partial Fulfillment of the Requirements

For the Degree of

Doctor of Philosophy (Biology) at

Concordia University

Montreal, Quebec, Canada

June 2014

CONCORDIA UNIVERSITY
SCHOOL OF GRADUATE STUDIES

This is to certify that the thesis prepared

By: Corinne Cluis

Entitled: Metabolic engineering of Escherichia coli for the production of coenzyme Q10

and submitted in partial fulfillment of the requirements for the degree of

Doctor of Philosophy (Biology)

complies with the regulations of the University and meets the accepted standards with respect to originality and quality.

Signed by the final examining committee:

Dajana Vuckovic — Chair

Rhadakrishnan Mahadevan — External Examiner

Joanne Turnbull — External to Program

Luc Varin — Examiner

David Walsh — Examiner

Vincent Martin — Thesis Supervisor

Approved by

Chair of Department or Graduate Program Director

2014

Dean of Faculty

Abstract

Metabolic engineering of *Escherichia coli* for the production of coenzyme Q10

Corinne Cluis

Concordia University, 2014

Coenzyme Q10 is required for respiratory electron transport and protects biological membranes against oxidative damage. As coenzyme Q10 supplements are used to treat or to alleviate symptoms associated with an increasing number of health conditions, there is growing interest in the development of bioprocesses for its production. The biosynthesis of coenzyme Q10 involves the condensation of an isoprenoid, decaprenyl diphosphate, with an aromatic compound, *para*-hydroxybenzoate, followed by a series of modifications of the aromatic moiety of the molecule via the ubiquinone pathway. *Escherichia coli* naturally produces coenzyme Q8, but replacement of its octaprenyl diphosphate synthase by a decaprenyl diphosphate synthase is sufficient to eliminate the production of coenzyme Q8 and favor the synthesis of coenzyme Q10.

A rational genetic engineering approach was used to create a strain of *E. coli* capable of producing high levels of coenzyme Q10. First, the endogenous octaprenyl diphosphate synthase gene was deleted and functionally replaced by a decaprenyl diphosphate synthase-encoding gene derived from *Sphingomonas baekryungensis*. Additionally, this strain was engineered to produce elevated levels of *para*-hydroxybenzoate by over-expressing genes encoding enzymes of the *E. coli* shikimate pathway. The production of isoprenoid was increased by introducing a heterologous mevalonate pathway. Decaprenyl diphosphate and *para*-hydroxybenzoate were further

directed toward the ubiquinone pathway by overexpressing a *para*-hydroxybenzoate prenyltransferase. The resulting recombinant strain was capable of producing elevated levels of coenzyme Q10. In order to further enhance production of this antioxidant, an investigation into the interplay between coenzyme Q10 biosynthesis and primary metabolism was conducted. This investigation revealed a link between sorbitol catabolism and coenzyme Q10 production in the engineered strain. Moreover, abrogating carbon flux to acetate by selected gene knock-outs also enhanced coenzyme Q10 accumulation. However, the engineered strains developed through this research were found to be highly unstable, leading to high variability in coenzyme Q10 production. This instability was hypothesized to result from the burden exerted by the engineered aromatic and foreign mevalonate pathways on primary metabolism. As a result, further optimization of these engineered strains of *E. coli* will be required in order to develop a suitable platform for coenzyme Q10 production.

Acknowledgement

I wish to thank, first and foremost, my supervisor, Vincent Martin, for his mentorship throughout this thesis. Through his knowledge, experience and vision of the field, he helped me progress as a scientist, encouraging creativity and autonomy in my research while remaining available for advice and direction. He also took at heart my professional future, and was always supportive of my efforts to balance research work with family life.

I am also grateful to Adam Burja, formerly of Ocean Nutrition Canada, for his contagious enthusiasm and early advice on the project. I am indebted to my teammate, Andy Ekins, for insightful discussions and for his help on numerous aspects of my research. I also thank my committee members, Luc Varin and David Walsh, for their constructive criticisms throughout my degree.

The years spent at Concordia University would not have been the same without the many friends I have made among the Martin lab. Special thanks to Andrew, Dominic, Euan, Nick and Elena, for their friendship, their humor, their moral support, and for great memories.

To my husband, Vincent, who was always there in good like in difficult times, and who encouraged me to persist when life challenges and struggles in my research cast doubts on my decision to pursue this doctorate degree. To my children, Mathias and Jérémie, who were born during the course of my Ph.D., and who fill me with purpose and joy. To my mother, Paulette, who was my friend and my guide, and who I miss every day. To my father, Daniel, who passed away just as I was writing this thesis, and whose

intelligence always inspired me. Himself a brilliant scientist, he would have loved to be by my side to celebrate this achievement, and it is with great regret that I complete my degree without him.

Contribution of authors

The text presented in Chapter 1 is derived from the following published articles:

> Cluis, C.P., Burja A.M., and Martin, V.J. (2007) Current prospects for the production of coenzyme Q10 in microbes. Trends in Biotechnology 25 (11): 514-21
>
> Cluis, C.P., Pinel, D., and Martin, V.J. (2012) The production of coenzyme Q10 in microorganisms. Subcellular Biochemistry. 64:303-26.

I was the primary author in both these publications. Figure 1.2, Table 1.1 and Table 1.2 in this thesis are adapted from material published in Subcellular Biochemistry.

Part of the text and data presented in Chapter 2 is derived from the following published article:

> Cluis, C.P., Ekins, A., Narcross, L, Jiang, H, Gold, N.D., Burja, A.M., and Martin, V.J. (2011) Identification of bottlenecks in Escherichia coli engineered for the production of CoQ10. Metabolic Engineering. 13(6):733-44

All figures presented in this manuscript result from my own experiments. However, a significant body of preliminary work that has led to this publication was done by Andy Ekins. With respect to specific elements included in the paper and in this thesis, Andy Ekins elaborated the strategy and performed experiments for the cloning of the plasmid pALLACC, elaborated the strategy for the integration of the aromatic operons on the chromosome and for the cloning of *ubiA* from *Erythrobacter* sp. NAP1. Lauren Narcross cloned the plasmid pALTAA under my supervision and the supervision of Andy Ekins. Heng Jiang performed mass spectrometry work to confirm the identification of 2-decaprenylphenol. Nicholas Gold performed preliminary analytical work on CoQ10-producing strains. Adam Burja was responsible for the isolation and characterization of

Sphingomonas baekryungensis. I wrote the manuscript in collaboration with Andy Ekins and Vincent Martin. Figure 2.4, Figure 2.5, Figure 2.6, Figure 2.7, Figure 2.9 and Figure 2.10 are adapted from material published in Metabolic Engineering.

In this thesis, the experiment presented in Figure 2.8 was done by Andy Ekins. Cloning of the plasmid pJUbiI (section 2.2.8), as well as the experiment presented in Figure 2.11, were done by David Papadopoli, under my supervision. Alain Tessier, of the Centre for Biological Applications of Mass Spectrometry, offered significant guidance for the development of the analytical method of quinone intermediates analysis and identification. Jean-Pierre Falgueyret provided expert advice and technical support during my attempts to identify *Unknown 1*.

Table of Contents

List of Figures

List of Tables

List of abbreviations

10P-AB	3-decaprenyl-4-aminobenzoate
10P-Ph	2-decaprenylphenol
8P-Ph	2-octaprenylphenol
ATP	adenosine triphosphate
CoQ10	Coenzyme Q10
CoQn	ubiquinone
DCW	dry cell weight
DMAPP	dimethylallyl diphosphate
DPP	decaprenyl diphosphate
DPS	decaprenyl diphosphate synthase
DXP	1-deoxy-D-xylulose 5-phosphate
DXS	1-deoxy-D-xylulose 5-phosphate synthase
E4P	Erythrose-4-phosphate
FARM	first aspartate-rich motif
FPP	farnesyl diphosphate
FTMS	Fourier Transform Ion Cyclotron Resonance Mass Spectrometer
HMG-CoA	3-hydroxy-3-methylglutaryl-CoA
HMGR	HMG-CoA reductase
IPP	isopentenyl diphosphate
IPTG	isopropyl β-D-1-thiogalactopyranoside
LB	Luria Bertoli
MEP	2-C-methyl-D-erythritol 4-phosphate
NADPH/NADP+	nicotinamide adenine dinucleotide phosphate
OPP	octaprenyl diphosphate
PABA	*para*-aminobenzoate
PCR	polymerase chain reaction
PEP	phosphoenolpyruvate
PHB	*para*-hydroxybenzoate
rpm	revolutions per minute
TCA	tricarboxylic acid

Chapter 1. Introduction

1.1 Thesis statement

The goal of this project was to engineer the metabolism of the enterobacterium *Escherichia coli* for the production of the commercially-valuable molecule, coenzyme Q10 (CoQ10). As will be detailed in Chapter 1, the biosynthetic pathway leading to the formation of CoQ10 is complex, with precursors stemming from different branches of metabolism and a great number of enzymes involved. Moreover, the biological function of this molecule is linked to aerobic respiration and energy production, which presupposes strict control mechanisms to ensure that appropriate levels are present in the cell membrane. Efforts to obtain higher CoQ10 yields in microbes using genetic engineering have been scattered, often narrowed on one branch of the biosynthetic pathway (Huang et al., 2011; Zahiri et al., 2006b; Zhang et al., 2007). Some improvements obtained were enhanced due to enrichment of the fermentation medium or modifications in growth conditions, demonstrating *E. coli*'s capacity to accumulate higher concentrations of CoQ10, but offering little insight into the underlying biological mechanism(s) responsible for the reported enhanced accumulation levels.

My driving hypothesis was that a systematic identification and upregulation of gene expression for rate-limiting steps in CoQ10 biosynthesis would result in unprecedented accumulation of this molecule in *E. coli*. Corollary to this, I believed that the investigation of metabolic or physiological factors influencing the synthesis of CoQ10 in *E. coli* would provide useful insight for the design of novel engineering

strategies to improve CoQ10 production in microbes. Throughout my research, the identification and characterization of such limiting factors primed over the achievement of high CoQ10 contents in engineered *E. coli* strains. I used genetic tools, such as recombinant plasmids, gene deletions and insertions, and defined alterations in primary metabolism using the growth medium, in order to push carbon flux towards CoQ10 biosynthesis. As such, more than industrially-fit solutions, the strains engineered through this project serve to establish proof-of-concept demonstrations of novel ways to increase CoQ10 biosynthesis in microbes.

1.2 **Physiological functions and applications of coenzyme Q10 in medicine**

Coenzyme Qn (CoQn), also known as ubiquinone, is a lipid-soluble molecule with high redox potential. It is formed of a benzoic group conjugated to a long isoprenoid chain with a varying number (n) of isoprene units (Figure 1.1).

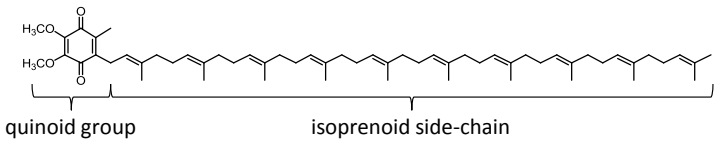

Figure 1.1 Structure of coenzyme Q10.

Humans naturally produce CoQ10, which plays a major role in the transfer of electrons between respiratory complexes of the electron transport chain, located within the inner mitochondrial membrane (Kroger and Klingenberg, 1973). CoQ10 also acts as an antioxidant, protecting membranes and proteins from oxidation by scavenging free radicals and by regenerating pools of tocopherols (Lass and Sohal, 1998; Martin et al., 2007; Yoshida et al., 2006). There is evidence that CoQ10 is involved in the

transcriptional regulation of genes, some of which play roles in inflammatory responses and in cholesterol metabolism (Schmelzer et al., 2007; Schmelzer et al., 2010). CoQ10 supplements have been demonstrated to have positive effects on patients suffering from certain cardio-vascular conditions, such as congestive heart failure and acute myocardial infarction (Hodgson et al., 2002; Shults et al., 2002; Singh et al., 1998; Yang et al., 2010). Additionally, it has been shown that patients taking statin drugs (3-hydroxy-3-methyl-glutaryl-CoA reductase inhibitors) to reduce cholesterol levels may suffer from diminished blood ubiquinone levels, which may be linked to muscle problems like myopathy and myositis that could be alleviated through CoQ10 supplementation (Schaars and Stalenhoef, 2008). Furthermore, early research has suggested that CoQ10 supplementation may benefit patients suffering from male infertility, neurodegenerative disease and diabetes-associated nephropathy (Mancini and Balercia, 2011; Sourris et al., 2012; Yang et al., 2010). Another major application of CoQ10 is as an ingredient of dermatological ointments, due to evidence that its topological application can reduce wrinkle formation (Inui et al., 2008).

This growing demand for CoQ10 from the pharmaceutical and cosmetic sectors has led to intensified efforts to decrease the cost of CoQ10 industrial production. Possible production methods for CoQ10 include: chemical synthesis (Negishi et al., 2002), semi-chemical synthesis using solanesol (Lipshutz et al., 2005), or microbial fermentation using yeasts or bacteria. Microbial biosynthesis offers several advantages over chemical and semi-chemical synthesis, including specificity towards the all-*trans* biologically active isomer of CoQ10, and the reduced production of environmentally hazardous waste. Indeed, the viability of a microbial biosynthesis approach has been demonstrated by

companies, such as Kaneka Corporation, that have already commercialized biologically-produced CoQ10 obtained from fermentation using proprietary yeast strains. In recent years, considerable research has emerged in attempts to isolate suitable microbial strains for the development of cost-effective bioprocesses for CoQ10 production.

1.3 **Quinone diversity between and within species**

The function and overall structure of ubiquinone is well conserved across species, but the length of its isoprenoid side-chain varies. For instance, humans mainly synthesize CoQ10 while rodents predominantly generate CoQ9; the budding yeast *Saccharomyces cerevisiae* makes CoQ6, but the closely related *Schizosaccharomyces pombe* makes CoQ10. Quinone diversity is also found among prokaryotes, where the ubiquinone chain length varies between eight-isoprene units (i.e. *Escherichia coli*, CoQ8), nine-isoprene units (i.e. *Acetobacter aceti*, CoQ9) or ten-units (i.e. *Paracoccus denitrificans*, CoQ10). In addition, prokaryotes may produce alternative quinone types bearing a naphthalene head group, depending on their species. These naphthoquinones include menaquinone and demethylmenaquinone. Typically, strictly aerobic gram-negative species of bacteria contain solely ubiquinone, while gram-negative facultative aerobic bacteria use both ubiquinone and menaquinone or demethylmenaquinone. Gram-positive bacteria, on the other hand, appear to largely use menaquinone or demethylmenaquinone (Collins and Jones, 1981).

1.4 **Physiological functions of ubiquinone in prokaryotes**

Similar to eukaryotes, prokaryotes use ubiquinone as an electron carrier during respiration. In *E. coli* ubiquinone is used when O_2 or nitrate are the final electron acceptors. Menaquinone and demethylmenaquinone, which have lower midpoint potentials than ubiquinone, are used during anaerobic respiration when final electron acceptors, such as fumarate, have a low midpoint potential (Ingledew and Poole, 1984). The redox state of ubiquinone also serves as a cue for cells to initiate aerobic or anaerobic cell functions. For example, in *E. coli*, the oxidized form of CoQ8 has been demonstrated to act as a direct negative signal for the Arc two-component signal transduction system (Georgellis et al., 2001). This regulatory switch consists of the membrane-associated sensor kinase ArcB, which undergoes autophosphorylation under anaerobic conditions, turning on its kinase activity. Activated ArcB then phosphorylates the transcription regulator ArcA, resulting in the transcription of genes involved in anaerobic metabolism and in the repression of genes taking part in aerobic metabolism. Therefore, by inhibiting the autophosphorylation of ArcB during aerobiosis, CoQ8 thus prevents the onset of anaerobic metabolism (Georgellis et al., 2001; Malpica et al., 2004). Also in *E. coli*, CoQ8 participates in disulfide bond formation by providing oxidizing power to the cytoplasmic membrane protein DsbB, which then oxidizes the periplasmic enzyme DsbA, responsible for introducing disulfide bonds to newly synthesized proteins (Bader et al., 2000). The various roles for CoQ8 that have been elucidated in *E. coli* demonstrate the importance of quinones in many facets of cellular function.

1.5 **Biosynthesis of ubiquinone in prokaryotes**

Genetic and biochemical studies have led to almost complete elucidation of the CoQ8 biosynthesis pathway in *E. coli*. Homologues of genes involved in this pathway were identified in several other bacterial species, suggesting that ubiquinone synthesis is highly conserved among prokaryotes (Figure 1.2).

The aromatic core of the CoQn molecule is derived from the shikimate pathway, which starts with the condensation of erythrose-4-phosphate (E4P) and phosphoenolpyruvate (PEP). The shikimate pathway leads to the production of the aromatic intermediate chorismate, a precursor for several essential aromatic molecules including folate and aromatic amino acids, which is converted to *para*-hydroxybenzoate (PHB) by the chorismate lyase UbiC. PHB, the first committed intermediate to ubiquinone biosynthesis, is then prenylated with an isoprenoid of varying length, depending on the species (Figure 1.2).

In prokaryotes, long chain isoprenoids are derived from the 2-C-methyl-D-erythritol 4-phosphate (MEP) pathway. The MEP pathway leads to the formation of two isoprenoid building blocks, isopentenyl diphosphate (IPP) and dimethylallyl diphosphate (DMAPP). DMAPP then serves as a primer for the elongation of a fifteen-carbon isoprenoid by the farnesyl diphosphate (FPP) synthase IspA, which successively condenses IPP molecules to form FPP. This fifteen-carbon isoprenoid is the substrate for a polyprenyl diphosphate synthase, which further elongates the isoprenoid chain that will eventually form the prenyl side-chain constituent for ubiquinone synthesis (Figure 1.2). *E. coli* endogenously expresses an octaprenyl diphosphate (OPP) synthase, IspB, leading

to the formation of OPP and finally to CoQ8. In this way, the product formation catalyzed by a given polyprenyl synthase determines the chain length of the ubiquinone produced in each organism. Indeed, the heterologous expression in a microbial host of a polyprenyl diphosphate synthase, catalyzing the formation of an isoprenoid of n subunits, is sufficient for the accumulation of CoQn species with the corresponding chain length, n. For instance, the expression in *E. coli* of *sdsA*, encoding the solanesyl diphosphate synthase from *Rhodobacter capsulatus*, results in the production of both CoQ8 from the endogenous IspB and CoQ9 from the heterologous SdsA (Okada et al., 1997a).

The enzymatic steps downstream of PHB and isoprenoid formation, leading to the formation of ubiquinone, further described in this paragraph, will be referred to here as the ubiquinone pathway (Figure 1.2). The prenylation of PHB is carried out by an integral membrane protein, UbiA, forming the quinoid intermediate 3-polyprenyl-4-hydroxybenzoate (Young et al., 1972). In *E. coli*, UbiA competes for OPP with MenA, which directs OPP towards the biosynthesis of menaquinone and demethylmenaquinone. The product of UbiA is then decarboxylated into the intermediate 2-polyprenylphenol. In *E. coli*, two decarboxylases, UbiD and UbiX, participate in this reaction (Cox et al., 1969; Gulmezian et al., 2007; Leppik et al., 1976a). The next step of the ubiquinone pathway consists of the hydroxylation of 2-polyprenylphenol into 2-polyprenyl-6-hydroxyphenol. Genetic studies in *E. coli* had previously linked this reaction to the product of *ubiB* (Poon et al., 2000). However, UbiB is a kinase-like protein with no homology to known hydroxylases. A more recent study demonstrates that UbiI, an enzyme with structural characteristics of flavin adenine dinucleotide-dependent monooxygenases, is the main enzyme responsible for the hydroxylation of 2-polyprenylphenol (Hajj Chehade et al.,

2013). The product of this reaction, 2-polyprenyl-6-hydroxyphenol, is then methylated by UbiG, forming 2-polyprenyl-6-methoxyphenol, which is further hydroxylated by UbiH to form 2-polyprenyl-6-methoxy-1,4-benzoquinol (Alexander and Young, 1978; Hsu et al., 1996; Young et al., 1973). A second methyltransferase, UbiE, transfers a methyl group from S-adenosylmethionine to 2-polyprenyl-6-methoxy-1,4-benzoquinol, resulting in 2-polyprenyl-3-methyl-6-methoxy-1,4-benzoquinol (Lee et al., 1997; Young et al., 1971). The hydroxylase UbiF then adds a hydroxyl group, forming 2-polyprenyl-3-methyl-5-hydroxy-6-methoxy-1,4-benzoquinol (Young et al., 1971). Finally, this last intermediate is methylated in a second reaction carried out by UbiG, completing the formation of CoQn, in its reduced form (Leppik et al., 1976a; Stroobant et al., 1972) (Figure 1.2).

All ubiquinone pathway intermediates have a hydrophobic isoprenoid side chain that localizes them to the cytoplasmic membrane. It follows that a number of ubiquinone biosynthetic enzymes are or have been predicted to be membrane-associated (Bhasin et al., 2005; Claros and von Heijne, 1994; Leppik et al., 1976a; Leppik et al., 1976b; Young et al., 1972). Furthermore, strains with mutations in *ubiB*, *ubiG* or *ubiH* accumulate the intermediate 2-octaprenylphenol (Alexander and Young, 1978; Poon et al., 2000; Young et al., 1973), indicating that a loss of activity of any of these three enzymes blocks the hydroxylation of this intermediate (Figure 1.2). This phenotype suggests interdependency or a complex between these three proteins. Such a complex has indeed been isolated from the cytoplasmic membranes and was capable of converting 2-octaprenylphenol to CoQ8 *in vitro*. It is hypothesized to remain in standby position during anaerobiosis and resume the conversion of 2-octaprenylphenol to ubiquinone upon transition to aerobic conditions (Knoell, 1979; Knoell, 1981). There is also increasing evidence for the existence of such

a complex in *S. cerevisiae*, and given the similarities between the two pathways, a related complex might be functional in *E. coli* (Baba et al., 2004; Gin and Clarke, 2005; Hsu et al., 2000; Marbois et al., 2005). Studies with yeast also suggest that ubiquinone is synthesized in two phases: the first phase involves interactions between multiple proteins and CoQ6, leading to the formation of 2-hexaprenyl-6-methoxy-1,4-benzoquinol, while the second phase, ultimately leading to the conversion of 2-hexaprenyl-6-methoxy-1,4-benzoquinol into CoQ6 (Figure 1.2), is triggered by the transition to stationary phase and by linolenic acid-induced oxidative stress (Padilla et al., 2009). The activity of Coq7p, the monooxygenase responsible for the conversion of 2-hexaprenyl-6-methoxy-1,4-benzoquinol to 2-hexaprenyl-3-methyl-5-hydroxy-6-methoxy-1,4-benzoquinol, is modulated by its phosphorylation state: phosphorylated Coq7p is deactivated and thus indirectly leads to a decrease in CoQ6 accumulation, while dephosphorylated Coq7p results in increased CoQ6 synthesis (Martin-Montalvo et al., 2011). This suggests that in *S. cerevisiae*, the biosynthesis of ubiquinone is modulated post-translationally by protein kinases and phosphatases, thereby fine-tuning quinone production with the respiratory needs of the cell. Supporting a similar model in prokaryotes, *E. coli* studies using the translation inhibitor chloroamphenicol suggest that the increase in cellular ubiquinone pools that follow a switch from anaerobic to aerobic conditions can be attributed to a post-translational mechanism (Shestopalov et al., 1997).

Overall, the biosynthesis of ubiquinone is complex, incorporating precursors generated from different branches of central metabolism, requiring a great number of enzymes working in synchrony and a myriad of genes whose timely expression is essential for the proper unfolding of the pathway. Understanding of the different steps of

this biosynthetic pathway, as well as of the regulatory mechanisms underlying its functionality, is key to rationally engineer an industrially-viable biocatalyst capable of high CoQ10 yields.

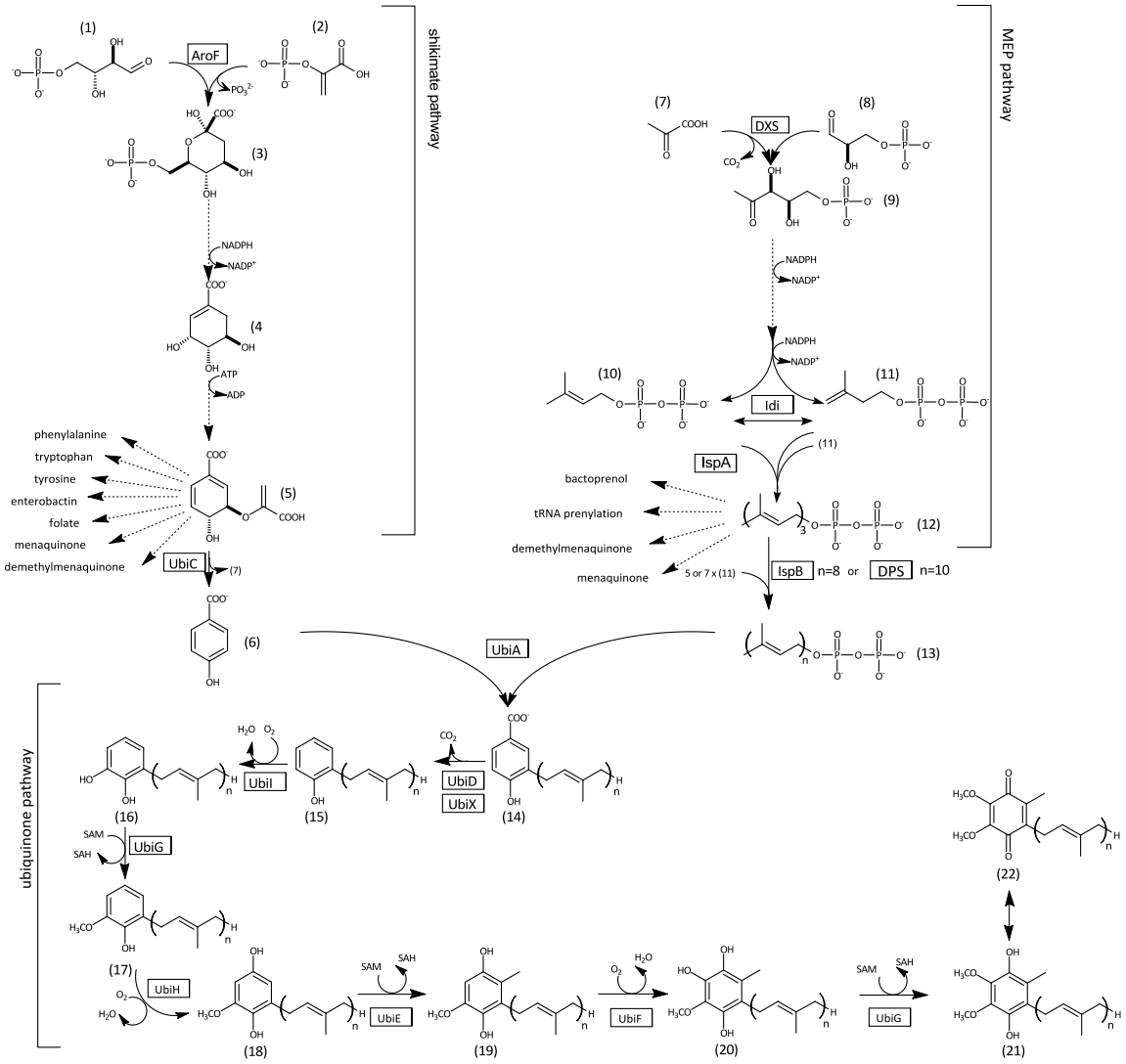

Figure 1.2 Biosynthetic pathway of ubiquinone in prokaryotes
Enzyme names and intermediates are inferred from research studies in *E. coli*. The chain length of isoprenoids and ubiquinone pathway intermediates is kept unspecified (n) to generalize the pathway model to encompass all prokaryotes. (1) erythrose-4-phosphate; (2) phosphoenolpyruvate; (3) 3-deoxy-arabino-heptulosonate 7-phosphate; (4) shikimate; (5) chorismate; (6) *para*-hydroxybenzoate; (7) pyruvate; (8) glyceraldehyde-3-phosphate; (9) 1-deoxy-D-xylulose-5-phosphate; (10) demethylallyl diphosphate; (11) isopentenyl diphosphate; (12) farnesyl diphosphate; (13) polyprenyl diphosphate; (14) 3-polyprenyl-4-hydrobenzoate; (15) 2-polyprenylphenol; (16) 2-polyprenyl-6-hydroxyphenol; (17) 2-polyprenyl-6-methoxyphenol; (18) 2-polyprenyl-6-methoxy-1,4-benzoquinol; (19) 2-polyprenyl-3-methyl-6-methoxy-1,4-benzoquinol; (20) 2-polyprenyl-3-methyl-5-hydroxy-

6-methoxy-1,4-benzoquinol; (21) ubiquinol; (22) ubiquinone (CoQn). Abbreviations: ATP, adenosine triphosphate; ADP, adenosine diphosphate; NADPH/$NADP^+$, nicotinamide adenine dinucleotide phosphate; SAM, *S*-adenosylmethionine; SAH, *S*-adenosylhomocysteine.

1.6 **Natural producers of CoQ10**

CoQ10 is produced in naturally high quantities by several microorganisms including strains of gram-negative soil bacteria such as *Rhizobium radiobacter* (a.k.a. *Agrobacterium tumefaciens*), *Paracoccus denitrificans,* and *Protomonas extorquens*, as well some photoautotrophs including *Rhodobacter sphaeroides* (a.k.a. *Rhodopseudomonas sphaeroides*), and yeast species such as *Sporidiobolus johnsonii,* which accumulate intracellular CoQ10 to levels between 0.8 and 3.3 mg/g dry cell weight (DCW) (Dixson et al., 2011; Urakami and Hori-Okubo, 1988; Yoshida et al., 1998).

Furthermore, the innate CoQ10 content of a number of naturally producing strains has been increased through chemical mutagenesis. In order to select high CoQ10-producing mutant strains, a number of indirect phenotypes were used as surrogate screens. For example, *R. radiobacter* mutants that could produce up to 2-fold higher CoQ10 content than the wild type parental strain were selected for their ability to grow on daunomycin, menadinone (quinone-like molecules generating hydroxyl radicals) and/or the methionine antagonist ethionine (Farr and Kogoma, 1991; Myers et al., 1987; Yoshida et al., 1998). The mutations resulting in enhanced CoQ10 production in such mutants remain largely undetermined. However, in one instance, it was determined that an *R. radiobacter* mutant strain with a high CoQ10 content displayed up-regulated expression levels of a number of genes involved in the tricarboxylic acid (TCA) cycle (Koo et al., 2010). In another example of screening for enhanced CoQ10 producers, *R.*

sphaeroides mutants were chosen based on their colony colour as a surrogate selection for increased CoQ10 accumulation. In this case, a green colony colour was used to indicate reduced accumulation of cellular carotenoids, which are synthesized from the same isoprenoid precursors as CoQ10 and could indicate the allocation of more cellular isoprenoid resources towards CoQ10 production (Sakato et al., 1992; Urakami and Hori-Okubo, 1988; Yoshida et al., 1998). It is also possible that CoQ10 synthesis was up-regulated in carotenoid-reduced mutant strains in order to balance the loss of one antioxidant (carotenoid), with another (CoQ10). The selected mutants display 1.3 to 3-fold increases in CoQ10 production compared to their parental strains.

1.7 *R. radiobacter* as a production platform for CoQ10

Despite their high CoQ10 contents, most natural producers of CoQ10, wild type or mutant, are unsuitable for industrial applications due to their limited growth rate and yields. For instance, even under optimized fermentor conditions, the cell mass obtained with a mutant strain of *R. sphaeroides* did not exceed 18.6 g DCW/L (Kien et al., 2010). One exception is *R. radiobacter*, which is gaining popularity as a host for the production of CoQ10. *R. radiobacter* mutants isolated for their improved CoQ10 content can be cultivated in fermentors at densities exceeding 65 g DCW/L (Ha et al., 2007a). There are two accounts where *R. radiobacter* was engineered for higher CoQ10 production by either over-expressing its (DXP) synthase 1-deoxy-D-xylulose 5-phosphate or its glyceraldehyde-3-phosphate dehydrogenase (Koo et al., 2010; Lee et al., 2007). However, most improvements in CoQ10 titers were obtained by modifications in culture growth conditions and media composition (Ha et al., 2009; Ha et al., 2007a; Ha et al.,

2007b). Various optimization strategies involving media composition and growth conditions are presented in section 1.10.

1.8 *E. coli* as a production platform for CoQ10

E. coli is commonly used as a model for the heterologous production of CoQ10 in microbes. It is an attractive host for development as an industrial production platform due to the following: (1) its robust fermentation characteristics, including fast growth rate; (2) its amenability to genetic engineering and; (3) the extensive knowledge that exists regarding its ubiquinone pathway and primary metabolism. As a result, rational genetic engineering strategies have been developed to allow production of CoQ10 in *E. coli*, and are presented in section 1.9. These strategies have led to improvements in the yields of CoQ10 obtained from engineered *E. coli* strains (Table 1.1). However, such yields still fall below those obtained from natural CoQ10 producers, such as *R. radiobacter*, indicating that the factors limiting CoQ10 accumulation in *E. coli* bear further investigation.

1.9 Engineering strategies for high CoQ10 production in microbes

1.9.1 *Heterologous expression of a decaprenyl diphosphate synthase*

As mentioned above (section 1.3), wild type *E. coli* produces CoQ8 as its predominant ubiquinone molecule. However, it is possible for *E. coli* to produce CoQ10 by the expression of a heterologous decaprenyl diphosphate (DPP) synthase (DPS), which catalyzes the sequential condensation reaction between IPP and FPP to form DPP

(Figure 1.2). For example, the *dps* genes from CoQ10-producing bacterial species, including *R. radiobacter*, *R. sphaeroides*, and *Gluconobacter suboxydans,* have been isolated and expressed in *E. coli* (Lee et al., 2004; Park et al., 2005; Zhang et al., 2007). Additionally, a given heterologous DPS must be expressed in a Δ*ispB* background, where expression of *E. coli*'s endogenous OPP synthase has been abolished, in order to eliminate CoQ8 synthesis in favor of CoQ10 production (Choi et al., 2009; Huang et al., 2011; Kim et al., 2006; Lee et al., 2004; Okada et al., 1998; Park et al., 2005; Takahashi et al., 2003; Zahiri et al., 2006a; Zahiri et al., 2006b). *E. coli* Δ*ispB* strains expressing a foreign DPS accumulate CoQ10, along with varying levels of CoQ8 and CoQ9, depending on the DPS expressed (Okada et al., 1998; Takahashi et al., 2003; Zahiri et al., 2006a). Most bacteria surveyed to date produce minor amounts of differing CoQn forms with shorter-length isoprenoid side-chains in addition to their main ubiquinone species, suggesting that DPS enzymes generally make other prenyl diphosphates in addition to DPP. The production of shorter or longer ubiquinone species in *E. coli* strains engineered for CoQ10 production poses a problem from an industrial point of view due to the reduced yields of CoQ10 that result when precursors are channeled towards non-desired products and the extra costs associated with purifying CoQ10 from additional quinone species.

1.9.2 *Increasing production of precursors of CoQ10*

As described in section 1.5, the formation of ubiquinone in bacteria occurs through condensation between the aromatic molecule PHB, derived from the shikimate pathway, and the long-chain isoprenoid, DPP, formed via the MEP pathway. A current

strategy to improve the heterologous production of CoQ10 in *E. coli* is to overexpress rate-limiting enzymes leading to the production of these precursor molecules (Zahiri et al., 2006b; Zhang et al., 2007).

1.9.2.1 Increasing the production of isoprenoid precursors

The first step of the MEP pathway is the condensation of pyruvate and glyceraldehyde-3-phosphase to yield DXP, catalyzed by the DXP synthase, DXS (Figure 1.2). The heterologous production of the carotenoid lycopene in *E. coli*, which also requires isoprenoid precursors, has been improved by the overexpression of DXS (Harker and Bramley, 1999; Kim and Keasling, 2001). Using the same rationale, higher titers of CoQ10 have been achieved by overexpressing the *dxs* gene isolated from *Pseudomonas aeruginosa* in *E. coli* strains engineered for CoQ10 production (Choi et al., 2009; Kim et al., 2006). Up to 1.8-fold improvement in specific CoQ10 content was obtained in strains over-expressing both DPS and DXS compared to those expressing solely DPS (Table 1.1). An alternative to the overexpression of the endogenous MEP pathway in *E. coli* is to express a heterologous mevalonate pathway, generally found in eukaryotes. Synthetic mevalonate pathways are typically divided into two parts: an upper pathway that converts acetyl-CoA to mevalonate and a lower pathway that converts mevalonate into DMAPP and IPP. Both parts of the pathway can be co-expressed, enabling the formation of isoprenoids from acetyl-CoA. Alternatively, one can express the lower part of the pathway alone and supplement the growth medium with mevalonate to enable the production of IPP and DMAPP. The expression of the lower part of the mevalonate pathway in *E. coli* strains expressing a recombinant *dps* has led to two-fold improvements in CoQ10 accumulation, while the expression of both the upper and lower sections of the

pathway has thus far led to more modest improvements (1.5-fold) (Zahiri et al., 2006b) (Table 1.1).

1.9.2.2 Increasing the production of aromatic precursors

As described in section 1.5, the first committed aromatic precursor to ubiquinone, PHB, is formed through the shikimate pathway leading to chorismate (Figure 1.2). As chorismate is a precursor molecule in several essential metabolic routes, the conversion of chorismate to PHB may limit the rate of production of ubiquinone in *E. coli*. It has been shown that the overexpression of the chorismate lyase UbiC in engineered *E. coli* increased the production of CoQ10 when the downstream PHB polyprenyltransferase, UbiA, was coexpressed (Zhang et al., 2007; Zhu et al., 1995). Another study reports that the exogenous addition of PHB improved CoQ10 production by two-fold, but only when the supply of isoprenoid precursors was concomitantly increased (Zahiri et al., 2006b). Overall, these experiments suggest that the availability of PHB becomes rate-limiting to CoQ10 production mainly when the supply of isoprenoid increases, resulting in more DPP available for CoQ10 biosynthesis, or when the activity of UbiA goes up, leading to an increased flux of PHB to the ubiquinone pathway.

1.9.2.3 Overexpression of the ubiquinone pathway

In *E. coli* it has been shown that the rate-limiting step to CoQ10 production occurs at the condensation reaction between the aromatic PHB and isoprenoid DPP, catalyzed by UbiA (Zhang et al., 2007; Zhu et al., 1995). The overexpression of UbiA, along with DPS, resulted in as much as a 3.4-fold increase in CoQ10 content compared to strain expressing DPS alone (Zhang et al., 2007). Additionally, to overcome any

potentially limiting steps stemming from the native regulatory mechanisms, the *ubiB*, *ubiG* and *ubiH* genes have been overexpressed in *E. coli*. The overexpression of these genes had only a limited effect on ubiquinone production (Table 1.1) (Zhang et al., 2007; Zhu et al., 1995). However, the *E. coli* background strains used in these experiments were subjected to endogenous regulation of aromatic and isoprenoid precursors. Therefore, it is possible that limited carbon flux to the ubiquinone pathway resulted in the modest increases in ubiquinone content reported in these studies. When precursors are produced in excess, CoQ10 biosynthesis may then become limited by the activity of one or more enzymes of the ubiquinone pathway.

1.9.3 *Improving CoQ10 production using central metabolism*

As an alternative or complementary strategy to increase carbon flux towards CoQ10 production in engineered *E. coli* strains, one may consider introducing alterations into the central metabolic pathways. The glycolysis intermediate glyceraldehyde-3-phosphate is, along with pyruvate, an initial building block of the MEP pathway, which in turn supplies the isoprenoid precursors necessary for the prenylation of ubiquinone (Figure 1.2). By deleting *pykA* and *pykF*, coding for pyruvate kinases, and over-expressing the PEP carboxykinase Pck, carbon flux can be redirected towards glyceraldehyde-3-phosphate, which favours increased flux through the MEP pathway (Farmer and Liao, 2001). Applying this approach to CoQ10 production, a 1.7-fold increase in CoQ10 content was obtained in an *E. coli* strain expressing a *G. suboxydans* DPS (Huang et al., 2011) (Table 1.1).

Another attractive strategy to improve the production of a molecule of interest in a microbial host is to manipulate the levels of redox cofactors required for its synthesis. The production of one molecule of CoQ10 from glucose requires 21 molecules of nicotinamide adenine dinucleotide phosphate (NADPH) (20 molecules from the MEP pathway and one NADPH from the shikimate pathway) (Figure 1.2). In order to increase the availability of NADPH, the nicotinamide adenine dinucleotide (NAD^+)-dependent glyceraldehyde-3-phosphate dehydrogenase, GapA, of *E. coli* can be replaced with the $NADP^+$-dependent glyceraldehyde-3-phosphate dehydrogenase, GapC, from *Clostridium acetobutylicum* (Huang et al., 2011; Martinez et al., 2008). When this approach was used to improve CoQ10 biosynthesis in engineered *E. coli* strains, a 1.25-fold increase in CoQ10 content was observed (Table 1.1). In a high CoQ10-producing mutant strain of *R. radiobacter*, a positive correlation was demonstrated between the $NADH/NAD^+$ ratio and the specific CoQ10 content (Koo et al., 2010). Based on this finding, the native NAD^+-dependent GapA, was over-expressed to increase the $NADH/NAD^+$ ratio and further improve CoQ10 production. This strategy resulted in a 25% increase in $NADH/NAD^+$ and in over two-fold improvement in CoQ10 content (Koo et al., 2010) (Table 1.1). The results of these two studies, which both take advantage of glyceraldehyde-3-phosphate dehydrogenases to alter the pools of redox factors, appear somewhat conflicting (Huang et al., 2011; Koo et al., 2010). Nevertheless, these studies highlight the necessity to explore in more detail the relationship between central metabolism and CoQ10 production in microbes.

Table 1.1 Production of CoQ10 by engineered microorganisms

Organism	Overexpressed enzymes	Gene deletions	Metabolic pathways affected	Specific CoQ10 content (mg/g DCW)	CoQ10 productivity (mg/L·h)	CoQ10 titer (mg/L)	Reference
E. coli	DPS_{Gsub}	N/A	Isoprenoid	0.29	0.67	25.5	(Park et al., 2005)
E. coli	DXS	N/A	Isoprenoid (MEP)	~0.80	N/A	N/A	(Harker and Bramley, 1999)
E. coli	DPS_{Gsub}, DXS	N/A	Isoprenoid (MEP)	0.94	0.94	46.1	(Kim et al., 2006)
E. coli	DPS_{Atum}, DXS	*ispB*	Isoprenoid (MEP)	1.41	3.1	100	(Choi et al., 2009)
E. coli	DPS_{Atum}, PhbA, MvaK1, MvaD, MvaK2, MvaA, MvaS, idi	N/A	Isoprenoid (mevalonate)	2.428	N/A	N/A	(Zahiri et al., 2006b)
E. coli	DPS_{Gsub}, Pck	*ispB, pykA, pykF*	Isoprenoid, glycolysis	0.44	0.01	0.31	(Huang et al., 2011)
E. coli	DPS_{Gsub}, GapC	*ispB, pykA, pykF, gapA*	Isoprenoid, glycolysis	0.45	0.02	0.37	(Huang et al., 2011)
E. coli	DPS_{Gsub}, DXS, Idi, IspA, UbiC, UbiA, Pck, GapC	*ispB, pykA, pykF, gapA*	Isoprenoid, glycolysis, ubiquinone	3.24	2.82	5.64	(Huang et al., 2011)
E. coli	DPS_{Atum}, UbiA	N/A	Isoprenoid, ubiquinone	0.51	N/A	N/A	(Zhang et al., 2007)
E. coli	DPS_{Atum}, UbiA, UbiC	N/A	Isoprenoid, ubiquinone	0.59	1.55	50.29	(Zhang et al., 2007)
E. coli	DPS_{Atum}, UbiG	N/A	Isoprenoid, ubiquinone	0.19	N/A	N/A	(Zhang et al., 2007)
E. coli	UbiC, UbiA	N/A	Ubiquinone	~0.45	N/A	N/A	(Zhu et al., 1995)
E. coli	IspB, UbiC, UbiA	N/A	Isoprenoid, ubiquinone	~0.80	N/A	N/A	(Zhu et al., 1995)
E. coli	IspB, UbiC, UbiA, UbiB	N/A	Isoprenoid, ubiquinone	~0.85	N/A	N/A	(Zhu et al., 1995)
E. coli	IspB, UbiC, UbiA, UbiG, UbiH	N/A	Isoprenoid, ubiquinone	~0.95	N/A	N/A	(Zhu et al., 1995)
R. radiobacter	GapA	N/A	Glycolysis	5.27	N/A	N/A	(Koo et al., 2010)
R. radiobacter	DXS		Isoprenoid	8.3	4.5	502.4	(Lee et al., 2007)

1.10 **Improving CoQ10 yields through growth conditions**

As discussed in section 1.6, the CoQ10 content of natural producers, such as *R. radiobater* and *R. sphaeroides* has been improved by random mutagenesis and selection. However, because of the limited genetic tools available for these organisms, the rational genetic strategies that can be applied to *E. coli* are largely impractical. As a result, most research has focused on increasing CoQ10 production by fine-tuning the growth conditions of these organisms, both in flasks and in fermentors.

Although there is still conflicting evidence on this matter (Wu et al., 2003), a number of reports have shown that CoQ10 production tends to increase under low aeration conditions, both in *R. radiobacter* and *R. sphaeroides* (Choi et al., 2005; Ha et al., 2007b; Seo and Kim, 2010; Yen and Chiu, 2007; Yen and Shih, 2009). For instance, the CoQ10 content of a mutant strain of *R. radiobacter* increased four-fold by reducing dissolved oxygen concentrations from 20 to 5% (Choi et al., 2005) (Table 1.2). As part of the electron transport chain, it is possible that CoQ10 levels are modulated by variations in the electron flux or in the proton gradient brought about by the limited oxygen supply. To test these possibilities, the effect of the cytochrome *c* oxidase inhibitor, azide, and of 2,4-dinitrophenol, a proton ionophore that uncouples oxidative phosphorylation, on CoQ10 accumulation were assessed in *R. radiobacter* (Choi et al., 2005). The addition of 2,4-dinitrophenol had no effect on CoQ10 accumulation, indicating that large-scale changes in the cellular proton gradient do not affect CoQ10 production (Choi et al., 2005). The addition of increasing concentrations of sodium azide, on the other hand, correlated to increasing CoQ10 content of bacterial cultures (Choi et al., 2005; Seo and Kim, 2010). These results suggest that the restricted electron flux through the respiratory

chain brought about by low aeration conditions, mimicked by the azide treatment, triggers the synthesis of CoQ10. Though the precise mechanism behind this phenomenon is unclear, it has been hypothesized that when the transfer of electrons through the electron transport chain to the final acceptor is slowed by a decrease in oxygen availability, electrons are trapped in upstream constituents of the respiratory chain, potentially leading to an accumulation of the reduced form of CoQ10, $CoQ10H_2$ (Bekker et al., 2007). Cells may thus be forced to synthesize more CoQ10 in order to fix this imbalance of CoQ10/$CoQ10H_2$ (Choi et al., 2005). Alternatively, partial blockage of the respiratory chain may lead to an accumulation of toxic free electrons in the inner membrane, hence triggering the synthesis of more CoQ10 to scavenge these electrons (Choi et al., 2005).

In addition to respiration, facultative photoautotrophs such as *R. sphaeroides* also use CoQ10 to transfer electrons from the reaction center to the cytochrome bc_1 complex, within the photosynthetic apparatus (Vermeglio and Joliot, 1999). Growth of *R. sphaeroides* under anaerobic/light conditions increased the specific CoQ10 content over four-fold compared to the level attained under aerobic/dark growth conditions (Table 1.2). However, this growth strategy significantly decreased the growth rate of the already low biomass culture, therefore making it uncompetitive for industrial applications (Yen and Chiu, 2007). Nevertheless, this finding suggests that the complete shutdown of respiration associated with the onset of photosynthetic reactions triggers the cells to accumulate more CoQ10 within their inner membrane. This observation, coupled with the CoQ10 accumulation that accompanies a slowed electron transport chain, yields

strong evidence that hindering respiration is an effective strategy in increasing CoQ10 productivity.

Another successful strategy to improve CoQ10 yields in *R. radiobacter* was to increase the concentration of calcium in the growth media. It has been proposed that the increased Ca^{2+} concentration is a source of oxidative stress for the cell, triggering the onset of lipid peroxidation and the production of reactive oxygen species (Ha et al., 2009). Because CoQ10 has well-documented antioxidant properties, it may therefore be likely that increasing its production is the natural response to such oxidative stress. Supporting this hypothesis, an oxidative stress challenge, mediated by the addition of hydrogen peroxide to *R. radiobacter* cultures, also results in increases in CoQ10 content (Seo and Kim, 2010). The selection of high CoQ10-producing mutants on free radical-generating growth inhibitors, described in section 1.6, also supports this link between CoQ10 production and oxidative stress (Yoshida et al., 1998) .

The effect of growth on select carbon and nitrogen sources on CoQ10 production has been explored in mutant strains of *R. radiobacter*. There is conflicting evidence of the impact that growth on different carbon sources has on accumulated CoQ10 content, with one study reporting sucrose, glucose and fructose as having a positive impact on CoQ10 content compared to xylose, lactose and galactose (Koo et al., 2010), while another report shows no differences in CoQ10 content for growth on these carbon sources (Ha et al., 2007b). Plant based nitrogen sources such as corn steep powder and soytone yielded the highest CoQ10 specific content compared to other nitrogen sources including yeast extract, meat extract and tryptone (Ha et al., 2007b; Koo et al., 2010). Overall, modifying growth conditions in order to modulate central metabolic processes appears to be an

effective strategy in enhancing CoQ10 production in microbes (for further culture conditions that correspond to increased CoQ10 accumulation refer to Table 1.2).

Table 1.2 CoQ10 production and culture conditions of natural producer microbes.

Organism	CoQ10 titer (mg/L)	Specific CoQ10 content (mg/g DCW)	Optimized Culture Conditions	Reference
R. radiobacter ATTC4452	87.6	1.9	Not applicable	(Yoshida et al., 1998)
R. radiobacter WSH2601	32.1	1.91	Maximal DO of 40 % (of air saturation)	(Wu et al., 2003)
R. radiobacter ATCC4452	Not reported	5.3	Decreased DO, azide treatment	(Choi et al., 2005)
R. radiobacter KCCM 10413	458	8.54	Fed-batch with sucrose as carbon source, pH 7.0 and 0-10 % DO	(Ha et al., 2007b)
R. radiobacter KCCM 10413	638	9.71	Decreased sucrose feeding to 10% w/v, led to less byproducts/osmotic stress	(Ha et al., 2007a)
R. radiobacter KCCM 10413	763.7	11.84	$CaCl_2$ supplementation	(Ha et al., 2009)
R. radiobacter T6102	14.6	1.95	Decreased DO; H_2O_2 and azide treatement	(Seo and Kim, 2010)
R. radiobacter A603-35-gapA	Not reported	5.27	Increased NADH/NAD^+ ratio	(Koo et al., 2010)
R. spheroides KY 8598	770	Not reported	Controlled agitation speed and oxygen supply	(Sakato et al., 1992)
R. sphaeroides KY 4113	350	8.7	Decreased aeration	(Yoshida et al., 1998)
R. sphaeroides BCRC13100	10.5	8	0 % DO and cultivation without light	(Yen and Chiu, 2007)
R. sphaeroides BCRC13100	45.65	4.4	Use of airlift bioreactor for low aeration	(Yen and Shih, 2009)
R. sphaeroides BCRC13100	83.8	4.5	Fed-batch system with molasses at 1 % w/v	(Yen et al., 2010)
S. johnsonii	Not reported	10.5	Post log growth phase addition of PHB	(Dixson et al., 2011)

1.11 **Thesis objectives**

Current literature offers hints regarding the biochemical steps and metabolite availability that most limit CoQ10 accumulation in microbes. Moreover, the modulation of biological processes such as catabolism, redox balance and respiration, all of which have links to the functions of ubiquinone, has the potential to increase the production of CoQ10 in *E. coli*. Based on this evidence, this thesis is structured around two objectives:

1) To use rational design to address all known rate-limiting factors to CoQ10 biosynthesis. In Chapter 2, I describe the steps taken to build a strain of *E. coli* capable of producing high levels of CoQ10, but most importantly, a strain where each pathway limiting carbon flux towards ubiquinone are addressed individually, in a systematic manner.

2) To expand current knowledge on the physiological and/or metabolic factors limiting CoQ10 accumulation in *E. coli*. In Chapter 3, I investigate whether CoQ10 production in engineered *E. coli* strains can be further enhanced by harnessing the bacteria's capacity to direct carbon flow towards given directions either to fulfill its energy needs or to achieve redox balance.

Chapter 2. Rational design of *E. coli* for increased CoQ10 biosynthesis

2.1 Introduction

Previous studies, summarized in Chapter 1, have shown that the production of CoQ10 is feasible in *E. coli*. However, despite its great potential as a production host, the CoQ10 content currently obtained in engineered *E. coli* still falls below those obtained in mutant strains of *R. radiobacter* and *R. sphaeroides* (Table 1.1, Table 1.2) (Ha et al., 2009; Yoshida et al., 1998; Zahiri et al., 2006b). Strategies used to improve CoQ10 content in *E. coli* range from increasing the biosynthesis of isoprenoid precursors, to supplementation of aromatic intermediates, or over-expressing individual enzymes of the ubiquinone pathway. These studies, although unsuccessful in increasing CoQ10 production levels above those of natural producers, offer hints into the factors limiting the production of this antioxidant in *E. coli*.

Several microbes are capable of CoQ10 biosynthesis, some of them in naturally high concentration. Their poor amenability to growth in the laboratory and to genetic modifications excludes them as hosts for industrial production. However, I may harness some of their inherent qualities by heterologously expressing selected genetic loci in the chosen host, *E. coli.* Ocean Nutrition Canada, a company using marine microbes and microscopic algae for the production of nutraceuticals, was our partner during initial stages of this project. They have collected and characterized a collection of marine microbes capable of CoQ10 production, which were made available as source of genetic material. As mentioned in section 1.9.1, DPS enzymes are known to have relaxed product specificity, resulting in the production of ubiquinone species of varying length. A

first objective was therefore to identify an organism where CoQ10 is the only quinone species produced, which presupposes a DPS with strict product specificity. A second hypothesis was that a PHB prenyltransferase derived from a natural high CoQ10 producer would be more apt to convert high concentrations of substrates into ubiquinone intermediates. Previous literature has also shown that overexpression of UbiA is sufficient to increase CoQ10 production (Zhang et al., 2007). I attempted to express a foreign UbiA in *E. coli*, derived from the high CoQ10 producer *Erythrobacter* sp. NAP1, and evaluated the resulting impact on CoQ10 production.

It has been demonstrated that the effect of deregulated isoprenoid production on CoQ10 is potentiated by an exogenous supply of the aromatic precursor, PHB (Zahiri et al., 2006b). However, as no transporter for this organic acid has been characterized to date in *E. coli*, it is unclear to what extent exogenous PHB can be actively brought into *E. coli* cells. Moreover, the addition of PHB is impractical in the context of an industrial microbial platform. To ensure unrestricted supply of this molecule to the first enzyme of the ubiquinone pathway, the PHB prenyltransferase UbiA, I propose to increase the endogenous production of PHB. Elevated production of PHB from glucose has been achieved in *E. coli* (Barker and Frost, 2001). The strategy employed was to over-express *E. coli*'s *tktA,* coding for a tranketolase, $aroF^{FBR}$, coding for a feedback-insensitive isozyme of 3-deoxy-arabino-heptulosonate synthase, *aroB*, coding for a dehydroquinate synthase, *aroL*, coding for a shikimate synthase, *aroA*, coding for a 5-enolpyruvylshikimate 3-phosphate synthase, *aroC*, coding for a chorismate synthase, and *ubiC*, coding for a chorismate lyase. Maximum yields of PHB were obtained using a strain defective in aromatic amino acid biosynthesis, in order to reduce enzymatic

competition with UbiC for chorismate. However, the resulting strain required supplementation of the culture medium with aromatic amino acids, and suffered cytotoxic effects associated with high concentrations of organic acid. In the context of a CoQ10 production strain, achieving such high titers of PHB is not necessarily desirable. The combined effects of PHB toxicity and metabolic burden associated with multiple plasmid expression may prevent cell growth and optimal production of CoQ10. Alternatively, I aimed at engineering moderate but sustained PHB production in *E. coli*, which could be temporally coupled with the production of isoprenoid precursors.

As the synthesis of one mole of CoQ10 requires ten moles of the isoprenoid building blocks, IPP/DMAPP, it is expected that flux through the isoprenoid pathway is to become rapidly restrictive in a CoQ10 production strain. Accordingly, increased CoQ10 production has been reported in strains overexpressing enzymes of the MEP pathway, or of a foreign mevalonate pathway (Choi et al., 2009; Kim et al., 2006; Zahiri et al., 2006b). The latter strategy has an added advantage over the endogenous MEP pathway in that it bypasses native regulatory mechanisms that may make up-regulation for overproduction more problematic (Martin et al., 2003). For IPP/DMAPP and FPP synthesis, I used the pMevT and pMBIS plasmids developed as part of the initial demonstration that the mevalonate pathway may be expressed in *E. coli* for the production of amorphadiene (Martin et al., 2003). The plasmid pMevT contains the "top" mevalonate operon, formed by *atoB* (*E. coli*), coding for an acetoacetyl-CoA thiolase, *HMGS* (*S. cerevisiae*), coding for 3-hydroxy-3-methylglutaryl-CoA (HMG-CoA) synthase, and *tHMGR* (*S. cerevisiae*), coding for a truncated HMG-CoA reductase (HMGR). The top operon results in the conversion of acetyl-CoA to mevalonate (Figure

2.1). The plasmid pMBIS encodes the "bottom" mevalonate operon, allowing the conversion of mevalonate to DMAPP/IPP and FPP. This operon contains *ERG12* (*S. cerevisiae*), coding for a mevalonate kinase, *ERG8* (*S. cerevisiae*), coding for a phosphomevalonate kinase, *MVD1* (*S. cerevisiae*), coding for a mevalonate pyrophosphate decarboxylase, *idi* (*E. coli*), coding for an IPP isomerase, and *ispA* (*E. coli*), coding for a FPP synthase. Both parts of the pathway may be co-expressed, enabling the formation of isoprenoids from acetyl-CoA. Alternatively, one may express the lower part of the pathway alone and supplement cultures with exogenous mevalonate to enable the production of IPP/DMAPP and FPP. The expression of the top mevalonate operon, in the version present on pMevT, is associated with growth defects, due to an imbalanced pathway leading to the accumulation of a toxic intermediate, HMG-CoA (Pitera et al., 2007). I therefore chose to develop initial CoQ10 production strains with the bottom mevalonate pathway alone. Further along in this project, I obtained plasmids containing upgraded version of the top mevalonate pathway and was able to use them in my CoQ10 production strains.

In this chapter, I report on the stepwise construction of a CoQ10 production strain where endogenous restrictions in precursor production are bypassed, and where flux through the ubiquinone pathway is augmented by the overexpression of a PHB prenyltransferase (Figure 2.1). Using this approach, I sought to identify bottlenecks limiting the accumulation of CoQ10 in this host. I report that the deregulated, over-production of both aromatic and isoprenoid precursors of CoQ10 results in the accumulation of 2-decaprenylphenol, and that the production of this intermediate is

modulated by the expression of UbiA, as well as by the flux through the isoprenoid pathway.

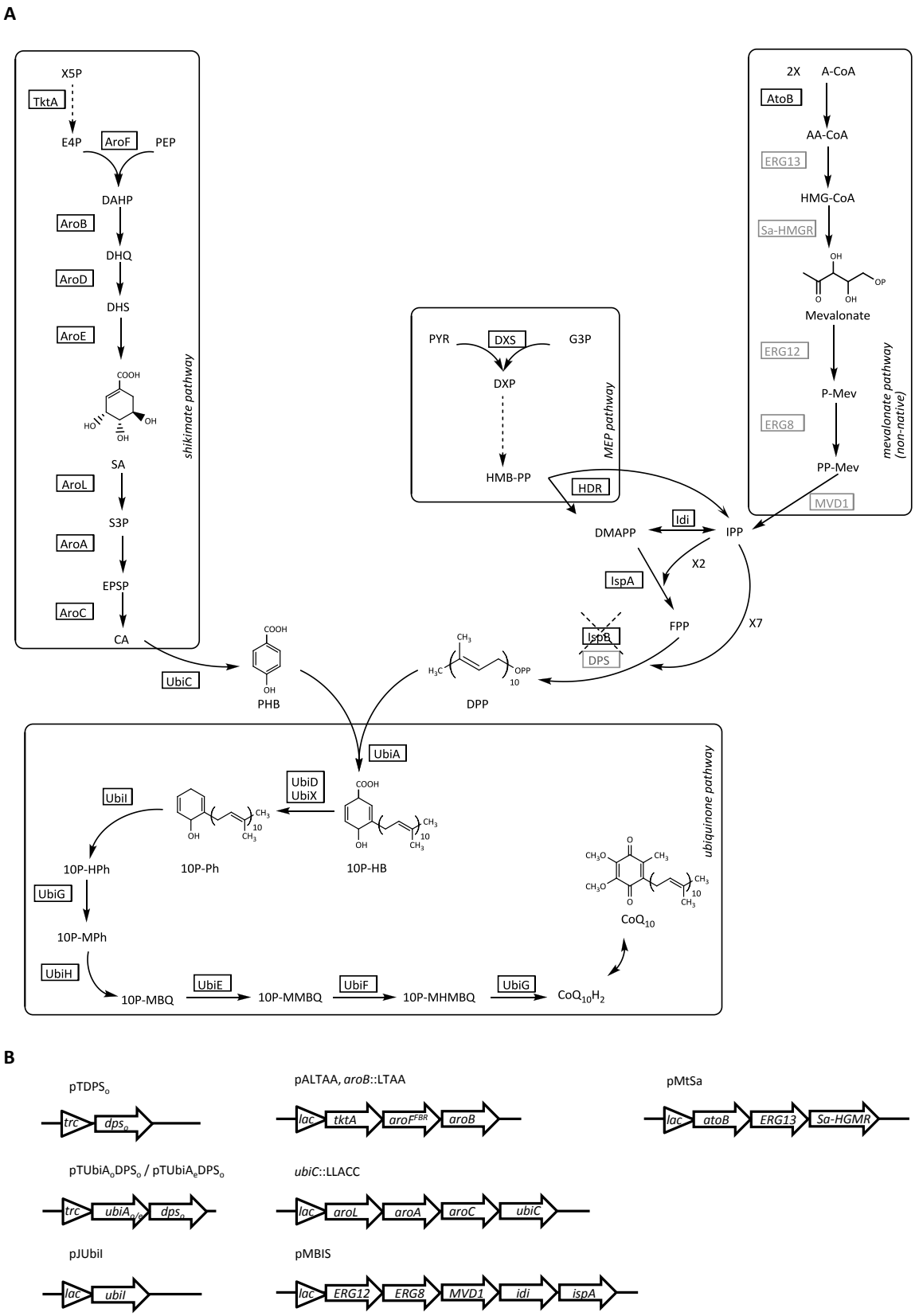

Figure 2.1 Engineering *E. coli* for CoQ10 production

A. Endogenous and foreign biosynthetic pathways engineered for the production of CoQ10 in *E. coli*. Enzymes in black are endogenous to *E. coli*. Enzymes in grey are non-native or modified. Abbreviations; E4P, erythrose-4-phosphate; PEP, phosphoenolpyruvate; DAHP, 3-deoxy-arabino-heptulosonate 7-phosphate; EPSP, 5-enolpyruvyl-shikimate-3-phosphate; PHB, *para*-hydroxybenzoate; GAP, glyceraldehyde-3-phosphate, DXP, 1-deoxy-D-xylulose-5-phosphate; HMB-PP, 1-hydroxy-2-methyl-2-(E)-butenyl 4-diphosphate; HMG-CoA, 3-hydroxy-3-methylglutaryl-CoA; DMAPP, demethylallyl diphosphate; IPP, isopentenyl diphosphate; FPP, farnesyl diphosphate; DPP, decaprenyl diphosphate; 10P-HB, 3-decaprenyl-4-hydrobenzoate; 10P-Ph, 2-decaprenylphenol; 10P-HPh, 2-decaprenyl-6-hydroxyphenol; 10P-MPh, 2-decaprenyl-6-methoxyphenol; 10P-MBQ, 2-octaprenyl-6-methoxy-1,4-benzoquinol; 10P-MMBQ, 2-octaprenyl-3-methyl-6-methoxy-1,4-benzoquinol; 10-MHMBQ, 2-octaprenyl-3-methyl-5-hydroxy-6-methoxy-1,4-benzoquinol; $CoQ10H_2$, ubiquinol-10; CoQ10, coenzyme Q10. **B.** Synthetic operons used in this study. $pTDPS_o$ contains dps_o, coding for a decaprenyl diphosphate synthase, and driven by the *trc* promoter. $pTUbiA_oDPS_o$, and $pTUbiA_eDPS_o$ contains $ubiA_o$ or *ubiA,* respectively, coding for a PHB decaprenyl transferase, and dps_o, driven by the *trc* promoter. pJUbiI contains *ubiI* driven by *lacZ*p. pALTAA and *aroB*::LTAA (integrated downstream of *aroB* on the chromosome) contain *tktA*, coding for transketolase, $aroF^{FBR}$, coding for a tyrosine-insensitive 3-deoxy-D-arabino-heptulosonate 7-phosphate synthase, and *aroB*, coding for a 3-dehydroquinate synthase, driven by *lacZ*p. *ubiC*::LLACC contains *aroL*, coding for a shikimate kinase, *aroA,* coding for a 5-enolpyruvyl-shikimate-3-phosphate synthase, *aroC,* coding for a chorismate synthase, and *ubiC*, coding for and a chorismate lyase, driven by *lacZ*p and integrated downstream of *ubiC* on the chromosome. pMBIS contains *ERG12*, coding for a mevalonate kinase, *ERG8*, coding for a phosphomevalonate kinase, *MVD1*, coding for a mevalonate pyrophosphate decarboxylase, *idi*, coding for an IPP isomerase, and *ispA*, coding for a FPP synthase, driven by *lacZ*p. pMtSa contains *atoB*, coding for a acetyl-CoA acetyltransferase, *ERG13*, coding for a 3-hydroxy-3-methylglutaryl-CoA synthase and *SaHMGR*, coding for a 3-hydroxy-3-methylglutaryl-CoA reductase, driven by *lacZ*p.

2.2 **Materials and methods**

2.2.1 *Reagents, strains and culture conditions*

E. coli strains and plasmids used in this chapter are listed in Table 2.1. *E. coli* DH5α was used for cloning whereas CoQ10-producing strains were constructed in *E. coli* MG1655. *E. coli* strains containing the individual gene knockouts Δ*aroK::kan*, *ΔaroL::kan*, *ΔaroA::kan* and *ΔaroC::kan* were obtained from the Keio collection (Baba et al., 2006). When required, strains were propagated on Luria Bertani (LB) medium (Sambrook et al., 1989) supplemented with 100 µg/mL ampicillin, 20 µg/mL

chloramphenicol, 12.5 μg/mL tetracycline, and/or 25 μg/mL kanamycin. Polymerase chain reactions (PCR) for cloning purposes were performed with Phusion High-Fidelity DNA Polymerase (New England Biolabs) while colony PCR reactions to identify positive clones were conducted using *Taq* DNA polymerase (Fermentas). DNA isolated from agarose gels and PCR reactions were purified using the QIAquick Gel and QIAquick PCR purification kit (Qiagen), respectively. Plasmid extractions were done using the GeneJET Plasmid Miniprep Kit (Fermentas). All plasmids used or constructed in Chapter 2 are described in Table 2.1. Sequences for all primers used in Chapter 2 are reported in Table 2.2. Chemicals were obtained from Sigma-Aldrich. Mevalonate was prepared by mixing 1 volume of 2 M D,L-mevalolactone to 1.02 volumes of 2 M KOH and incubating for 30 minutes at 37°C, as previously described (Martin et al., 2003). Growth experiments presented in sections 2.3.1 to 2.3.5 were performed in M9 medium (Sambrook et al., 1989) supplemented with 1.5% yeast extract, 3% glucose and appropriate antibiotics at ½ concentration, in order to reduce the initial lag phase. Optical densities were converted to DCW using a standard curve, which determined a conversion factor of 1 OD_{600}= 0.37 g/L DCW. Experiments presented in sections 2.3.6 to 2.3.8 were done in M9 medium supplemented with 3% glucose and antibiotics at full concentration. To prepare starter cultures for testing the engineered strains, one colony was used to inoculate a 10-mL culture, which was grown overnight and adjusted to OD_{600}=1. The starter cultures were then diluted ten-fold in 50 mL of medium in 250-mL shake flasks and shaken at 200 revolutions per minute (rpm) and 37°C. When the cultures reached an OD_{600} of 0.5-0.7, they were supplemented with 10 mM mevalonate as necessary and 0.5 mM isopropyl β-D-1-thiogalactopyranoside (IPTG), unless noted otherwise.

Table 2.1 Strains and plasmids used in Chapter 2

Strain	Genotype / description	Reference
DH5α	*fhuA2* Δ*(argF-lacZ)U169 phoA glnV44 Φ80* Δ*(lacZ)M15 gyrA96 recA1 relA1 endA1 thi-1 hsdR17*	Invitrogen
BW25113	$rrnB_{T14}$ Δ$lacZ_{WJ16}$ *hsdR*514 Δ$araBAD_{AH33}$ Δ$rhaBAD_{LD78}$	(Datsenko and Wanner, 2000)
MG1655	F-λ-*ilvG-rfb*-50 *rph*-1	ATCC 700926
CC001	MG1655 + $pTDPS_o$	This study
CC002	MG1655, Δ*ispB* + $pTDPS_o$	This study
CC003	MG1655 + pALac	This study
CC004	MG1655 + pALTAA	This study
CC005	MG1655, Δ*aroK*, Δ*aroL* + pALac	This study
CC006	MG1655, Δ*aroK*, Δ*aroL* + pALTAA	This study
CC007	MG1655, *ubiC::LLACC* + pALac	This study
CC008	MG1655, *ubiC::LLACC* + pALTAA	This study
CC009	MG1655, Δ*ispB* + $pTDPS_o$ + pALac + pBBR1MCS3	This study
CC010	MG1655, Δ*ispB* + $pTDPS_o$ + pALac + pMBIS	This study
CC011	MG1655, Δ*ispB, ubiC::LLACC* + $pTDPS_o$ + pALTAA + pBBR1MCS3	This study
CC012	MG1655, Δ*ispB, ubiC::LLACC* + $pTDPS_o$ + pALTAA + pMBIS	This study
CC013	MG1655, Δ*ispB* + $pTUbiA_oDPS_o$ + pALac + pBBR1MCS3	This study
CC014	MG1655, Δ*ispB* + $pTUbiA_oDPS_o$ + pALac + pMBIS	This study
CC015	MG1655, Δ*ispB, ubiC::LLACC* + $pTUbiA_oDPS_o$ + pALTAA + pBBR1MCS3	This study
CC016	MG1655, Δ*ispB, ubiC::LLACC* + $pTUbiA_oDPS_o$ + pALTAA + pMBIS	This study
CC017	MG1655, Δ*ispB, ubiC::LLACC* + pTDPSo + pALTAA + pMBIS + pJUbiI	This study
CC018	MG1655, Δ*ispB, ubiC::LLACC* + pTDPSo + pALTAA + pMBIS + pJPK12	This study
CC019	MG1655, Δ*ispB, ubiC::LLACC*, *aroB::LTAA* + pTUbiAeDPSo + pMBIS + pMtSa	This study
CC020	MG1655, Δ*ispB*, *ubiC::LLACC*, *aroB::LTAA* + pTUbiAeDPSo + pMBIS + pMtDa	This study
CC021	MG1655, Δ*ispB* + pTUbiAoDPSo	This study
CC022	MG1655, Δ*ispB* + pTUbiAeDPSo	This study
CC023	MG1655, Δ*ispB, ubiC::LLACC*, *aroB::LTAA* + pTUbiAeDPSo + pMBIS + pMtSa	This study
Plasmid	**Description**	**Reference**
pACYC184	Low-copy expression plasmid; Tet^R, Cm^R	ATCC 37033
pALac	pACYC184 derivative containing the *lacZ* promoter; Cm^R	This study
$pALDPS_o$	pALac derivative containing DPS_o; Cm^R	This study
pTrc99A	High-copy expression plasmid; Amp^R	Pharmacia
$pTDPS_o$	pTrc99A derivative containing DPS_o; Amp^R	This study
$pTUbiA_NDPS$	pTrc99A derivative containing $ubiA_N$ (*Erythrobacter* sp. NAP1) and *DPS*; Amp^R	This study
$pTUbiA_EDPS$	pTrc99A derivative containing *ubiA* (*E. coli*) and *DPS*; Amp^R	This study
$pTUbiA_oDPS_o$	pTrc99A derivative containing $ubiA_o$ and DPS_o; Amp^R	This study

pKD4	plasmid with the RK6γ origin containing a Kan^R cassette flanked by FRT sites; Amp^R	(Datsenko and Wanner, 2000)
pKD46	plasmid with repA101(ts) origin containing *araBp-gam-bet-exo* for λ red recombibation; Amp^R	(Datsenko and Wanner, 2000)
pCP20	plamid with temperature sensitive origin of replication containing the *FLP;*Amp^R, Cm^R	(Datsenko and Wanner, 2000)
pGEM-T Easy	High-copy cloning plasmid; Amp^R	Promega
pG-TktA	pGEM-T Easy derivative containing *tktA*; Amp^R	This study
pG-AroF	pGEM-T Easy derivative containing *aroF;* Amp^R	This study
pG-AroFFBR	pGEM-T Easy derivative containing $aroF^{FBR}$; Amp^R	This study
pG-AroB	pGEM-T Easy derivative containing *aroB*; Amp^R	This study
pGFPuv	High-copy plasmid containing *lacZ*p-*GFPuv;* Amp^R	ClonTech
pUC19	High-copy cloning plasmid; Amp^R	Fermentas
pUSERGFP	pUC19 derivative containing a USER cloning cassette and *GFPuv*; Amp^R	This study
pUTAAG	pUSERGFP derivative containing *tktA, aroF*^{FBR} and *aroB;* Amp^R	This study
pALTAA	pALac derivative containing tktA, $aroF^{FBR}$ and aroB; Cm^R	This study
pALLACC	pALac derivative containing *aroL*, *aroA, aroC* and *ubiC*; Cm^R	This study
pLOI2224	plasmif with the RK6γ origin containing a Kan^R cassette and two FRT sites, for chromosomal integration of DNA; kan^R	(Martinez-Morales et al., 1999)
pBBR1MCS3	Low-copy expression plasmid; Tet^R	(Kovach et al., 1995)
pMBIS	pBBR1MCS3 derivative containing *ERG12, ERG8, MVD1, idi* and *ispA*; Tet^R	(Martin et al., 2003)
pJPK12	Medium-copy expression plasmid; Kan^R	(Peterson and Phillips, 2008)
pJUbiI	pJPK12 derivative containing ubiI; Kan^R	This study
$pTUbiAeDPS_o$	pTrc99A derivative containing $ubiA_o$ and DPS_o; Amp^R	This study
pMtSa	pBAD33 derivative containing *atoB*, *HMGS*, *SaHMGR*; Cm^R	(Ma et al., 2011)
pMtDa	pBAD33 derivative containing *atoB*, *HMGS*, *DaHMGR*; Cm^R	(Ma et al., 2011)

Table 2.2 Oligonucleotides used in Chapter 2

Primer name	5' to 3' sequence
DPSF6	CTSCTSCAYGAYGATGTG
DPSR4	GCCTTCCAGCTYGYYGAY
DPS-iPCR-F1	GAAGAACGCTACCTCACCATTATC
DPS-iPCR-R1	GTCTTCCACCATCAGTTCAAAAG
DPSF1	ATGAGCGACAACGTCGTACCAATC
DPSR1	CTAGTAGCCCCGCGCTACGGCGAATT
RBSDPSoKpnIF	ACGTGGTACCAGGAGGTAAAACATATGTCTGATAATGTGGTGCCGATTAAAC
DPSoHindIIIR	CGATAAGCTTTCAATAACCACGAGCGAC
RBSDPSBamHIF	TTAAGGATCCAGGAGGTAAAACATATGTCTGATAATGTGGTGCCGATTAAAC
DPSNotIR	GATCGCGGCCGCTCAATAACCACGAGCGACGGCAA

Primer name	5' to 3' sequence
pACYC184F	GATCATGCATGCGGCCGCACCTCGCTAACGGATTCACC
pACYC184R	GATCATGCATGGCGCGCCAATTTAACTGTGATAAACTACCGC
IspBko-F	TTGCCTTTGTTCACAGTAAGGTAATCGGGGCGAAAAGCCCGGCTTTTGCGGTGTAG GCTGGAGCTGCTTC
IspBko-R	AGCATCACTATACTCCTGATGGCCTATTGCTCTAAAAAGTTCCTGTAAAGAATGGG AATTAGCCATGGTCC
LacPAscI F	ATATGGCGCGCCCGCAACGCAATTAATGTGAGTTAGCTCA
LacP-PmeI-R1	TCCGACTGTTTAAACTGTGAAATTGTTATCCGCTCACAA
LacP-PmI-BH1-ScI-R2	GCAGGAGCTCATCGGATCCGACTGTTTAAACTGTGAAATTG
LaP-NotI-R3	TTTTCCTTTTGCGGCCGCAGGAGCTCATCGGATCCGACTG
TktAF1	GATCTGGAGTCAAAATGTCCTCA
TktAR1	TTACCCGAAATGCTAATTACAGC
AroFF2	AACTATCGCAAACGAGCATAAA
AroFR2	CGGTCAATTCAGCAACCATAATA
AroBF2	TAATTAAGGTGGATGTCGCGTTA
AroBR2	CCTTTCTTGTTACGCTGATT
AroF-PL-F1	CGACGGAAGCGTTAGATCTGAATAGCCCGCAATACC
AroF-PL-R1	GGTATTGCGGGCTATTCAGATCTAACGCTTCCGTCG
USER-GFP-F1	CTCAGCCACCGGTGTAGGAGGAAAATTATGAGTAAAGGAGAAGAACTT
USER-GFP-R1	ATTAGGCGGGCTCACCGGTGTTATTTGTACAGCTCATCCATGCCA
USER-GFP-F2	CTTAATTAAGGATCCTTAATTAAACCTCAGCCACCGGTGTAGGA
USER-GFP-R2	CGCCAAAAAAAAGCCCGCTCATTAGGCGGGCTCACCGGT
USER-GFP-F3	TGCAGGATCGGGCCGGCCGGCTGAGGCTTAATTAAGGATCCTTAATTAAACCTC
USER-GFP-R3	GTCTCTAGAGGCGCGCCAAAAAAAAGCCCGCTCA
USER-GFP-F4	GACGAGCTCGCGGCCGCCCTGCAGGATCGGGCCGGCCGGCTG
TktAUF1	GGCTTAAUCGGACCGAGGAGGAAAAATTATGTCCTCACGTAAAGAGCTTGCAATG
TktAUR1	ATCTCCUTTACAGCAGTTCTTTTGCTTTCGCA
AroFUF2	AGGAGAUAGGAGGAAAAATTATGCAAAAAGACGCGCTGAATAACGT
AroFUR2	ACCACAAGUTTAAGCCACGCGAGCCGTCAGCT
AroBUF4	ACTTGTGGUAGGAGGAAAAATTATGGAGAGGATTGTCGTTACTCT
AroBUR4	GGTTTAAUTAAGGATCCTTAATTAAGCCTCAGCTTACGCTGATTGACAATCGGCAA TG
TkTAF2	AATTAGATCTACCGAGGAGGAAAAATTATGTCCT
AroBR3	AATTGCGGCCGCCTTACGCTGATTGACAATCGGCAA
AroL F	TTAAAGATCTAGGAGGTAAAACATATGACACAACCTCTTTTTCTGATCG
AroL R	GTACCCTAGGTCAACAATTGATCGTCTGTGCCAG
AroA F	GTACTCTAGAGGAGTGAAACGATGGAATCCCTGACGTTACAACC
AroA R	GTACCCTAGGTCAGGCTGCCTGGCTAATCC
AroC F	GTACTCTAGAGGAGTGAAACGATGGCTGGAAACACAATTGGACAAC
AroC R	GTACCCTAGGTTACCAGCGTGGAATATCAGTCTTC
UbiC F	GTACTCTAGAGGAGTGAAACGATGTCACACCCCGCGTTAACG
UbiC R	GTACGCGGCCGCCCTAGGTTAGTACAACGGTGACGCCGG

Primer name	5' to 3' sequence
VisC-BHI-F	AGCTGGATCCACCGAGGAGGAAAAATTATGCAAAGTGTTGATGTAGCCATTG
VisC-Nt-R	AGGTGCGGCCGCTTAACGCAGCCATTCAGGCAAATCGTTTAATC

2.2.2 *P1 phage transduction of deleted loci and inserted operons*

Multiple gene knockouts and insertions in *E. coli* MG1655 were generated by P1 transduction (Thomason et al., 2007). To generate phage lysate from a donor strain, the latter was grown in 5 mL LB medium supplemented with 5 mM $CaCl_2$ and 0.2% glucose to OD_{600}=0.2, at which point 100 µL of P1 phage lysate (from *E. coli* MG1655) was added. The culture was shaken at 37°C and 200 rpm for 3 hours, until cell lysis. Lysate was transferred into 1.5 mL tubes to which was added 25 µL chloroform, vortexed for 30 seconds, then spun down at 16,000 x g for 1 minute. The supernatant was transferred in a new 1.5 mL tube with 15 µL chloroform and kept at 4°C. For the transduction of donor DNA into a recipient strain, the latter was grown in 5 mL LB supplemented with 5 mM $CaCl_2$ and 0.2% glucose to OD_{600}=0.8. Cells were then concentrated 4 times into LB supplemented with 5 mM $CaCl_2$ and 100 mM $MgSO_4$. A 1/10 dilution of donor phage lysate in the same medium was also prepared. In a 1.5 mL tube, 100 µL of recipient cells were mixed to 100 µL of diluted phage and incubated at 37°C for 30 minutes. The phage transduction process was then stopped by adding 200 µL 1M sodium citrate (pH=5.5). One mL of LB was added and cells were incubated at 200 rpm and 37°C for one hour, then plated on LB supplemented with 25 µg/mL kanamycin. Positive transductants were confirmed by colony PCR.

2.2.3 *Construction of cloning and expression vectors*

pALac: The pALac expression vector is derived from the low-copy plasmid pACYC184. The vector was amplified using the primers pACYC184F and pACYC184R (Table S1), which anneal to regions flanking the tetracycline resistance cassette, and carry 5'-*Nsi*I and *Not*I sites (pACYC184F) or 5'-*Nsi*I and *Asc*I sites (pACYC184R). The PCR product was digested with *Nsi*I and *Dpn*I and self-ligated, yielding pACCM. *lacZ*p was amplified from *E. coli* MG1655 by colony PCR using the primers lacPAscIF and LacPPme1R1, and then with the primers LacPPMIBHI-R2 and LacPNotIR3. The *lacZ*p cassette was then introduced into pACCM using the *Asc*I and the *Not*I sites, yielding pALac.

pG-USER-GFP: In order to create a cloning vector to assemble the upper aromatic operon by the USER method (Geu-Flores et al., 2007), I created a module flanked by *Fse*I, *Sbf*I, *Not*I and *Sac*I sites at the 5' end, and by *Asc*I and *Xba*I at the 3' end, containing a *Pac*I/*NtBbvC*I cassette, a ribosomal binding site and the coding sequence of *GFP*. This module was created by PCR using the primer pair USER-GFP-F1/USER-GFP-R1 and pGFPuv as a template. The primer pairs USER-GFP-F2/USER-GFP-R2, USER-GFP-F3/ USER-GFP-R3, and USER-GFP-F4/USER-GFP-R3 were then used in sequential overlapping PCR reactions. The cassette was digested with *Sac*I and *Xba*I and inserted into pUC19, yielding pUSER-GFP.

2.2.4 *Isolation of the dps gene from Sphingomonas baekryungensis*

Sphingomonas baekryungensis was isolated from seawater in Advocate Bay (Nova Scotia, Canada) and identified as a high producer of CoQ10 (patent

WO2008023264: Coenzyme Q10 production from marine bacteria). To isolate the *dps* gene from *S. baekryungensis*, degenerate PCR primers (DPSF6 and DPSR4) were first designed based on the conserved DPS amino acid regions LLHDDV and AFQLVD (Lee et al., 2004). A 384-bp PCR fragment was amplified from *S. baekryungensis* genomic DNA, cloned into pGEM-T Easy (Promega), and sequenced. To generate the template for inverse PCR and isolate the 5' and 3' regions of the *dps* gene, genomic DNA from *S. baekryungensis* was digested with *Nco*I, and the purified fragments were self-ligated. This template was used to amplify a 2.5-kb fragment containing the 5' and 3' ends of the *S. baekryungensis dps* gene, using primers DPS-iPCR-F1 and DPS-iPC-R1, designed based on the 384-bp $dps_{S.bae}$ internal fragment. The entire coding sequence of $dps_{S.bae}$ was then amplified using the primers DPSF1 and DPSR1. A synthetic version of the $dps_{S.bae}$ gene was codon-optimized for *E. coli* by GeneScript, yielding dps_o. The synthetic gene was amplified using the primers RBSDPSoKpnIF and DPSoHindIIIR, adding an optimized RBS (Ringquist et al., 1992) at the 5' end, and cloned into pTrc99A, yielding $pTDPS_o$ (Figure 1B). The dps_o gene was also amplified with the primers RBSDPSBamHIF and DPSNotIR, introducing an optimized RBS at the 5' end, then cloned into pALac, yielding $pALDPS_o$.

2.2.5 *Deletion of ispB from E. coli*

To minimize the production of CoQ8, the *ispB* gene was deleted from the chromosome of *E. coli* using lambda Red recombination (Datsenko and Wanner, 2000). A 1597-bp deletion cassette was amplified using primers IspBkoF and IspBkoR, and the plasmid pKD4 as a template. The reactions were treated with *Dpn*I, and dialyzed using a

0.025 µm disc (Millipore). Cells of *E. coli* BW25113 harboring pKD46 and pALDPS$_o$ that were previously grown on LB containing L-arabinose (1 mM), were electroporated using ~475 ng of the purified DNA cassette. The Δ*ispB::*kan locus was transferred to MG1655 harboring pTDPS$_o$ by P1 transduction. The kanamycin marker flanked by FRT sites was removed using the helper plasmid pCP20, as previously described (Datsenko and Wanner, 2000).

2.2.6 *Isolation of the ubiA gene from Erythrobacter sp. NAP1*

The amino acid sequence of the PHB decaprenyl transferase (UbiA) from *Erythrobacter* sp. NAP1 was retrieved from GenBank (EAQ29552.1). The corresponding coding sequence was codon-optimized for *E. coli* and synthesized by DNA2.0, yielding *ubiA$_o$*. The optimized gene and an optimized ribosomal binding site (Ringquist et al., 1992) were inserted into pTDPS$_o$ using *Eco*RI and *Kpn*I, upstream of *dps$_o$*, yielding pTUbiA$_o$DPS$_o$ (Figure 1B).

2.2.7 *Construction of the synthetic aromatic pathway operons*

The coding regions of *tktA*, *aroF* and *aroB* were amplified from MG1655 genomic DNA using the primer pairs TktAF1/TktAR1, AroFF2/AroFR2 and AroBF2/AroBR2, respectively, then cloned into pGEM-T Easy, yielding pG-TktA, pG-AroF and pG-AroB. The primers AroF-PL-F1 and AroF-PL-R1 were used to introduce the base pair modification (C444T) required to introduce Pro (148) →Leu mutation in AroF^{FBR} (Weaver and Herrmann, 1990). The resulting pG-AroF^{FBR} was further modified by site-directed mutagenesis using the primers AroF-T327C-F and AroF-T327C-R, in

order to remove a *Pac*I recognition site. For USER cloning (Geu-Flores et al., 2007), *tktA* was amplified using *PfuTurbo* Cx hotstart DNA polymerase (Agilent Technologies) from pG-TktA using the primers TktAUF1/TktAUR1, $aroF^{FBR}$ from pG-AroF^{FBR} with the primers AroFUF2/AroFUR2, and *aroB* from pG-AroB with the primers AroBUF4/AroBUR4. The fragments were *Dpn*I-treated, purified and mixed with pUSER-GFP pre-digested with *Pac*I and *Nt.Bbv*CI, as well as one unit of USER enzyme. After 20 minutes at 37°C and 20 minutes at 25°C, the whole reaction was transformed into *E. coli*, yielding plasmid pUTAAG. The *tktA*-$aroF^{FBR}$-*aroB* operon was amplified from pUTAAG using the primers TktAF2 and AroBR3, and then cloned into pALac, yielding pALTAA (Figure 1B). The coding regions of *aroL*, *aroA*, *aroC* and *ubiC* were amplified from MG1655 genomic DNA using the primer pairs AroLF/AroLR, AroAF/AroAR, AroCF/AroCR and UbiCF/UbiCR, respectively. The operon was built by iterative digestion, ligation, and amplification of the ligated coding regions. Briefly, the amplified coding region of *aroL* was digested with *Avr*II at the 3' end while the amplified coding region of *aroA* was digested with *Xba*I at the 5' end. The two digested products were then ligated, which destroyed both the *Avr*II and *Xba*I sites, and subsequently amplified with AroLF and AroAR. The same procedure was repeated for the addition of the amplified *aroC* and *ubiC* to the operon. Once the entire operon was constructed, it was digested with *Bgl*II and *Not*I and then cloned into *Bam*HI-*Not*I-digested pALac, yielding pALLACC.

2.2.8 *Construction of pJUbiI*

The open reading frame of the *ubiI* locus was amplified from the chromosome of *E. coli* by colony PCR, using primers VisC-BHI-F and VisC-Nt-R, adding a *Bam*HI site and a *Not*I site at the 5' and 3' end, respectively. The PCR product was purified, then digested with *Bam*HI and *Not*I and cloned into the plasmid pALac, downstream of the *lacZ* promoter. After the identity of the coding sequence was verified by Sanger sequencing, the *lacZ*p:*ubiI* cassette was excised using *Hind*III/*Not*I and inserted into the low-copy expression vector, pJPK12, yielding pJUbiI.

2.2.9 *Integration of the synthetic aromatic operons on the chromosome of E. coli*

The *LacZp*:*tktA-aroF*^{FBR}*-aroB* and the *LacZp*:*aroL-aroA-aroC-ubiC* operons were integrated on the chromosome of *E. coli* at the *aroB* and *ubiC* loci, respectively, by homologous recombination using the method of Martinez-Morales (1999). A GFP cassette flanked by *Not*I and *Asc*I sites was first cloned at the *Not*I site of pALTAA and pALLACC, and allowed the excision of *Asc*I-flanked fragments. Each operon was cloned into the *Asc*I site of pLOI2224, yielding p24LTAA and p24LLACC. The plasmid p24LTAA was subsequently electroporated into MG1655 Δ*tktA, ΔaroF*, and p24LLACC into MG1655 Δ*aroL, ΔaroA*, *ΔaroC,* yielding *aroB*::LTAA-kan and *ubiC*::LLACC-kan. The *ubiC::*LLACC-kan locus was transferred into MG1655, and the kanamycin cassette excised using pCP20, yielding MG1655 *ubiC*::LLACC. The *aroB*::LTAA-kan locus was transferred into MG1655 *ubiC*::LLACC by P1 transduction, and the kanamycin cassette excised using pCP20, yielding MG1655 *ubiC*::LLACC*, aroB*::LTAA.

2.2.10 *Analysis of shikimic acid and PHB from culture supernatants*

For HPLC analysis of shikimic acid and PHB from culture supernatants, one-mL aliquots from *E. coli* cultures were centrifuged at 16,100 x g to remove the cells. The supernatant was filtered using a 13 mm 0.2 µM nylon filter (Acrodisc, VWR), and 10 µL was injected into a 1200 Series HPLC system (Agilent technologies) equipped with an Aminex HPX-87H column (Bio-Rad) heated to 65°C. Shikimic acid was resolved using 0.1% trifluoroacetic acid at a flow rate of 0.6 mL/minute and detected with a 1200 Series UV/Vis diode array detector (Agilent Technologies) at 215 nm. PHB was resolved using 0.1% trifluoroacetic acid and 15% acetonitrile at a flow rate of 0.6 mL/minute and detected at 254 nm. Shikimic acid and PHB were quantified using standard curves of authentic standards.

2.2.11 *Quinone extraction and analysis*

To analyze cellular quinone content, cells from one-mL aliquots of *E. coli* cultures were harvested at 16,100 x g prior to quinone extraction. The pelleted cells were washed with 1 mL of 50 mM Tris-HCl pH 7.5, and re-suspended in 450 µL Cell Lytic B (Sigma-Aldrich). After 30 minutes at room temperature, a first extraction was performed with 900 µL of hexane:2-propanol (5:3). The upper phase was transferred into a new tube and a second extraction was done using 500 µL of hexane. The combined extracts were dried under an air stream, and re-suspended in 50 µL acetone. A 10-µL aliquot was injected into a 1200 Series HPLC system equipped with a ZORBAX Eclipse XDB-C18 (4.6 x 150 mm, 5 µm, Agilent technologies). The mobile phase consisted of acetonitrile (A) and ethanol (B), ran at 0.5 mL/minute with the following elution profile: 0-5 minutes,

40% B; 5-18 minutes, 40%-100% B; 18-32 minutes, 100% B. The quinones were detected at 275 nm. CoQ10 was quantified using a standard curve of an authentic standard. For identification by LC-MS-MS, the extracted quinones were separated by HPLC as described above, except that the mobile phase was acidified with 0.1% formic acid and 10 μM ammonium formate. The HPLC eluent was then channeled to a Quattro LC triple quadrupole mass spectrometer (Waters) with electrospray ionization in the positive mode. The source block temperature was set to 80 °C, the disolvation temperature to 200 °C, and a voltage of 3.5 kV was applied to the electrospray needle. Nitrogen was used as the nebulizer, disolvation, and collision gas. The precursor ions were manually selected and directed to the collision cell where they were fragmented with 30 kV or 40kV of collision energy, depending on the metabolite. The identity of 10P-Ph was confirmed by LC-MS-MS on a LTQ Orbitrap Velos MS (Thermo Electron). The mass spectrometer was equipped with a heated-electrospray ionization source, which was operated in positive ion mode with a source voltage of 3.0 kV and a capillary temperature of 380 °C, and the spectra were recorded at a normalized collision energy of 25 with pulsed-Q dissociation.

2.3 **Results**

2.3.1 *Cloning and functional expression of a dps in E. coli*

Ocean Nutrition Canada has established a vast collection of marine microbes, isolated from sea water, sediments and sea weeds collected from Advocate Bay, Nova Scotia. The marine bacterium *S. baekryungensis* was identified in a screen for high producers of CoQ10. Analysis of its quinone profile also revealed negligible amounts of

shorter quinone species such as CoQ9 (Figure 2.2). Since previous studies have shown that the chain length of CoQn species is dictated by the polyprenyl synthase (Okada et al., 1996), I hypothesized that the DPS expressed by this species had higher stringency for DPP compared to other CoQ10 producers who also produce shorter coenzyme species (Okada et al., 1998; Park et al., 2005; Takahashi et al., 2003; Zahiri et al., 2006a).

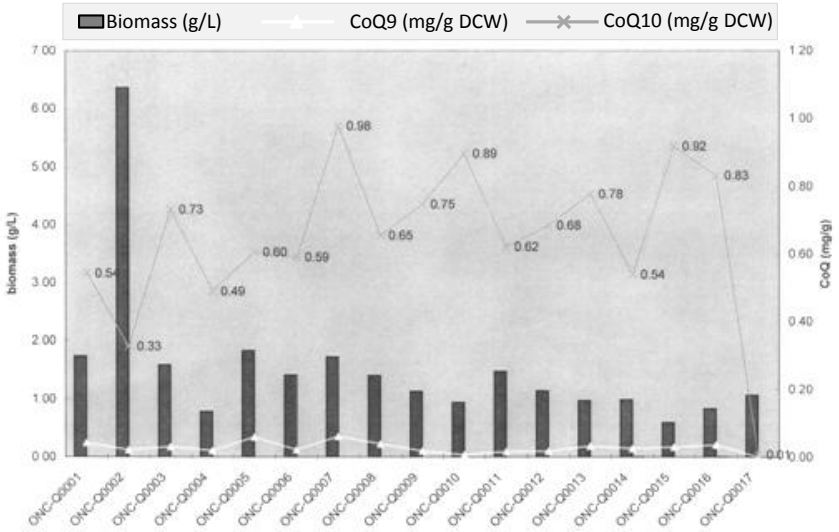

Figure 2.2 Screen of marine bacteria for high CoQ10 content.
Strain ONC-Q0010 was identified as *Sphingomonas baekryungensis*. Data graciously provided by Ocean Nutrition Canada.

In order to engineer a strain highly enriched in CoQ10, I isolated the open-reading frame of a putative *dps* ($dps_{S.bae}$) from *S. baekryungensis*. As detailed in section 2.2.4, this was done using degenerate primers designed to anneal the coding sequence of a highly conserved motif characterizing long-chain prenyl diphosphate synthases. The amino acid sequence of $DPS_{S.bae}$ was deducted and aligned with previously characterized DPS proteins. This revealed that the putative $DPS_{S.bae}$ shared several conserved domains with other DPS's. Amino acids at the 8th, 5th and 4th position before the first aspartate-rich motif (FARM) determine the chain length of the product of the prenyl disphosphate

synthase (Wang and Ohnuma, 2000). Enzymes that make short products, such as geranylgeranyl diphosphate synthases have large amino acids, while enzymes that make longer products (C_{30}-C_{50}) contain short amino acids at these positions, such as alanine, threonine and isoleucine, which were found in $DPS_{S.bae}$ and conserved in DPS enzymes of other species (Figure 2.3).

Figure 2.3 Multiple alignment of DPS proteins from *S. baekryungensis* and other representative microbial species

The amino acid sequence the $DPS_{S.bae}$ from *S. baekryungensis* was deducted from the sequenced open-reading frame. The amino acid sequences of the other DPS proteins were obtained from GenBank. The alignment was done using Clustal W2. Stars indicate conserved residues among all species. The conserved FARM motifs are framed. The arrows indicate the 4th, 5th and 8th residues preceding the first FARM motif.

The nucleotide sequence of $DPS_{S.bae}$ was codon-optimized (dps_o) in order to improve expression and the activity of DPS_o was confirmed by the accumulation of CoQ10, in addition to CoQ8, in *E. coli* MG1655 transformed with $pTDPS_o$ (Figure 2.4B, strain CC001). In order to exclusively produce CoQ10, the *ispB* gene was deleted and complemented by dps_o, yielding CC002. When comparing the quinone profile of the *ΔispB* strain CC002 with that of a control strain (MG1655 + pTrc99A), I observed that while the control exclusively produced octaprenyl quinones (CoQ8 and menaquinone-8), CC002 produced the decaprenyl quinones CoQ10 and menaquinone-10, as well as longer CoQ11 (Figure 2.4B and C). Although some CoQ9 was found in cells expressing both *ispB* and dps_o (strain CC001, Figure 2.4B), I did not observe detectable amounts of CoQ9 in CC002 (Figure 2.4C).

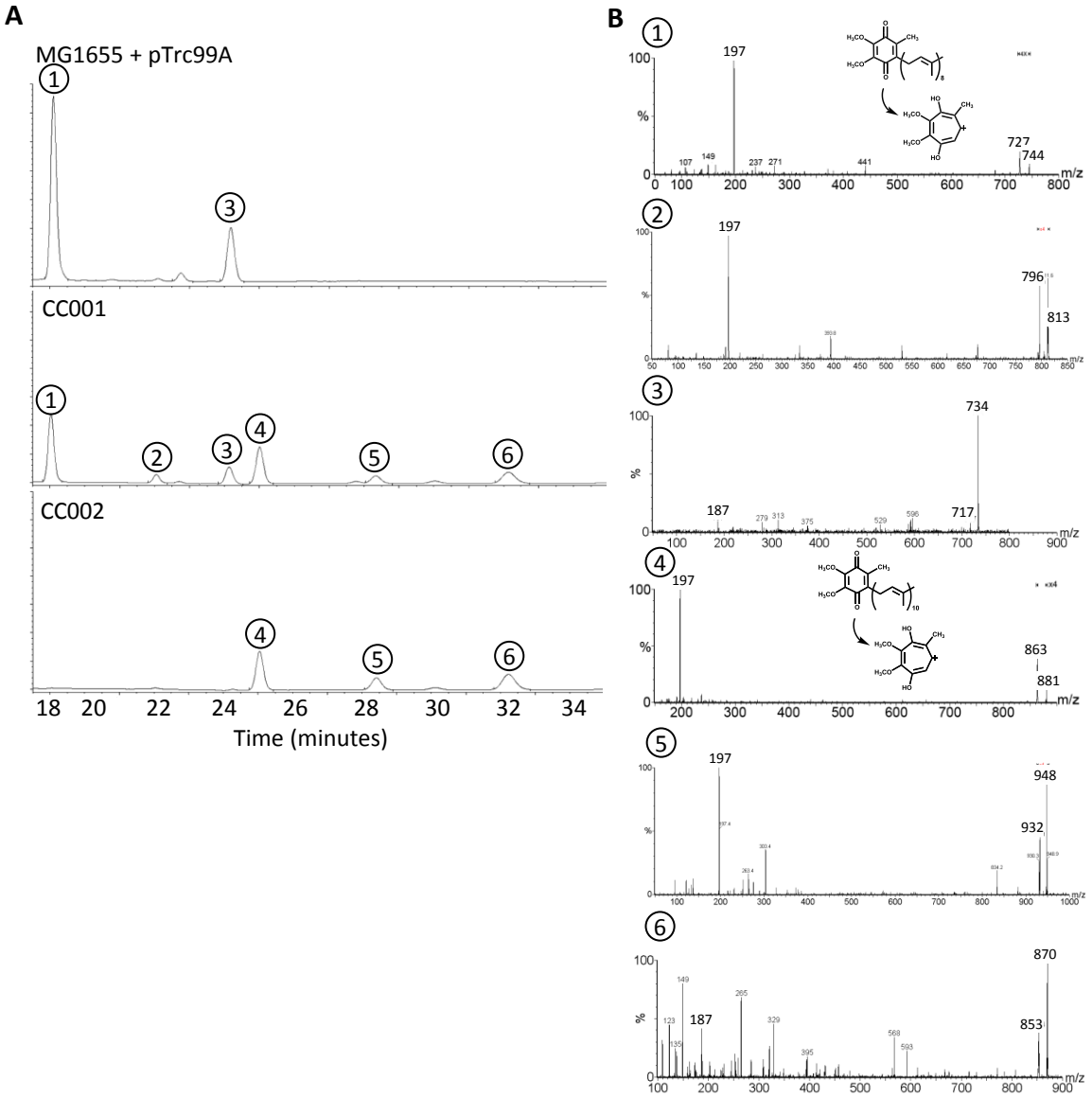

Figure 2.4 Quinone profile and identification from recombinant *E. coli* strains
A) HPLC chromatogram of extracted quinones from MG1655+pTrc99A, CC001 and CC002. Labelled peaks were identified by LC-MS-MS, and are shown in **B)** Peak 1: MS-MS spectrum of CoQ8, ammonium adduct $[M+NH_4]^+$ ($C_{49}H_{78}O_4N^+$; exact mass 744.6), protonated adduct $[M+H]^+$ ($C_{49}H_{75}O_4^+$; exact mass 727.7), and tropylium ion $[M]^+$ ($C_{10}H_{13}O_4^+$, exact mass 197.1). Peak 2: MS-MS spectrum of CoQ9, ammonium adduct $[M+NH_4]^+$ ($C_{54}H_{85}O_4N^+$; exact mass 812.6), protonated adduct $[M+H]^+$ ($C_{54}H_{83}O_4^+$; exact mass 795.6), and tropylium ion $[M]^+$ ($C_{10}H_{13}O_4^+$, exact mass 197.1). Peak 3: MS-MS spectrum of menaquinone-8, ammonium adduct $[M+NH_4]^+$ ($C_{51}H_{76}O_2N^+$; exact mass 734.6), protonated adduct $[M+H]^+$ ($C_{51}H_{73}O_2^+$; exact mass 717.6), and tropylium ion $[M]^+$ ($C_{12}H_{11}O_2^+$, exact mass 187.1). Peak 4: MS-MS spectrum of CoQ10, ammonium adduct $[M+NH_4]^+$ ($C_{59}H_{94}O_4N^+$; exact mass 880.7), protonated adduct $[M+H]^+$ ($C_{59}H_{91}O_4^+$; exact mass 863.7), and tropylium ion $[M]^+$ ($C_{10}H_{13}O_4$+, exact mass 197.1). Peak 5: MS-MS spectrum of CoQ11, ammonium adduct $[M+NH_4]^+$ ($C_{64}H_{102}O_4N^+$; exact mass 948.7), protonated adduct $[M+H]^+$ ($C_{64}H_{99}O_4^+$; exact mass 931.7), and tropylium ion $[M]^+$ ($C_{10}H_{13}O_4^+$, exact mass 197.1). Peak 6: MS-MS spectrum of menaquinone-10, ammonium

adduct $[M+NH_4]^+$ ($C_{61}H_{92}O_2N^+$; exact mass 870.7), protonated adduct $[M+H]^+$ ($C_{61}H_{89}O_2^+$; exact mass 853.7), and tropylium ion $[M]^+$ ($C_{12}H_{11}O_2^+$, exact mass 187.1).

2.3.2 *Deregulation of PHB biosynthesis*

The benzoic head of CoQ10 is derived from the shikimate pathway leading to the biosynthesis of chorismate, which is then converted to PHB by the chorismate lyase, UbiC (Figure 2.1A). The overexpression of the rate-limiting enzymes of the shikimate pathway, along with UbiC, allows for the production of high PHB titers in *E. coli* (Barker and Frost, 2001). Based on this strategy, I created two synthetic operons, referred to as the upper and lower aromatic operons, aimed at increasing the expression of selected genes coding for enzymes of the PHB pathway (Figure 2.1B).

The upper aromatic operon, designed to increase the production of shikimate, comprises the genes coding for TktA, a feedback resistant AroF ($AroF^{FBR}$), and AroB, driven by the *lacZ* promoter (Figure 2.1B). $AroF^{FBR}$ is a mutated version of AroF, made insensitive to feedback inhibition by tyrosine via a single proline-to-leucine modification (Weaver and Herrmann, 1990). I tested the functionality of the upper aromatic operon by following the accumulation of shikimic acid over time in MG1655 harboring pALTAA (CC004). Strain CC004 secreted 0.7 mM of shikimic acid (Figure 2.5A). To prevent the rapid conversion of shikimate to downstream aromatic intermediates, and get a better estimate of shikimate production, I expressed pALTAA in *E. coli* MG1655 Δ*aroK*Δ*aroL*, a strain deficient in shikimate kinase activity, yielding CC006. Using this genetic background, the production of shikimate increased 21-fold compared to the control CC005 (MG1655 Δ*aroK*Δ*aroL*, pALac) and 2.5-fold compared to CC006, leading to the

excretion of 1.7mM shikimic acid (Figure 2.4A). The expression of the upper operon alone in CC004 resulted in the accumulation of 0.05 mM of PHB (Figure 2.5C).

The lower aromatic operon (LACC) includes the genes coding for AroL, AroA, AroC, and UbiC. The expression of these four enzymes leads to the conversion of shikimate to PHB (Figure 2.1A). The lower operon was placed under the control of *lacZ*p, and integrated on the chromosome downstream of the *ubiC* locus (*ubiC*::LLACC, Figure 2.1B) of CC003 and CC004, yielding CC007 and CC008, respectively. I did not observe an increase in PHB productivity in CC007, expressing solely the lower aromatic operon, indicating that availability of shikimate is limiting for PHB biosynthesis (Figure 2.5C). However, CC008, expressing both upper and the lower operons, produced over 0.4 mM of PHB, representing a 220-fold increase compared to the control CC003 , and a 25% yield from shikimate (Figure 2.5C). No residual shikimate was detected in the media of CC008, suggesting that the fraction of shikimate that was not converted to PHB was channeled to other aromatic molecules.

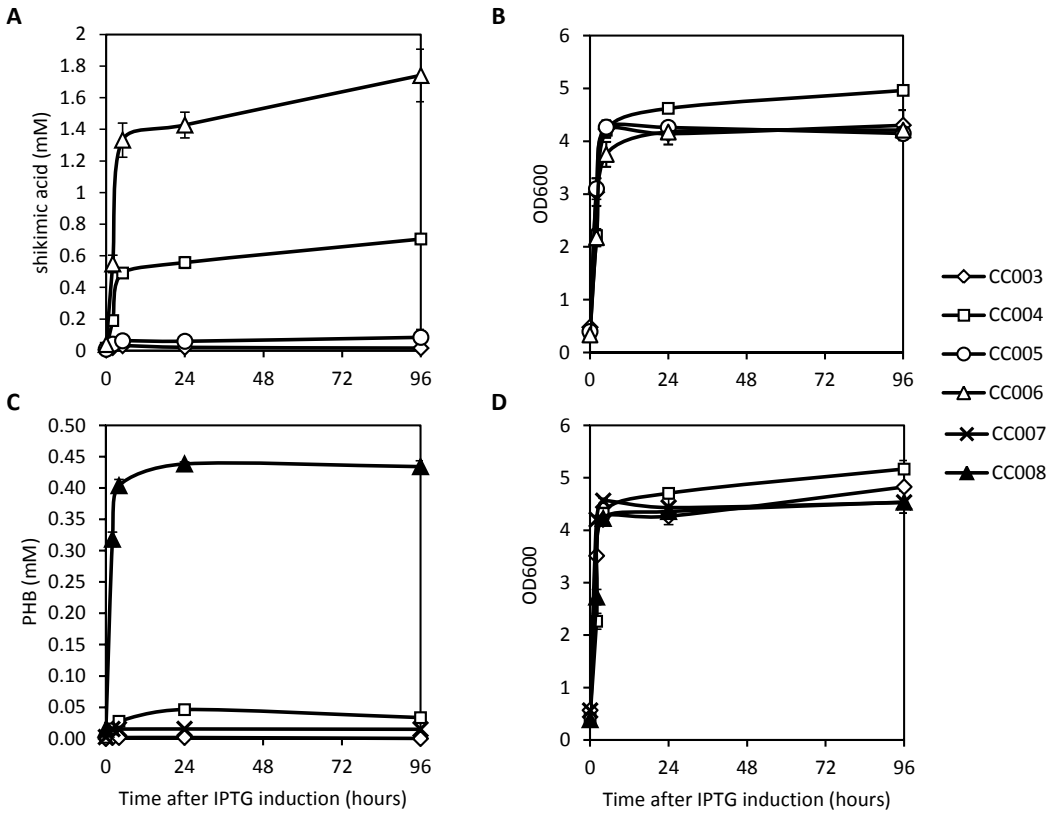

Figure 2.5 Production of aromatic intermediates following the expression of the upper and lower synthetic aromatic pathway operons
Tested strains were grown to exponential phase, and induced with 0.5 mM IPTG. Samples were taken at 0, 4, 24, and 96 hours after induction. Strains CC003, CC004, CC005 and CC006 were compared for A) secretion of shikimic acid in the growth medium B) optical density. Strains CC003, CC004, CC007 and CC008 were compared for C) secretion of PHB in the growth medium D) optical density. Error bars show the standard deviation for two biological replicates.

2.3.3 *Assessment of CoQ10 production following the overexpression of PHB and/or FPP biosynthetic pathways*

As the availability of PHB limits the carbon flux toward ubiquinone biosynthesis (Zahiri et al., 2006b; Zhu et al., 1995), I hypothesized that a deregulation of PHB biosynthesis would translate into higher production of CoQ10 in an engineered *E. coli* strain. The upper and lower aromatic operons were introduced into the CoQ10-producing strain CC002, yielding CC011, and CoQ10 production was followed over time. Strain CC009, expressing pTDPS$_o$ in a Δ*ispB* background, as well as empty vectors, was used as

a control in order to determine basal production levels of CoQ10, when the biosynthesis of precursors is endogenously regulated. As shown in Figure 2.6A, CC011 produced up to 0.24 mg/g DCW of CoQ10, corresponding to a 1.3-fold increase compared to the control CC009. In addition, CC011 produced 0.09 mM of PHB (Figure 2.6C), a four-fold decrease compared to CC008 (Figure 2.5C).

In addition to aromatic precursors, the biosynthesis of CoQ10 in recombinant *E. coli* is limited by the availability of DPP for the prenylation of PHB (Choi et al., 2009; Kim et al., 2006; Zahiri et al., 2006b). DPP is formed by the successive condensation of IPP with FPP (Wang and Ohnuma, 2000). In *E. coli*, the biosynthesis of these isoprenoid molecules can be dramatically increased by the heterologous expression in *E. coli* of the typically eukaryotic mevalonate pathway (Martin et al., 2003). The pMBIS plasmid harbors the lower mevalonate operon, which enables the conversion of mevalonate into IPP, DMAPP and FPP (Figure 2.1A, B). The expression of pMBIS results in significant increases in the production of FPP and IPP in the presence of exogenously supplied mevalonate (Martin et al., 2003). In order to increase the availability of FPP for CoQ10 biosynthesis, I transformed pMBIS into CC002, yielding CC010. The expression of the lower mevalonate pathway in CC010 resulted in a 2-fold increase in CoQ10 content (0.33 mg/g DCW) over the control CC09 (Figure 2.6A).

I then hypothesized that an even greater increase in CoQ10 production would be observed if both the PHB and the isoprenoid pathways were over-expressed in the same strain. The engineered aromatic and lower mevalonate pathways were introduced in strain CC002, resulting in strain CC012, and the latter was tested for CoQ10 production. As shown by Figure 2.6C, CC012 reached a CoQ10 content of 0.43 mg/g DCW, a 2.6-fold

increase over the control CC009. This demonstrates that both aromatic and isoprenoid precursors are rate-limiting for CoQ10 biosynthesis and that both of these pathways can be simultaneously engineered in *E. coli* to produce high CoQ10-producing strain without the need for feeding the PHB precursor. Only a slight difference was observed in PHB accumulation between CC012 and CC011 (Figure 2.5B).

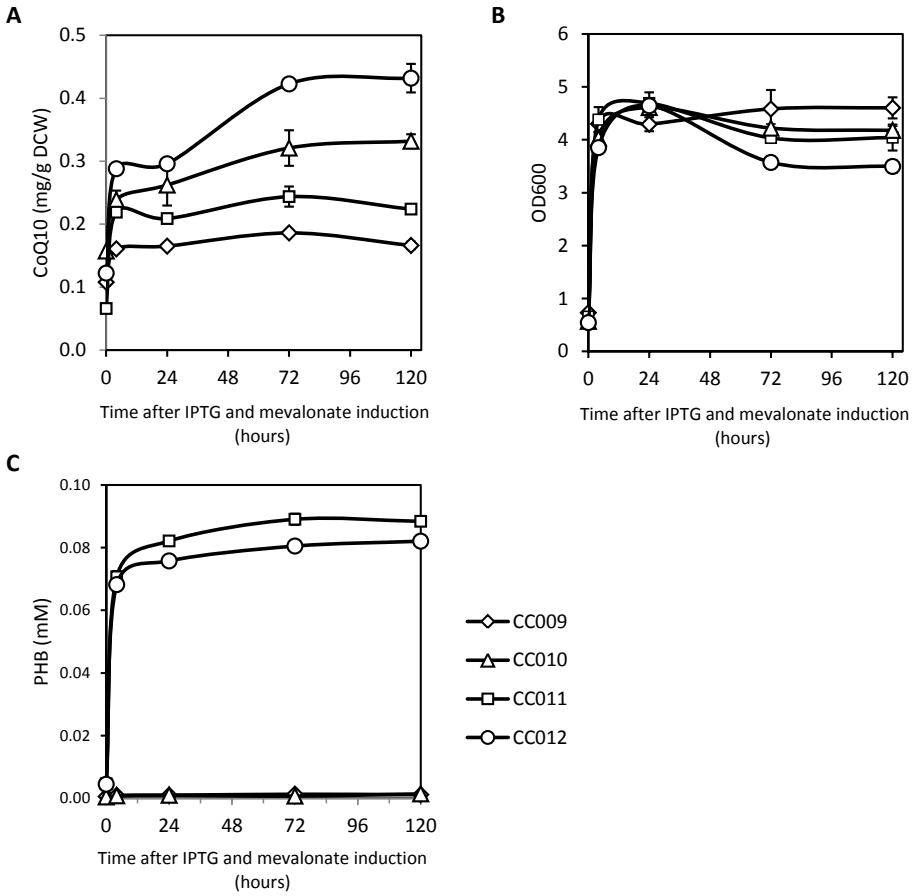

Figure 2.6 Production of CoQ10 and PHB in strains expressing the synthetic aromatic operons and/or the bottom mevalonate operon.
Strains CC009 (diamonds), CC010 (triangles), CC011 (squares) and CC012 (circles) were grown for five days. Cultures were induced during exponential phase with 0.5 mM IPTG and 10 mM mevalonate. Samples were taken at 0, 4, 24, 72 and 120 hours after induction in order to measure **A**) CoQ10 production **B**) optical density **C**) extracellular PHB. Error bars represent the standard deviation of two biological replicates.

In addition to its increased CoQ10 content, CC012 had elevated concentrations of an unknown molecule, which eluted one minute before CoQ10 on the HPLC

chromatogram (Figure 2.7A). Analysis of this unknown compound by LC-MS-MS revealed a precursor ion at m/z=792.7828 and a product ion at m/z=107.0493 (Figure 2.7C), characteristic of the ammonium adduct $[M+NH_4]^+$ and the tropylium ion $[M]^+$, respectively, derived from the CoQ10 intermediate, 2-decaprenylphenol (10P-Ph) (Cox et al., 1969; Hsu et al., 1996; Matsumura et al., 1983). 10P-Ph is the second intermediate of the ubiquinone pathway, formed by the hydroxylation of 3-decaprenyl-4-hydroxybenzoate (10P-HB) (Figure 2.1A) (Alexander and Young, 1978). Although the lack of an analytical standard precluded the quantification of this compound, a comparison of its relative abundance between different strains revealed that CC012 accumulated 14 times more 10P-Ph than CC010, while CC011 and CC009 did not accumulate detectable levels of this intermediate (Figure 2.7B).

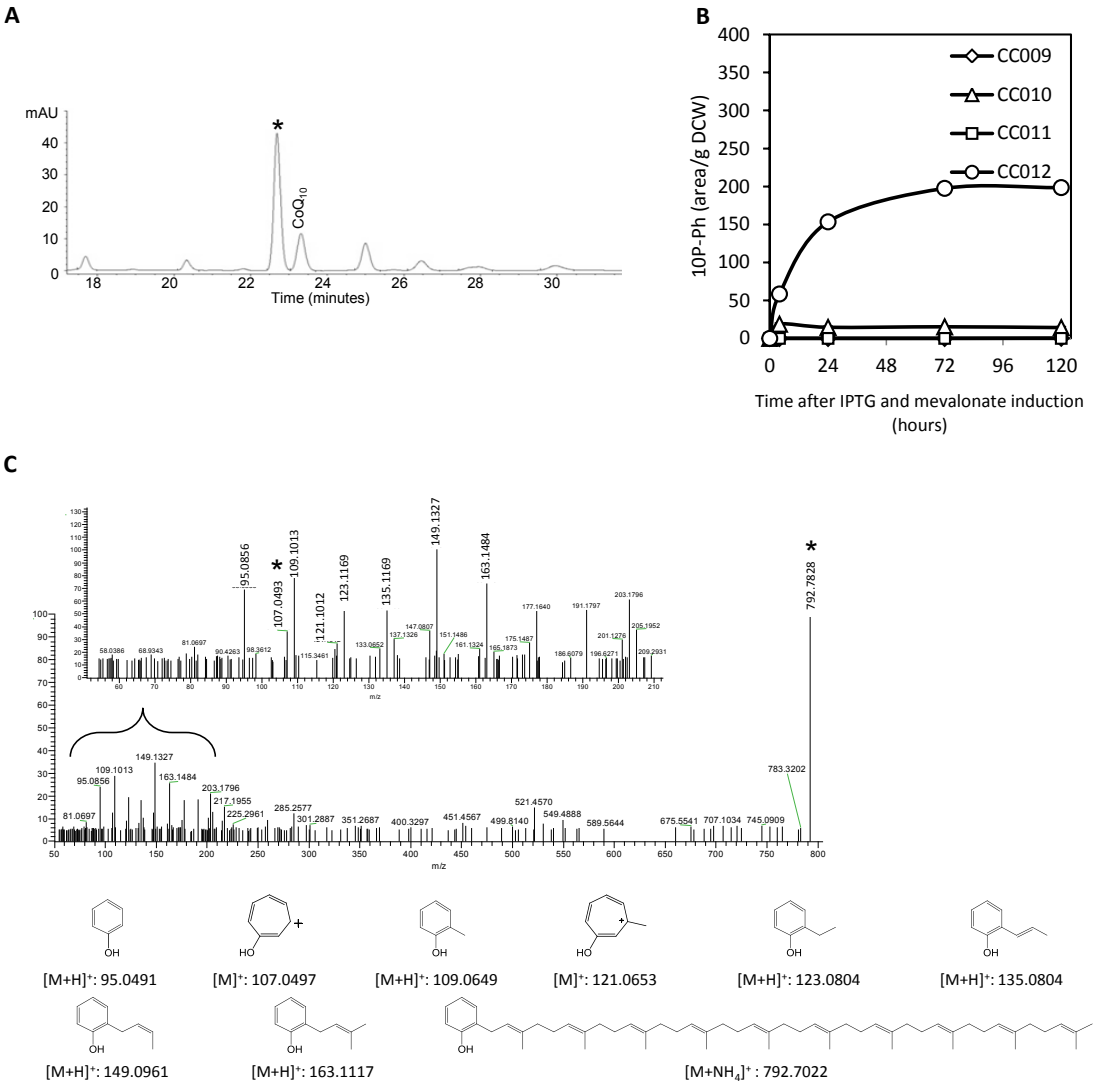

Figure 2.7 Identification and accumulation pattern of 10-Ph following the expression of the synthetic aromatic operons and of the bottom mevalonate operon.

The production of a ubiquinone pathway intermediate, 10P-Ph, was characterized. **A**) HPLC chromatogram of extracted quinones from CC012, 24 hours after induction with 0.5 mM IPTG and 10 mM mevalonate. The 10P-Ph peak is labelled with a star. **B**) Time-course of 10P-Ph production in strains CC009 (diamonds), CC010 (triangles), CC011 (squares) and CC012 (circles). Error bars represent the standard deviation of two biological replicates **C**) LC-MS-MS spectrum of 10P-Ph. The most abundant product ions identified from the MS-MS are illustrated below the spectra. In particular, the fragmented precursor ion yielded an ammonium adduct $[M+NH_4]^+$ ($C_{56}H_{90}ON^+$, exact mass 792.7022) and a tropiclium ion $[M]^+$ ($C_7H_7O^+$, exact mass 107.0497), both labelled by a star.

2.3.4 *Overexpression of a PHB decaprenyltransferase from Erythrobacter sp. NAP1*

Although I observed an increase in CoQ10 production following the overexpression of both the aromatic and the lower mevalonate pathways in CC012, I found that PHB accumulation levels by the latter and by CC011 were almost similar (Figure 2.6C). The entry of PHB and DPP into the ubiquinone pathway is catalyzed by the PHB prenyltransferase, UbiA, condensing DPP to PHB to form 10P-HB (Figure 2.1A). It is possible that the limited flux of PHB towards the ubiquinone pathway in CC012 reflects a bottleneck at the PHB prenylation step carried out by UbiA. I hypothesized that microorganisms naturally accumulating high levels of CoQ10 might express PHB prenyltransferases of increased efficiency. Preliminary experiments showed that expression of the PHB prenyltransferase from *Erythrobacter* sp. NAP1 (via pTUbiA$_N$DPS) restored growth defects associated with the production of high levels of IPP/DMAPP and FPP (via pMBIS), suggesting that this orthologue of UbiA was capable of pulling toxic isoprenoid intermediates down the ubiquinone pathway more efficiently than *E. coli*'s UbiA (via pTUbiA$_e$DPS) (Figure 2.8).

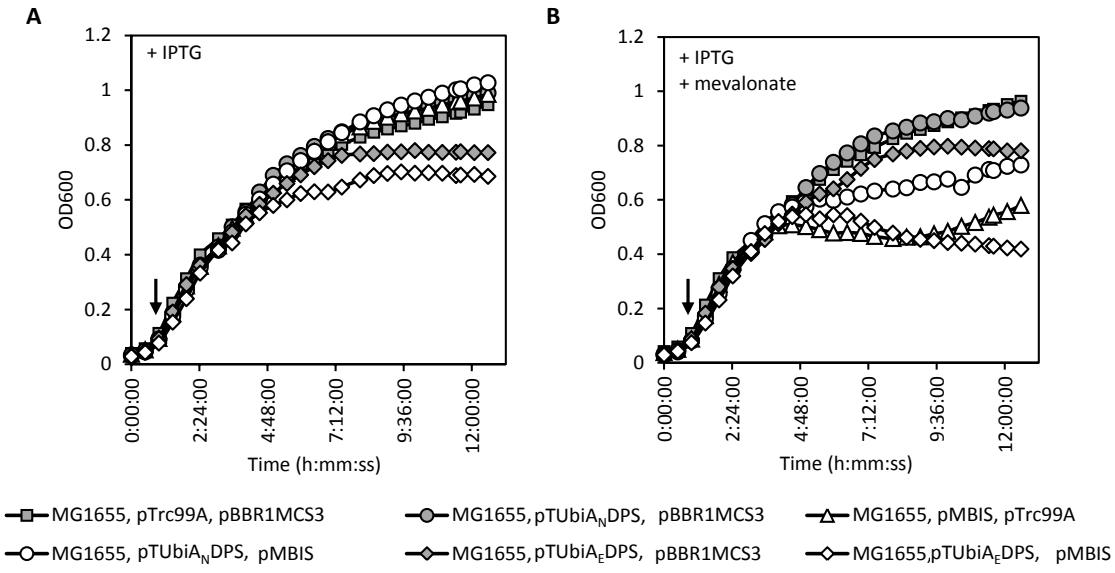

Figure 2.8 Effect of PHB prenyltransferase variants on growth of *E. coli* strains harboring pMBIS.
The following strains were grown in replicate (N=6) in a 96-well plate incubated in a microtiter plate reader with continuous shaking: MG1655, pTrc99A, pBBR1MCS3 (grey squares); MG1655, ptrc99A, pMBIS (white triangles); MG1655, pTUbiA$_N$DPS, pBBR1MCS3 (grey circles); MG1655, pTUbiA$_e$DPS, pBBR1MCS3 (grey diamonds); MG1655, pTUbiA$_N$DPS, pMBIS (white circles); MG1655, pTUbiA$_e$DPS, pMBIS (white diamonds). After one hour, triplicate cultures of each strain were induced with **A)** 0.5 mM IPTG or B) 0.5 mM IPTG and 10 mM mevalonate, as indicated by the arrow. Optical densities were measured automatically by the plate reader. Values show the average of triplicates. Data graciously provided by A. Ekins.

In order to overcome a potential bottleneck at the PHB prenylation step in my engineered *E. coli* strains, I expressed a codon-optimized version of *ubiA* (*ubiA$_o$*) that was isolated from the CoQ10-producing marine bacterium *Erythrobacter* sp. NAP1 (Figure 2.1B). The plasmid pTUbiA$_o$DPS$_o$ was expressed in a Δ*ispB* background along with empty vectors (CC013), the bottom mevalonate pathway (CC014), the aromatic operons (CC015), or both the bottom mevalonate and aromatic operons (CC016) (Table 2.1).

The heterologous expression of *ubiA$_o$* in CC013, CC014, CC015, and CC016 was associated with an extended initial lag phase and with reduced growth (Figure 2.9B). Extracellular PHB was 2.6-times lower in CC016 cultures compared to CC012 (Figure

2.9D). However, taking into consideration lower cell density in CC016 cultures, PHB secretion was in fact comparable between the two strains, with 0.04 mmol/g DCW PHB produced by CC016 and 0.05 mmol/g DCW by CC012. Consistent with the hypothesis that the overexpression of $UbiA_o$ favors the production of CoQ10 when high concentrations of aromatic and isoprenoid precursors are available, CC016 achieved the highest CoQ10 content amongst the strains tested. As shown by Figure 2.9A, CC016 produced up to 0.58 mg/g DCW of CoQ10, compared to 0.37 mg/g DCW for CC012 (Figure 2.9A). In contrast to its higher CoQ10 content, CC016 produced 2.8-fold less 10P-Ph than CC012 (Figure 2.9C). This suggests that the overexpression of $UbiA_o$ reduces the accumulation of 10P-Ph in CC016, and favors the accumulation of CoQ10.

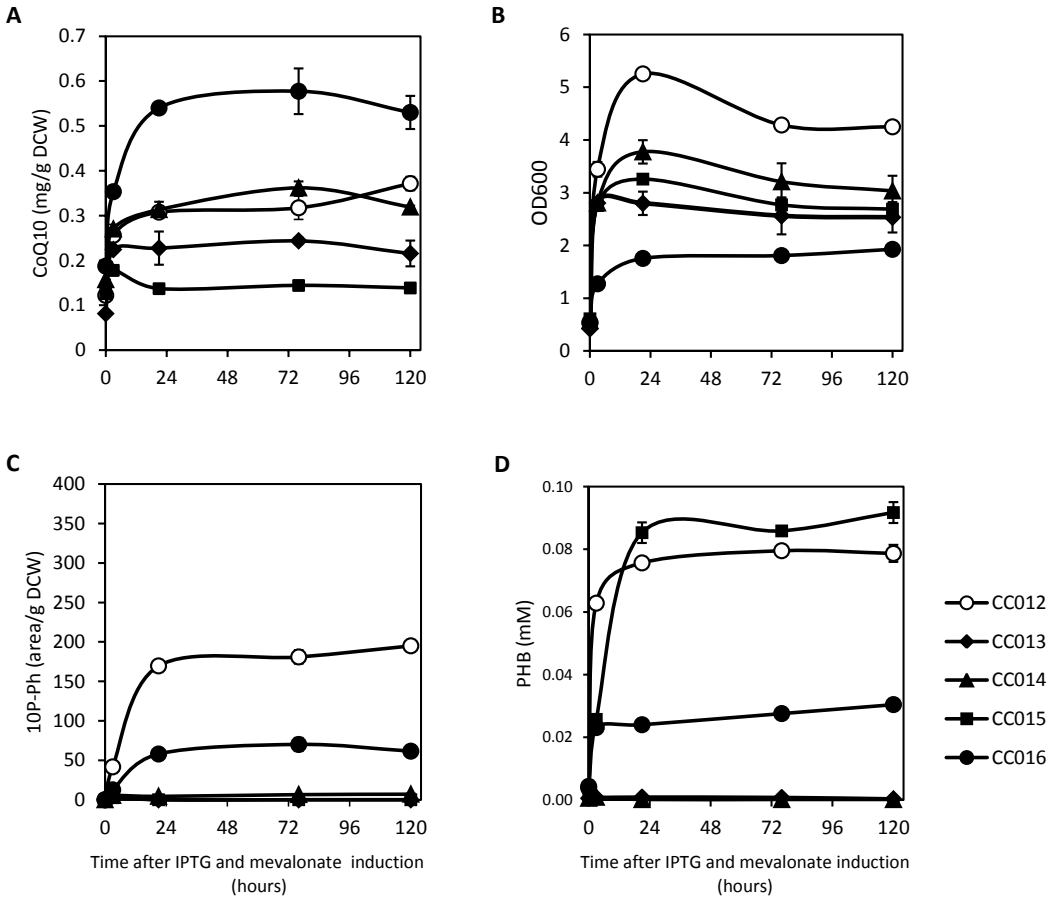

Figure 2.9 Time-course of CoQ10, 10P-Ph and PHB production following the expression of the aromatic operons, the bottom mevalonate operon and/or the PHB prenyltransferase $UbiA_o$

Strains CC012 (empty circles), CC013 (filled diamonds), CC014 (filled triangles), CC015 (filled squares) and CC016 (filled circles) were grown for five days. Cultures were induced during early exponential phase with 0.5 mM IPTG and 10 mM mevalonate. Samples were taken at 0, 3, 25, 72 and 120 hours after induction in order to measure **A**) CoQ10 production **B**) optical density **C**) 10P-Ph production **D**) extracellular PHB. Error bars represent the standard deviation of two biological replicates.

The overexpression of $UbiA_o$ along with the lower mevalonate pathway in CC014 resulted in the accumulation of a new compound, which eluted from the HPLC column 4.5 minutes before CoQ10 (Figure 2.10A). Analysis of this molecule by LC-MS-MS revealed a precursor ion of m/z 818 and a product ion of m/z 150, corresponding to the protonated precursor ion and to the tropylium product ion, respectively, of 3-decaprenyl-4-aminobenzoate (10P-AB) (Figure 2.10B) (Hamilton and Cox, 1971; Marbois et al.,

2010). The accumulation of this hybrid metabolite had never been observed in a CoQ10-producing *E. coli* strain, but had been reported in *E. coli* when UbiA uses *para*-aminobenzoate (PABA) as its substrate, typically when the production of PHB is defective (Hamilton and Cox, 1971; Lawrence et al., 1974). Interestingly, none of the other strains tested produced measurable amounts of 10P-AB (Figure 2.10C).

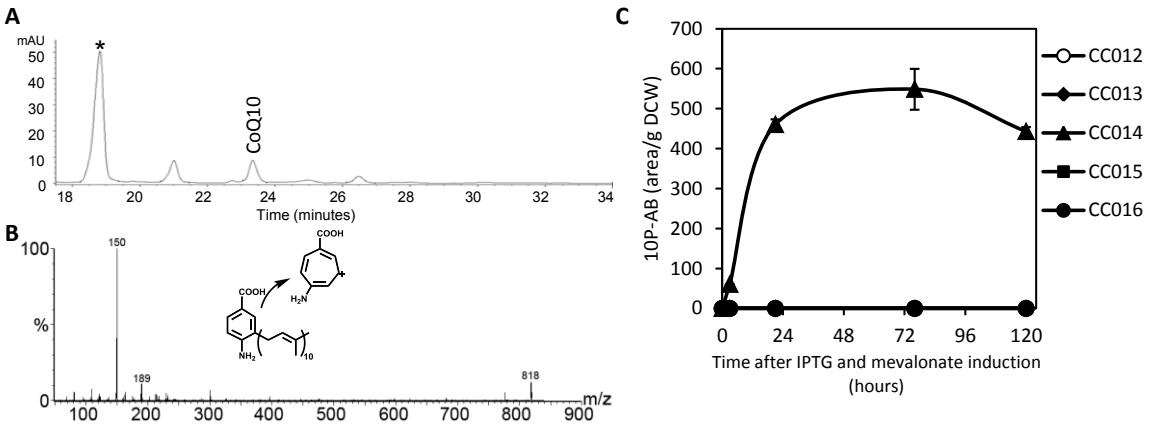

Figure 2.10 Identification and accumulation pattern of 10P-AB in a strain overexpressing a PHB prenyl transferase and the bottom mevalonate pathway
The production 10P-AB was characterized in CC014. **A)** HPLC chromatogram of extracted quinones from CC014, 24 hours after induction with 0.5 mM IPTG and 10 mM mevalonate. The 10P-AB peak is labeled with a star. **B)** LC-MS-MS spectrum of 10P-AB. The fragmented precursor ion yielded a protonated ion $[M+H]^+$ ($C_{57}H_{88}NO_2^+$, exact mass 818.7), and a tropylium ion $[M]^+$ ($C8H8NO_2^+$, exact mass 150.1). **C)** Time-course of 10P-AB production in stains CC012 (empty circles), CC013 (filled diamonds), CC014 (filled triangles), CC015 (filled squares) and CC016 (filled circles), after induction with 0.5 mM IPTG and 10 mM mevalonate. Error bars represent the standard deviation of two biological replicates.

2.3.5 *Overexpression of a putative monooxygenase of the ubiquinone pathway, UbiI*

The accumulation of 10P-Ph reported in sections 2.3.3 and 2.3.4 highlights the existence of a bottleneck in the ubiquinone pathway, preventing the conversion of 10P-Ph to the downstream intermediate, 2-decaprenyl-6-hydroxyphenol (Figure 2.1A). The overexpression of $UbiA_o$ partially relieved this bottleneck, but CoQ10 synthesis in my engineered strains remained low, with an undetermined portion of precursors sequestered

in the form of 10P-Ph. To address this problem, the open-reading frame of *ubiI*, coding for the putative monooxygenase responsible for the hydroxylation of 10P-Ph (Hajj Chehade et al., 2013), was placed under the control of a *lacZ* promoter and plasmid-localized. The resulting construct, pJUbiI, was expressed in strain CC012, yielding strain CC017. The corresponding empty plasmid, pJPK12, was also transformed into CC012, yielding the control strain CC018. I deliberately chose not perform initial tests in strains expressing $UbiA_o$ because of the growth defects associated with this heterologous enzyme, and the potential additional burden associated with the expression of a fourth plasmid, pJUbiI.

The expression of pJUbiI had no significant effect on CoQ10 production and on 10P-Ph accumulation in strain CC017 (Figure 2.11). Consequently, UbiI was not over-expressed in subsequent experiments.

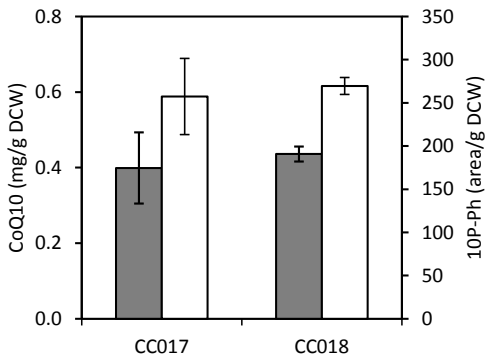

Figure 2.11 CoQ10 and 10P-Ph production following the expression of pJUbiI
Strain CC017 and CC018 were induced with 0.5 mM IPTG and 10 mM mevalonate during early exponential phase, and grown for five days. CoQ10 (grey bars) and 10P-Ph (white bars) were extracted at the end of fermentation. Error bars show the standard deviation of two biological replicates.

2.3.6 *Expression of the complete mevalonate pathway*

The CoQ10 production strains engineered so far expressed the bottom mevalonate pathway, enabling the conversion of exogenously supplied mevalonate into the isoprenoid building blocks, IPP, DMAPP and FPP (Martin et al., 2003). Biosynthesis of mevalonate from acetyl-CoA in *E. coli* is possible using the plasmid pMevT, bearing the top mevalonate operon, which contains the genes *atoB*, *HMGS* and *tHMGR* (Martin et al., 2003). However, the expression of this plasmid is associated with growth defects in *E. coli*, due to an imbalance in the pathway leading to the accumulation of the toxic intermediate, HMG-CoA (Pitera et al., 2007). For this reason, I initially chose to avoid its expression in my CoQ10 production strains. Over the last few years, considerable research has focused on the optimization of the top mevalonate pathway, and new plasmids variants allowing more streamlined conversion of acetyl-CoA to mevalonate have been constructed (Anthony et al., 2009; Ma et al., 2011; Pitera et al., 2007). I have obtained two of such variants, pMtSa and pMtDa (Ma et al., 2011). In these vectors, the *S. cerevisiae tHMGR* open-reading frame, is replaced by a *HMGR* from *Staphylococcus*

aureus (*SaHMGR*) or by a *HMGR* from *Delphia acidovorus* (*DaHMGR*), respectively. The plasmids pMtSa and pMtDa contain a chloroamphenicol resistance marker, as does the plasmid pALTAA. Therefore, in order to obtain strains expressing the full mevalonate pathway, I transferred the top aromatic operon, *lacZ*p:*tktA*-*aroF*^{FBR}-*aroB*, on the chromosome of *E. coli,* downstream of the *aroB* locus. The resulting strains, MG1655 Δ*ispB*, pTDPS$_o$, *ubiC*::LLACC, *aroB*::LTAA, pMBIS, pMtSa (CC019) and MG1655 Δ*ispB*, pTDPS$_o$, *ubiC::LLACC, aroB::LTAA,* pMBIS, pMtDa (CC020), were tested for CoQ10 production (Table 2.1). As shown by Figure 2.12, the expression of pMtSa in CC019 resulted in higher CoQ10 titers compared to CC020 (pMtDa) and CC012. The ratio of 10P-Ph to CoQ10 was also smaller in this strain, indicating the expression of pMtSa favored higher flux through ubiquinone pathway.

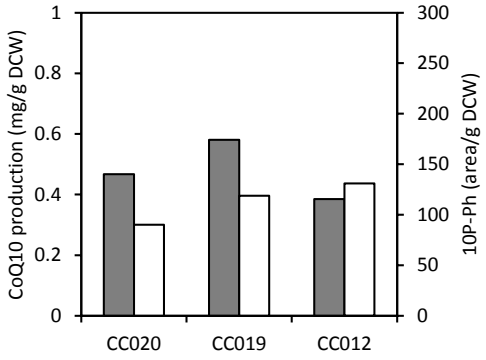

Figure 2.12 CoQ10 and 10P-Ph production following the expression of two variants of the top mevalonate operon.
Cultures of CC019 (pMtSa) , CC020 (pMtDa) and CC012 were induced with 0.5 mM IPTG and 10 mM mevalonate (CC012 only) during exponential phase. After five days fermentation, CoQ10 (grey bars) and 10P-Ph (white bars) were quantified. Values represent the average of two quinone extractions.

2.3.7 *Expression of a PHB prenyltransferase from E. coli, UbiA*

As reported in section 2.3.4, the expression of *ubiA$_o$*, the synthetic gene derived from *Sphingomonas* sp. NAP1, led to improvements in CoQ10 production, but had

deleterious effects on cell growth. I had originally concluded, from preliminary experiments, that replacing *ubiA*$_o$ by *E. coli*'s native PHB prenyltransferase, *ubiA*, would not alter this growth phenotype. However, I later revisited these results and was prompted to further investigate differences between *ubiA*$_o$ or *ubiA* overexpression. I replaced *ubiA*$_o$ on the expression plasmid pTubiA$_o$DPS$_o$ by the open reading frame of *E. coli*'s native PHB prenyltransferase, *ubiA*. The new plasmid was used to complement Δ*ispB*, and the resulting strain, Δ*ispB* pTubiA$_e$DPS$_o$ (CC022), was compared to strains Δ*ispB* pTubiA$_o$DPS$_o$ (CC021) and Δ*ispB* pTDPS$_o$ (CC002). I found that without IPTG induction, the growth pattern of CC021 and CC022 were comparable, both strains reaching lower densities than strain CC002 (Figure 2.13A). However, while the induction of the operon resulted in 29% reduction of growth in CC021, it had no noticeable effect on CC022 (Figure 2.13A). Furthermore, I found that CoQ10 production was higher following the expression of UbiA (CC022) than of UbiA$_o$ (CC021) (Figure 2.13B). Based on these findings, the plasmid pTubiA$_e$DPS$_o$ was used to build a new CoQ10 production strain, MG1655 Δ*ispB*, pTubiA$_e$DPS$_o$, *ubiC::LLACC, aroB::LTAA,* pMBIS, pMtSa (strain CC023, Table 2.1).

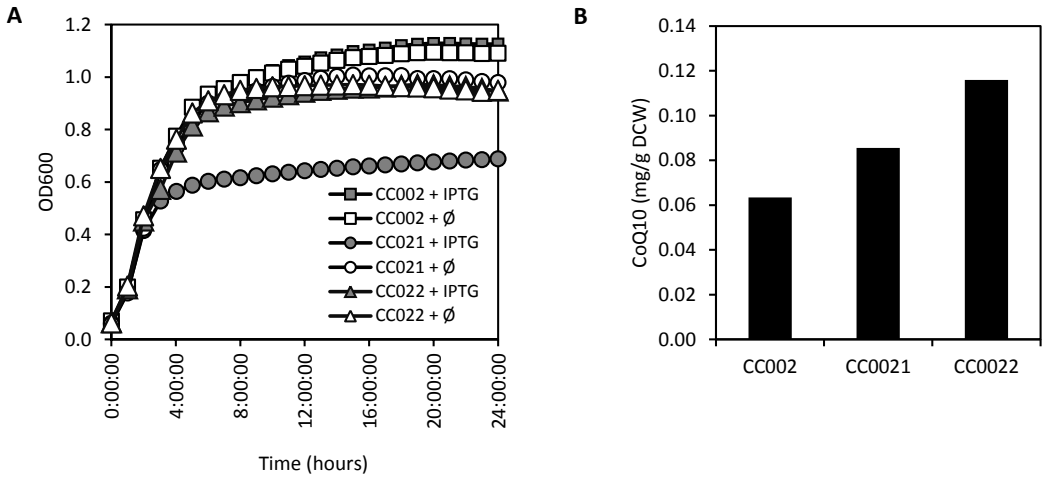

Figure 2.13 Growth and CoQ10 production following the expression of different PHB prenyltransferases

A) Strains CC002, CC021 and CC022 were grown in replicate (N=6) in a 96-well plate incubated in a microtiter plate reader with continuous shaking. Triplicate cultures of each strain were induced with 0.5 mM IPTG after two hours. Optical densities were measured automatically by the plate reader. Values show the average of triplicates. **B**) Strains CC002, CC021 and CC022 were grown for 48 hours and CoQ10 measured. Values show the average of duplicate extractions.

2.3.8 *Effect of IPTG induction on CoQ10 production*

The choice of the *lacZ* and *trc* promoters to drive the expression of synthetic operons was based on the premise that expression would remain low until an inducer (IPTG) was added to the culture. However, the leakiness of such promoters is well documented and IPTG can be omitted without undermining product accumulation following the expression of heterologous genes (Anthony et al., 2004; Zahiri et al., 2006b). As strain CC023 does not require the addition of mevalonate during early exponential phase, I was prompted to question the requirement for IPTG addition. I compared CoQ10 production following induction of CC023 with increasing concentrations of IPTG. As shown by Figure 2.14, IPTG induction had minimal effects on CoQ10 production. Moreover, the omission of IPTG diminished the synthesis of 10P-Ph, and of CoQ11 in CC023. These results indicate that the *lacZ* and *trc* promoters used

for the construction of the CoQ10 production strains are leaky and allow minimal control over the timing of expression of the synthetic operons. The addition of IPTG was henceforth omitted in subsequent experiments.

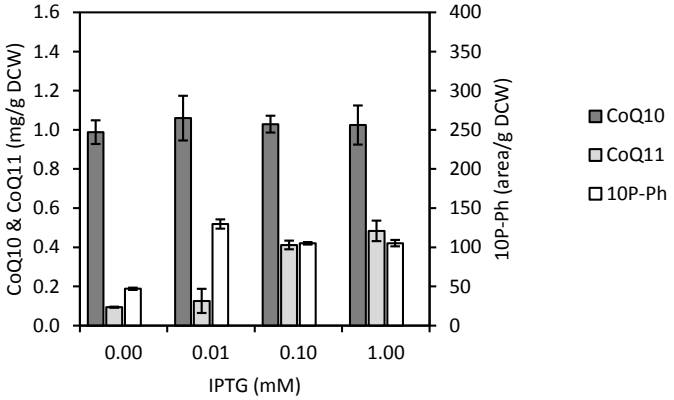

Figure 2.14 Effect of IPTG on CoQ10, CoQ11 and 10P-Ph accumulation
Strain CC023 was grown for five days. Different IPTG concentrations were added during early exponential phase. Error bars show the standard deviation of three biological replicates.

2.4 **Discussion**

The use of *E. coli* as a host for the production of CoQ10 offers several advantages, including a range of genetic tools allowing deletion and insertion of selected loci, the expression of foreign genes, and the capacity to alter metabolic pathways to increase the availability of precursors. As a first part in this thesis, I sought to systematically investigate how different approaches, both hypothesized and published, affect the flux of carbon towards CoQ10 in recombinant *E. coli* (Zahiri et al., 2006b; Zhang et al., 2007). As such, I set out to enhance flux of precursor molecules to the ubiquinone pathway by simultaneously increasing the production of both aromatic and isoprenoid intermediates. I also explored the potential of marine bacteria as a source of

genetic material, by overexpressing a DPS derived from *S. baekryungensis* and a PHB prenyltransferase from *Erythrobacter* sp. NAP1.

2.4.1 *Overexpression of the aromatic pathway*

In order to ensure the availability of increased levels of PHB *in situ*, rate-limiting enzymes of the shikimate pathway, along with UbiC, were over-expressed in a CoQ10-producing *E. coli* strain (Figure 2.1) (Barker and Frost, 2001). The expression of a first operon deregulated the conversion of E4P and PEP to shikimate, while enzymes encoded by a second operon ensured higher flux from shikimate to PHB. Expression of these two operons, upon IPTG induction, led to the accumulation of up to 0.43 mM of PHB when the synthetic aromatic operons were expressed alone (Figure 2.5C), and 0.08 mM of PHB when the mevalonate pathway and DPS_o were co-expressed. The additional burden brought by the maintenance of two additional plasmids, the expression of additional heterologous proteins, as well as the conversion of PHB to CoQ10 and ubiquinone intermediates, may account for this discrepancy. Although far from the yields previously obtained (Barker and Frost, 2001), the production of 0.08 mM of PHB corresponds to a 40-fold increase from the control strain CC009, and could yield up to 16 mg/g DCW of CoQ10.

2.4.2 *Overexpression of a heterologous mevalonate pathway*

Expression of the mevalonate pathway aimed at alleviating bottlenecks resulting from the rate-liming supply of isoprenoid precursors (Kim et al., 2006; Zahiri et al., 2006b). Increased production of FPP and IPP/DMAPP alone, resulting from the

expression of the bottom mevalonate pathway, augmented by 2-fold the CoQ10 content of CC010 (Figure 2.6A, Figure 2.9A). Expression of the top mevalonate pathway, through pMtDa or pMtSa, further enhanced CoQ10 production. Inadequate activity of the enzyme HMGR has bacteriostatic effects, due to the toxicity of HMG-CoA (Pitera et al., 2007). The pMtSa and pMtDa plasmids contain variant HMGRs, SaHMGR (*S. aureus*) and DaHGMR (*D. acidovorus*), respectively, mediating the conversion of HMG-CoA to mevalonate. SaHMG is NADPH-dependent, while DaHGMR is NADH-dependent (Ma et al., 2011). Close links exists between redox homeostasis and ubiquinone's functions and biosynthetic pathway (Bekker et al., 2007; Georgellis et al., 2001; Huang et al., 2011). Therefore, both plasmids were tested in the context of CoQ10 production. The expression of the NADPH-dependent SaHMGR favoured CoQ10 production over that of DaHMGR (Figure 2.12). These results may be due to differences in redox status between the two strains, or to kinetic properties of *S. aureus* HMGR, which favor higher mevalonate production than *D. acidovorans* HMGR during aerobic growth (Ma et al., 2011).

2.4.3 *Heterologous expression of a decaprenyl diphosphate synthase*

The increased flux of precursors towards the ubiquinone pathway substantially improved CoQ10 production in engineered *E. coli*. However, the 1 mg/g DCW of CoQ10 obtained in CC023 is lower than what was previously obtained (Zahiri et al., 2006b), and represents a fraction of the expected yield from PHB and isoprenoids in my strain, indicating that bottlenecks still prohibit maximum CoQ10 content. Despite the expression of the mevalonate pathway in strain CC023, the amount of isoprenoid committed to

CoQ10 biosynthesis might be limited by the activity of DPS_o, which may not fully convert FPP and IPP/DMAPP into DPP. I have shown that complementation of the Δ*ispB* deletion strain, an essential gene for *E. coli* (Okada et al., 1997b), with dps_o is sufficient to restore growth. However, assuming similar extinction coefficients between CoQ8 and CoQ10, the accumulation of CoQ10 in strain CC002 is less than the accumulation of CoQ8 in the wild-type strain MG1655 (Figure 2.2). This suggests that either catalytic properties of DPS_o are inferior to those of IspB, or that DPS_o is not adequately expressed. DPS_o activity also leads to the production of CoQ11, suggesting that this particular enzyme produces undecaprenyl diphosphate in addition to DPP. While the heterologous expression of several DPS proteins has been documented to result in the production of shorter polyprenyl species in addition to DPP, as inferred by the accumulation of a mixture of CoQ10, CoQ9 and CoQ8 (Okada et al., 1997a; Park et al., 2005; Takahashi et al., 2003; Zahiri et al., 2006a), the biosynthesis of undecaprenyl diphosphate and of CoQ11, has, to the best of my knowledge, never before been reported in *E. coli*. Interestingly, no CoQ11 was detected from quinone extracts of *S. baekryungensis* (personal communication, Adam Burja). This suggests a loss of specificity occurring exclusively during heterologous expression. The addition of the inducer, IPTG, favors the accumulation of CoQ11, supporting the idea that loss of specificity is a side effect of the deregulated overexpression of DPS_o. A more complete characterization and optimization of DPS_o activity and expression, or an investigation into alternative DPS enzymes with variable kinetic properties (Ma et al., 2011), may be necessary to ensure that the supply of DPP is not limiting CoQ10 production.

2.4.4 *Overexpression of a PHB prenyltransferase*

Supporting previous studies, the overexpression of a PHB prenyltransferase had a significant impact on CoQ10 production (Figure 2.9A) (Zhang et al., 2007). However, my results do not support the initial hypothesis that a PHB prenyltransferase derived from a high CoQ10 producer (*Erythrobacter* sp. NAP1) would have enhanced kinetic properties compared to the endogenous PHB prenyltransferase of *E. coli.* Moreover, the expression of $ubiA_o$ had cytotoxic effects on *E. coli*. It remains unclear why the replacement of $ubiA_o$ by *ubiA* (*E. coli*) was able to attenuate these effects. The codon-optimization of $UbiA_o$ might have had a negative effect on its expression. Rare codons sometimes increase the overall translational efficiency and may influence protein folding, particularly in the case of membrane proteins (Norholm et al., 2012). Increased production of isoprenoids coupled with the overexpression of $UbiA_o$ in CC014 led to the accumulation of a new metabolite, 10P-AB (Figure 2.10). This compound does not have a known biological function in *E. coli*, but accumulates in a mutant lacking chorismate lyase activity when grown in the presence of PABA (Hamilton and Cox, 1971). Growth inhibition of *E. coli* by high concentrations of exogenous PABA can be reversed by the addition PHB (Davis, 1951), suggesting that PABA may act as a competitive inhibitor of UbiA by displacing PHB within the active site of UbiA. In CC014, the increased PHB prenyltransferase ($UbiA_o$) activity combined with the higher availability of DPP may result in the exhaustion of the endogenously produced PHB, causing UbiA/$UbiA_o$ to accept PABA as an alternative substrate. In *S. cerevisiae,* PABA can also be used as a substrate for Coq2p and further channeled through the ubiquinone pathway (Marbois et al., 2010). Based on my results, it would appear that while UbiA can use PABA to form

10P-AB, the latter compound is not recognized by the *E. coli* decarboxylases UbiD and UbiX, therefore leading to an accumulation of this metabolite in CC014 (Figure 1.2). These findings demonstrate the importance of precursor stoichiometry in metabolic engineering complex multi-branch pathways.

2.4.5 *Accumulation of 2-decaprenylphenol*

The enhanced production of aromatic and isoprenoid precursors in CC012 and CC016 led to the accumulation of 10P-Ph, an intermediate of the ubiquinone pathway (Figure 2.7B; Figure 2.9C). While the accumulation of 10P-Ph and 2-octaprenylphenol (8P-Ph) as a by-product of CoQ10 and CoQ8 biosynthesis has been documented in anaerobic cultures of *P. denitrificans* (Matsumura et al., 1983) and *E. coli* (Alexander and Young, 1978), respectively, this is the first time that the accumulation of 10P-Ph is reported in an *E. coli* strain engineered to produce CoQ10. A recent study has identified UbiI as the monooxygenase converting 8P-Ph to 2-octaprenyl-6-hydroxyphenol (Hajj Chehade et al., 2013). However, an accumulation of 10P-Ph does not necessarily reflect insufficient UbiI expression, as *E. coli* strains bearing mutations in the ubiquinone pathway genes *ubiB*, *ubiH*, and *ubiG* all accumulate 8P-Ph (Young et al., 1973; Alexander and Young, 1978; Hsu et al., 1996; Poon et al., 2000). Accordingly, the overexpression of UbiI in strain CC017 did not reduce 10P-Ph accumulation nor lead to increase CoQ10 production (Figure 2.11). When flux through the ubiquinone pathway increases as a result of the augmented production of aromatic and isoprenoid precursors, the activity of one of the above-mentioned Ubi enzymes may become rate-limiting, resulting in the accumulation of 10P-Ph. Strain CC016, overexpressing $UbiA_o$, had a

lower 10P-Ph content compared to CC012, along with higher CoQ10 production (Figure 2.9A,C), suggesting that increasing PHB prenyltransferase activity improves flux within the ubiquinone pathway, downstream of the decarboxylation step. It is possible that one or more enzymes of the ubiquinone pathway are dependent on UbiA for their activity. Studies in *S. cerevisiae* provide compelling evidence for the existence of a multi-protein complex involved in the production of CoQ6 (Gin and Clarke, 2005; Gin et al., 2003; Johnson et al., 2005; Tran et al., 2006). It is hypothesized that Coq2p, the homologue of UbiA, does not physically interact with the complex, but that its product, 3-hexaprenyl-4-hydroxybenzoate, plays a role in the assembly and/or stability of the complex (Hsieh et al., 2007; Hsu et al., 2000; Suzuki et al., 1994). As described in more detail in Chapter 1 (section 1.5), physical interactions between Ubi proteins have not yet been demonstrated in *E.* coli, but early literature on the ubiquinone pathway hints at the existence of a soluble multi-protein complex capable of converting 8P-Ph to CoQ8 (Knoell, 1979; Knoell, 1981). The accumulation of 10P-Ph may reflect limitations in activity of stability of this putative complex. The introduction of pMtSa into CoQ10 production strains and the omission of IPTG from the fermentation medium also diminished the 10P-Ph/CoQ10 ratio, but these observations offer little insight on underlying mechanisms driving flux through the ubiquinone pathway. Moreover, as I was unable to quantify 10P-Ph, I cannot assert how much of the observed reduction in 10P-Ph accumulation translates into further CoQ10 biosynthesis. Further work focused on enzymes of the ubiquinone pathway will be key to completely eliminate the bottleneck resulting in 10P-Ph accumulation in CoQ10 production strains.

In summary, this chapter describes the development of a CoQ10-producing *E. coli* strain engineered to overproduce aromatic and isoprenoid precursors and to have increased PHB prenyltransferase activity. It is the first instance where both precursor pathways have been overexpressed and genetically deregulated in combination with the overexpression a PHB prenyltransferase, the enzyme bridging these two pathways. The results presented in this chapter highlight the existence of previously unreported bottlenecks in CoQ10 overproduction in *E. coli*, and will enhance our ability to design further improvements of this system. The resulting strain, CC023, achieved a 5.8-fold increase in CoQ10 content compared to the control strain CC009, over-expressing DPS_o alone (Figure 2.14; Figure 2.6A), thereby demonstrating the effectiveness of the chosen approach. The maximum specific content obtained, 1 mg/g DCW of CoQ10, is inferior to those reported when isoprenoid production and/or UbiA and UbiC expression were enhanced (Huang et al., 2011; Zahiri et al., 2006b). However, these studies presented CoQ10 yields obtained from engineered *E. coli* strains grown on rich, optimized growth media, which was beyond the scope of these initial experiments, and make comparisons difficult. The strain engineered in the first part of this thesis still requires optimization. In particular, a more extensive analysis of the accumulation patterns of intermediate metabolites will be required to ensure proper balancing of the pathway and optimal carbon flow. Nevertheless, this "base strain" had, at this point in my research, the potential to be used as tool to investigate the interplay between central metabolism and CoQ10 production, and to better understand inherent factors limiting the accumulation of this antioxidant in *E. coli.* The results of these investigations are presented in Chapter 3.

Chapter 3. Investigation into the interplay between central metabolism and CoQ10 production in an engineered strain of *E. coli*

3.1 Introduction

Chapter 2 describes the stepwise construction of a CoQ10-producing strain of *E. coli*. I showed that a simultaneous increase in the production of isoprenoid and aromatic precursors was beneficial to CoQ10 production, in particular when the expression of a PHB prenyltransferase was concurrently increased. I next wished to explore different strategies to further enhance CoQ10 production, with a special focus on central metabolism. Review of the literature pertaining to ubiquinone biosynthesis in microbes offers several hints that the production of this antioxidant is linked to the cell's primary metabolism. In particular, ubiquinone synthesis appears to have closed ties with catabolism, oxidative respiration as well as redox homeostasis.

CoQ10 production in *R. radiobacter* is upregulated on selected carbon sources (Ha et al., 2007b; Koo et al., 2010). In addition, the expression of a number of ubiquinone biosynthetic genes of *E. coli*, including *ubiA, ubiC, ubiG, ubiD* and *ubiX*, is higher on non-fermentable carbon sources compared to glucose, suggesting catabolite repression as a means of control (Gibert et al., 1988; Kwon et al., 2005; Zhang and Javor, 2003). The nature of the carbon substrate is also expected to have an impact on fluxes through the engineered precursor pathways. For instance, substrate import via a phosphotransferase system may decrease the availability of PEP as a building block in the synthesis of the aromatic intermediate, PHB (Patnaik and Liao, 1994). Accordingly, I investigated an

array of carbon sources representative of the different ways in which catabolism may exert influence on CoQ10 production.

As a major player in *E. coli*'s aerobic respiration, it is expected that ubiquinone biosynthesis is linked to the cell's respiratory state. Expression of *ubiC, ubiA* and *ubiG* is lower under anaerobic conditions, indicating transcriptional control of ubiquinone biosynthesis in response to respiratory state (Gibert et al., 1988; Kwon et al., 2005; Soballe and Poole, 1997). There is also evidence for post-transcriptional control over the ubiquinone to menaquinone ratio, upon a switch from anaerobic to aerobic conditions (Shestopalov et al., 1997). Interestingly, although aerobic respiration requires ubiquinone for electron transport, limiting the O_2 supply to growing cultures increases CoQ10 production in *R. radiobacter* and *R. sphaeroides* (Choi et al., 2005; Ha et al., 2007b; Sakato et al., 1992; Yoshida et al., 1998). As detailed in Chapter 1 (section 1.10), these observations, along with respiration inhibitors studies, suggest that cells may compensate restricted flux of electron through the respiratory chain by upregulating the biosynthesis of ubiquinone (Bekker et al., 2007; Choi et al., 2005). Overall, endogenous mechanisms controlling ubiquinone synthesis appear intricate and many fold. Under this premise, I chose to introduce genetic alterations in the electron transport chain of the engineered *E. coli*, as a mean to mimic restrictions in electron flux susceptible to trigger upregulation of CoQ10 production.

Both catabolism and oxidative respiration are closely linked to redox homeostasis, which is mainly driven by the ratios $NADH/NAD^+$ and $NADPH/NADP^+$. Manipulating the ratio of pyridine nucleotides for metabolic engineering purposes in *E. coli* is an effective strategy (Lin et al., 2005; Nikel et al., 2010). Nevertheless, these manipulations

may result in significant changes in metabolic partitioning, adding unforeseen complexity to the engineered system. For instance, when the NAD^+-dependent glyceraldehyde-3-phosphate dehydrogenase, GapA, was replaced with the $NADP^+$-dependent glyceraldehyde-3-phosphate dehydrogenase, GapC, from *C. acetobutylicum*, to increase the availability of NADPH in *E. coli*, there was a downregulation of the pentose-phosphate pathway, normally the major source of NAPDH in cells (Martinez et al., 2008). In the case of CoQ10 production, the down-regulation of the pentose-phosphate pathway would be detrimental, as it is essential for the production of aromatic precursors leading to PHB (Figure 3.1). In *R. radiobacter*, there is a positive correlation between the $NADH/NAD^+$ ratio and the resulting CoQ10 content (Koo et al., 2010). It is possible that higher $NADH/NAD^+$ ratio results in increased activity of the electron transport chain, which re-oxidizes NADH through the activity of NADH-dehydrogenases. Overall, little is known about the impact of redox homeostasis on CoQ10 production in *E. coli*, but the biological function of ubiquinone as an electron acceptor and the anecdotal evidence from *R. radiobacter* studies highlight the potential of this approach.

In this Chapter, I investigated the effect of different carbon sources on CoQ10 production in the base strain, CC023, as well as the impact of selected mutations, altering oxidative respiration or mixed-fermentation pathways. I found a link between sorbitol metabolism and CoQ10 production in the engineered strain, CC023. I also demonstrated that abrogating the production of acetate in the same strain can partly mimic the results obtained on sorbitol. My experiments were hindered by reproducibility and stability issues in all strains expressing the synthetic aromatic and mevalonate pathways. This has prevented a more thorough investigation regarding the link between acetate, sorbitol and

CoQ10 production. Nevertheless, the results presented in this Chapter suggest novel directions to engineer further improvements in CoQ10 production in *E. coli.*

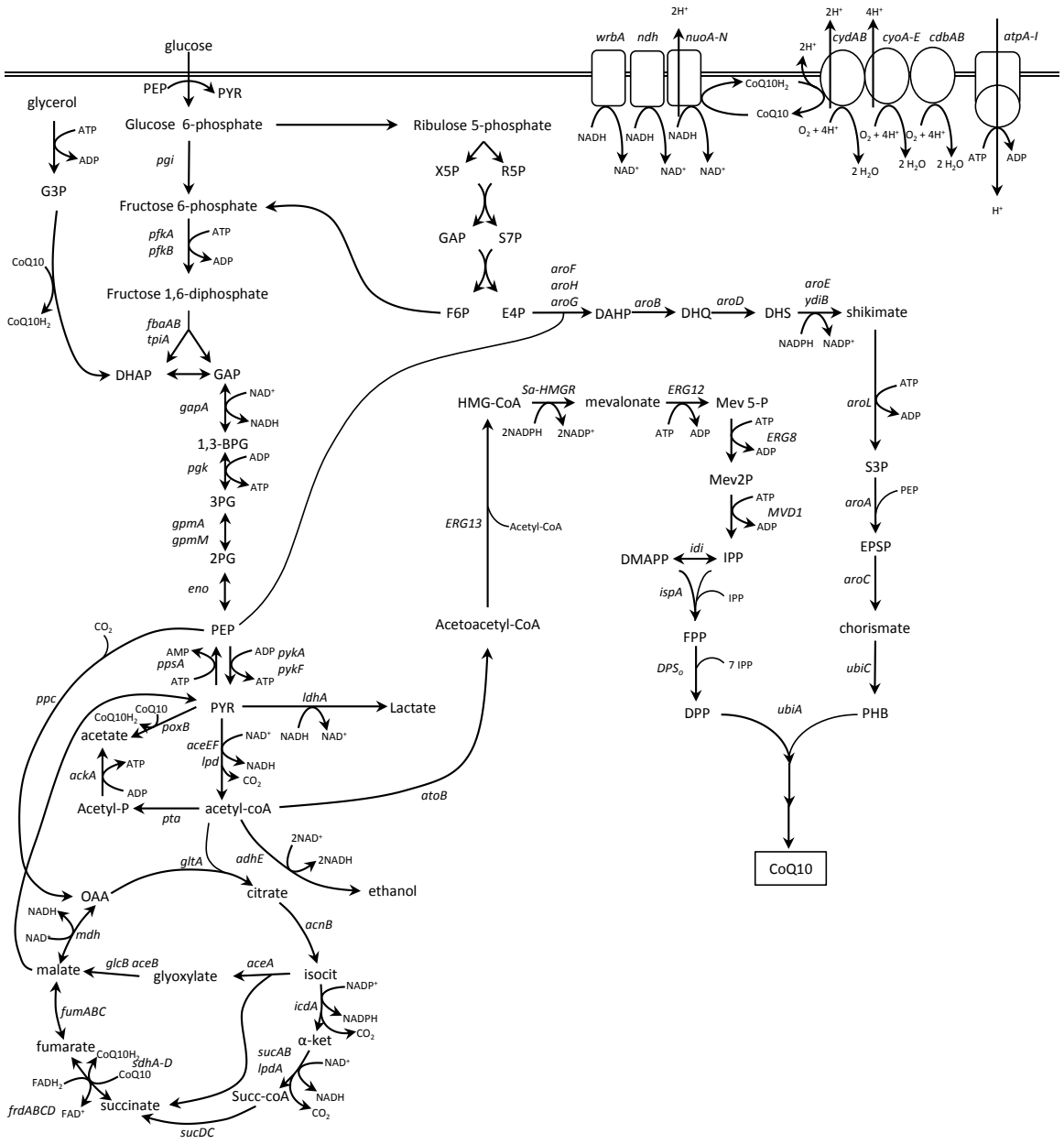

Figure 3.1 Central metabolism and engineered CoQ10 production in *E. coli*
Summary of the main reactions in *E. coli*'s central metabolism and oxidative respiration. ATP, adenosine triphosphate; ADP, adenosine diphosphate; NADH, nicotinamide adenine dinucleotide; NADPH, nicotinamide adenine dinucleotide phosphate. G3P, glycerol-3-phosphate; DHAP, dihydroxyacetone phosphate; GAP, glyceraldehyde-3-phosphate; 1,3-BPG, glycerate 1,3-bisphosphate; 3PG, 3-phospho-glycerate; 2PG, 2-phospho-glycerate; PEP, phosphoenolpyruvate; PYR, pyruvate; acetyl-P, acetyl phosphate; isocit, isocitrate; α-ket, α-ketoglutarate; Succ-CoA, succinyl-CoA; OAA, oxaloacetate; HMG-CoA, 3-

hydroxy-3-methylglutaryl-CoA; Mev 5-P, 5-phosphomevalonate; Mev2P, mevalonate pyrophosphate; IPP, isopentenyl diphosphate; DMAPP, dimethylallyl diphosphate; FPP, farnesyl diphosphate; DPP, decaprenyl diphosphate; X5P, xylulose 5-phosphate; R5P, ribose 5-phosphate; S7P, sedo-heptulose-7-phosphate; F6P, fructose 6-phosphate; E4P, erythrose-4-phosphate; DAHP, 3-deoxy-arabino-heptulosonate 7-phosphate; DHQ, 3-dehydroquinate; DHS, 3-dehydroshikimate; S3P, shikimate 3-phosphate; EPSP, 5-enolpyruvyl-shikimate 3-phosphate; PHB, *para*-hydroxybenzoate; $CoQ10H_2$, ubiquinol; CoQ10, coenzyme Q10.

3.2 **Materials and methods**

3.2.1 *Strains and reagents and culture conditions*

The strains of *E. coli*, and the plasmids used in this chapter are listed in Table 3.1. Plasmid construction and propagation was done using *E. coli* DH5-α. The strains developed for the production of CoQ10 are derived from MG1655. *E. coli* knock-out strains for *cyoE*, *nuoB*, *poxB* and *ldhA* were obtained from the Keio collection (Coli Genetic Stock Center) (Baba et al., 2006). Gene knockouts and insertions were transferred into the desired strains by P1 transduction, and kanamycin markers were removed using the plasmid pCP20, as previously described (section 2.2.2). Deletions and insertions were confirmed by colony PCR (Table 3.2). Chemicals were obtained from Sigma-Aldrich. Phusion polymerase (New England Biolabs) was used for cloning purposes, and Taq DNA polymerase (Fermentas) was used for colony PCR. Plasmids were isolated using the GeneJET Plasmid Miniprep Kit (Thermo Scientific) and PCR products were purified using the QIAQuick Gel Extraction Kit (QIAGEN). For routine propagation, strains were grown in LB. Appropriate antibiotics (100 μg/mL ampicillin, 20 μg/mL chloramphenicol, 12.5 μg/mL tetracycline and/or 25 μg/mL kanamycin) were added to cultures for plasmid maintenance. Primers used in this Chapter are listed in Table 3.2, while strains and plasmids used in this Chapter are listed in Table 3.1.

Table 3.1 Strains and plasmids used in Chapter 3

Strain	Genotype / description	Reference
DH5α	*fhuA2 Δ(argF-lacZ)U169 phoA glnV44 Φ80 Δ(lacZ)M15 gyrA96 recA1 relA1 endA1 thi-1 hsdR17*	Invitrogen
JW0418-1	*F-, Δ(araD-araB)567, ΔlacZ4787(::rrnB-3), ΔcyoE785::kan, λ-, rph-1, Δ(rhaD-rhaB)568, hsdR514*	(Baba et al., 2006)
JW5875-2	*F-, Δ(araD-araB)567, ΔlacZ4787(::rrnB-3), λ-, ΔnuoB769::kan, rph-1, Δ(rhaD-rhaB)568, hsdR514*	(Baba et al., 2006)
JW0855-1	*F-, Δ(araD-araB)567, ΔlacZ4787(::rrnB-3), λ-, ΔpoxB772::kan, rph-1, Δ(rhaD-rhaB)568, hsdR514*	(Baba et al., 2006)
JW1375-1	*F-, Δ(araD-araB)567, ΔlacZ4787(::rrnB-3), λ-, ΔldhA744::kan, rph-1, Δ(rhaD-rhaB)568, hsdR514*	(Baba et al., 2006)
CC023	MG1655, Δ*ispB, ubiC::LLACC*, *aroB::LTAA* + pTUbiA$_e$DPS$_o$ + pMBIS + pMtSa	This study
CC024	MG1655, Δ*ispB, ΔcyoE, ubiC::LLACC*, *aroB::LTAA* + pTUbiA$_e$DPS$_o$ + pMBIS + pMtSa	This study
CC025	MG1655, Δ*ispB, ΔnuoB, ubiC::LLACC*, *aroB::LTAA* + pTUbiA$_e$DPS$_o$ + pMBIS + pMtSa	This study
CC026	MG1655, Δ*ispB, ΔackA-pta, ubiC::LLACC*, *aroB::LTAA* + pTUbiA$_e$DPS$_o$ + pMBIS + pMtSa	This study
CC027	MG1655, Δ*ispB, ΔackA-pta, ΔpoxB, ubiC::LLACC*, *aroB::LTAA* + pTUbiA$_e$DPS$_o$ + pMBIS + pMtSa	This study
CC028	MG1655, Δ*ispB, ΔackA-pta, ΔpoxB, Δldha, ubiC::LLACC*, *aroB::LTAA* + pTUbiA$_e$DPS$_o$ + pMBIS + pMtSa	This study
CC029	MG1655, Δ*ispB, ΔackA-pta, ΔpoxB, Δldha, ubiC::LLACC*, *aroB::LTAA* + pTUbiA$_e$DPS$_o$ + pMBIS + pMtSaLTAA	This study
Plasmid	**Description**	**Reference**
pKD4	plasmid with the RK6γ origin containing a Kan^R cassette flanked by FRT sites; Amp^R	(Datsenko and Wanner, 2000)
pCP20	plamid with temperature sensitive origin of replication containing the *FLP;* Amp^R, Cm^R	(Datsenko and Wanner, 2000)
pTUbiA$_e$DPS$_o$	pTrc99A derivative containing *ubiA$_e$* and *DPS$_o$*; Amp^R	This study
pALTAA	pALac derivative containing *tktA*, *aroF^{FBR}* and *aroB*; Cm^R	This study
pMBIS	pTrc99A derivative containing *DPS$_o$*; Amp^R	This study
pMtSa	pBAD33 derivative containing *atoB*, *HMGS*, *SaHMGR* ; Cm^R	(Ma et al., 2011)
pMtSaLTAA	pBAD33 derivative containing *atoB*, *HMGS*, *SaHMGR*, tktA, aroF^{FBR} and aroB; Cm^R	This study

Table 3.2 Oligonucleotides used in Chapter 3

Primer name	**5' to 3' sequence**
cyoE5'	Caatggcagtggtacaggttct
cyoE3'	Ctagtgtaaagcggcaaacgaatg
nuoB5'	Gtttatctggtgcgtattggcg
nuoB3'	Catcaagatgatcgcgggtctgc
ackapta-koF	atcataaatgtcggtgtcatcatgcgctacgctctatggctccctgacgtgtgtaggctggagctgcttc
ackapta-koR	gattatttccggttcagatatccgcagcgcaaagctgcggatgatgacgagatgggaattagccatggtcc
ackaptaF	Aggtatcctttagcagcctgaag

ackaptaR	Caattcattgatgcagcgcagt
poxBF	Ctcgcataatcgccttatgcc
poxBR	Gcggccatcatcgcttcgag
ldhAF	Gcgtcaacggcacaagaataatcag
ldhAR	Tctggcggatttttatcgctgg
HGMR-F	Caaggttccattgagcatttgcaaag
HGMR-R	Gccgccaggcaaattctgttttatc
H1_F	Cttttgatttaggcgcgcccgcaacgcaattaatgtga
H2_R	Tcagcgcagccatacgtacggcgttacgtgcgtattc
H2_F	Aacgccgtacgtatggctgcgctgatgaaacagcgtca
H3_R	Accacggattctgccaccgcaggctgacggcgataatc
H3_F	Agcctgcggtggcagaatccgtggttgctcaaatc
H4_R	Gcaaaatcccttagcggccgccttacgctgattgac
H4_F	Gcgtaaggcggccgctaagggattttgccgatttcggc
H5_R	Gagcagatcctctacgccggacgcatcgtggcc
H5_F	Tgcgtccggcgtagaggatctgctcatgtttgacag
H6_R	Ccaatgcacagtgttgccagccccagcgttttatcg
H6_F	Tggggctggcaacactgtgcattggcggc
H7_R	Ctttgcaaatgctcaatggaaccttgaggtttgaagttc
H8_F	Gataaaacagaatttgcctggcggcagtagcgcggt
H1_R	Gcgttgcgggcgcgcctaaatcaaaagaatagc

3.2.2 *Aerobic flask fermentation*

Tested strains were streaked from glycerol stocks on M9 medium (Sambrook et al., 1989) supplemented with 1.5% agar and 2% glucose and appropriate antibiotics (100 µg/mL ampicillin, 20 µg/mL chloroamphenicol, 12.5 µg/mL tetracycline and/or 25 µg/mL kanamycin). After two days of incubation, several colonies were used to inoculate 5 mL pre-cultures on M9 medium supplemented with 3% glucose, or with an alternative carbon source and 0.1% glucose, and antibiotics. Pre-cultures were grown overnight, then spun down and adjusted to OD_{600}=1 in fresh M9 medium with 3% glucose or an alternative carbon source. Re-suspended pre-cultures were used to inoculate 50 mL medium in 250 mL flasks to OD_{600}=0.1. Flasks were shaken at 200 rpm and 37°C for five days, with regular sampling to monitor optical density, quinone production and

metabolite secretion. Sodium succinate and sodium pyruvate were used as a source of succinate and pyruvate, respectively.

3.2.3 *Deletion of the ackA-ptA locus*

The *ackA-pta* locus was deleted from the chromosome of *E. coli* using lambda Red recombination (Datsenko and Wanner, 2000). A 1597-bp deletion cassette was amplified using primers ackapta-koF and ackapta-koR, and the plasmid pKD4 as a template. The PCR reactions were purified, treated with *Dpn*I, and dialyzed using a 0.025 µm disc (Millipore). Cells of *E. coli* MG1655 *aroB::LTAA, ubiC::LLACC* harboring pKD46 that were previously grown on LB containing L-arabinose (15 mM), were transformed by electroporation using ~700 ng of the purified DNA cassette. Knock-outs were identified by colony PCR using primers ackaptaF and ackaptaR. The kanamycin marker flanked by FRT sites was removed using the helper plasmid pCP20, as previously described (Datsenko and Wanner, 2000).

3.2.4 *Construction of pMtSa-LTAA*

The plasmid pMtSaLTAA, where the *lacZ*p:*tktA*-*aroF*^{FBR}-*aroB* operon is inserted downstream of the MevT operon on the pACYC184 backbone, was constructed using Gibson assembly method (Gibson et al., 2009). The *lacZ*p:*tktA*-*aroF*^{FBR}-*aroB* operon was amplified in two parts, using primer pairs H1_F/H2_R and H2_F/H4_R and pALTAA as template. The pMtSa plasmid was amplified in three parts using primer pairs H4_F/H5_R, H6_F/HGMR-R and H8_F/H1_R. PCR products were treated with *Dpn*I and purified. Six hundred fmol of each part were pooled and evaporated in a speed

vacuum concentrator. DNA was re-suspended in 20 µL Gibson Assemby Mix (100 mM Tris-HCl (pH=7.5), 5 mM $MgCl_2$, 20 µM dNTPs, 250 µM DTT, 63 µg PEG-8000, 313 nM NAD, 0.08 U T5 exonuclease, 0.5 U Phusion DNA polymerase, 80 U Taq DNA ligase), then incubated at 50°C for 60 minutes. Ten µL of the completed reaction was used for transformation in DH5α. Positive clones were screened by colony PCR using primer pairs H3_F/H5_R and H8_F/H2_R.

3.2.5 *Quinone extraction and analysis*

Cells from one-mL aliquots of *E. coli* cultures were harvested at 16,100 x g for analysis of their quinone content. The pelleted cells were washed with 1 mL of 50 mM Tris-HCl pH 7.5, and re-suspended in 450 µL Cell Lytic B (Sigma-Aldrich). After 30 minutes at room temperature, a first extraction was performed with 900 µL of hexane:2-propanol (5:3). The upper phase was transferred into a new tube and a second extraction was done using 500 µL of hexane. The combined extracts were dried under a nitrogen stream, and re-suspended in 100 µL acetone. A 10-µL aliquot was injected into a 1200 Series HPLC system equipped with a ZORBAX Eclipse XDB-C18 (4.6 x 150 mm, 5 µm, Agilent technologies). The mobile phase consisted of acetonitrile (A) and ethanol (B), ran at 0.5 mL/minute with the following elution profile: 0-5 minutes, 40% B; 5-11 minutes, 40%-100% B; 11-22 minutes, 100% B. The quinones were detected at 275 nm. CoQ10 was quantified using a standard curve of an authentic standard.

3.2.6 *Extracellular metabolite analysis*

For HPLC analysis of extracellular metabolites, one-mL aliquots from *E. coli* cultures were centrifuged at 16,100 x g to remove the cells. The supernatant was filtered using a 13 mm 0.2 μM nylon filter (Acrodisc, VWR), and 10 μL was injected into a Finnigan Surveyor HPLC System (Thermo) equipped with an Aminex HPX-87H column (Bio-Rad) heated to 65°C. Acetic acid, pyruvic acid, lactic acid and glucose were resolved using 10 mM H_2SO_4 at a flow rate of 0.6 mL/minute and detected with a Finnigan Surveyor UV/Vis Plus Detector (Thermo) at 210 nm, except glucose which was detected using a Differential Refractometer (Waters 410). PHB and *Unknown 1* were resolved using 10 mM H_2SO_4 and 15% acetonitrile at a flow rate of 0.6 mL/minute and detected at 254 nm. All metabolites were quantified using a standard curve of authentic standards.

3.3 **Results**

3.3.1 *CoQ10 production on different carbon sources*

As a first step to explore the interplay between central metabolism and CoQ10 production, I tested the impact of different carbon sources on strain CC023, under aerobic shake-flask conditions. To simplify carbon fluxes and data interpretation, experiments were done in M9 minimal medium. Carbon sources were chosen to reflect different entry points in central metabolism, different uptake mechanisms and different oxidation states. Glucose is transported inside the cell and concomitantly phosphorylated at the expense of PEP, entering glycolysis, and then the TCA cycle. Glycerol enters the cell by facilitated diffusion and is then metabolized mainly to glycerol-3-phosphate, then to

dihydroxyacetone phosphate, where it enters glycolysis (Voegele et al., 1993). Pyruvate is transported into cells by an active transport system, and may then undergo decarboxylation to acetyl-CoA, oxidation to acetate or phosphorylation to PEP (Lang et al., 1987). The C4-carbon succinate is imported by a proton-coupled transporter, then enters the TCA cycle and triggers the onset of gluconeogenesis reactions (Gutowski and Rosenberg, 1975) (Figure 3.1). Figure 3.2 summarizes the growth pattern and CoQ10 contents obtained on different concentrations of glucose, glycerol, pyruvate and succinate. In this experiment, excess glucose (3%) allowed the most robust growth and the largest CoQ10 production (Figure 3.2A). However, growth and CoQ10 production of CC023 on the selected carbon sources was variable between experiments and replicates (see Appendix, section A2). Reduced growth rate and final biomass on substrates other than glucose suggest that they can difficultly sustain both growth and the strong pull exerted by the engineered aromatic and isoprenoid pathways in strain CC023 (Figure 3.2C, D). Growth on glycerol did not markedly increase CoQ10 production, indicating that neither catabolite repression nor the transport of glucose at the expense of PEP limits CoQ10 production in strain CC023 (Figure 3.2B). Based on these results, I concluded that alternative patterns of catabolic and anabolic reactions brought about by glycerol, pyruvate and succinate did not markedly favor CoQ10 production.

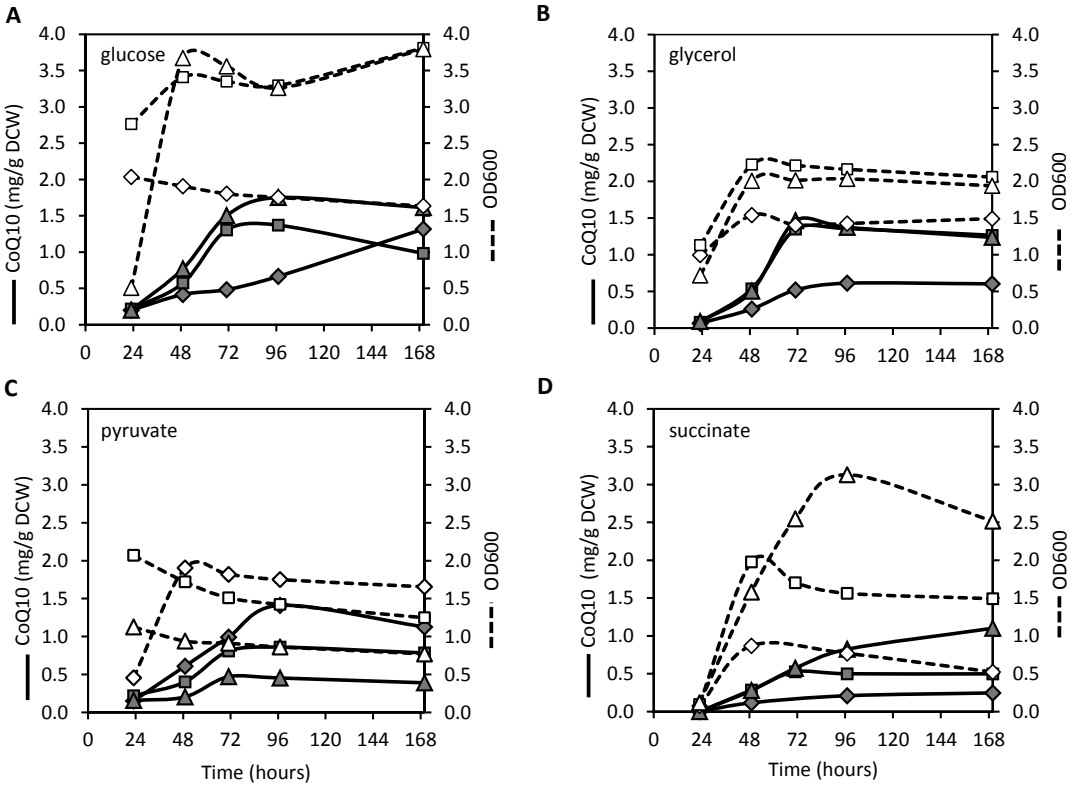

Figure 3.2 Growth and production of CoQ10 on difference carbon sources
Strain CC023 was grown on **A**) glucose **B**) glycerol **C**) pyruvate **D**) succinate. For each substrate, three concentrations were tested: 0.3% (diamonds), 1% (squares) or 3% (triangles). Samples were taken after 23, 29, 71 and 160 hours in order to monitor optical density (dashed lines, empty shapes) and CoQ10 production (full lines, filled shapes).

3.3.2 *Altering the electron transport chain for CoQ10 production*

CoQ10 is an essential component of the electron transport chain of *E. coli*. As such, inherent control mechanisms allow cells to modulate the biosynthesis of ubiquinone depending on their respiratory state (Shestopalov et al., 1997). Such mechanisms are complex with multiple layers of control, hindering our capacity to engineer precise modulations in their onset. By altering the electron transport chain directly, I hypothesized that transcriptional and/or post-translational control mechanisms of ubiquinone production could be harnessed, increasing CoQ10 accumulation in CC023. The *nuoB* gene encodes a subunit of NADH-dehydrogenase I, the most energy efficient

membrane-bound NADH dehydrogenase (4 H^+ translocated/ 2 electrons) (Figure 3.1) (Erhardt et al., 2012). A Δ*nuoB* strain may undergo respiration using NADH dehydrogenase II (*ndh*) and WrbA, but with lower efficiency (0 H^+/2 eletrons) (Bekker et al., 2009; Ingledew and Poole, 1984). The gene *cyoE* encodes a farnesyl transferase catalyzing the condensation between a prenyl group and proheme IV, to form heme *o*, as part of the cytochrome *bo*' oxidase (Saiki et al., 1992). Three terminal oxydases may be expressed during aerobic respiration: cytochrome *bd* I oxidase (*cydAB*), cytochrome *bd* II oxidase (*appCB*) and cytochrom *bo*' oxidase (*cyoABCDE*) (Figure 3.1). Cytochrome *bd* has high affinity to O_2 and is expressed during microoxic conditions, while cytochrome *bo'*, with lower affinity to O_2, is highly expressed in aerobic conditions and is the only terminal oxidase acting as a proton pump (Ingledew and Poole, 1984). Deletion of *cyoE* results in the replacement of heme *o* by heme *b*, and in a structurally intact but inactive cytochrome *bo'* oxidase (Saiki et al., 1992). I hypothesized that mutations in either Δ*nuoB* or Δ*cyoE*, although not entirely disruptive of aerobic respiration, would restrict the activity of the respiratory chain and trigger endogenous mechanisms for the upregulation of ubiquinone biosynthesis. The Δ*cyoE* and Δ*nuoB* mutations were thus introduced in CC023, yielding CC024 and CC025, respectively. As shown by Figure 3.3, neither Δ*nuoB* nor Δ*cyoE* had a significant impact on CoQ10 accumulation.

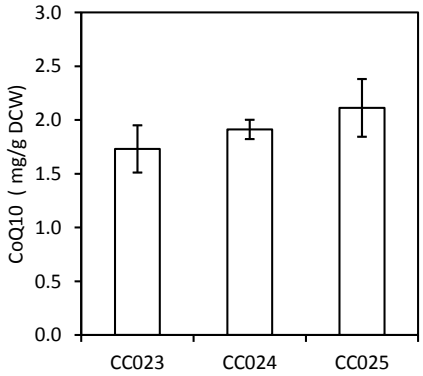

Figure 3.3 CoQ10 production in response to mutations in the aerobic respiratory chain
Strains CC023, CC024 and CC025 were grown for five days and sampled for CoQ10 production. Error bars show the standard deviation of three biological replicates.

3.3.3 *Effect of redox change on CoQ10 production*

Despite the absence of significant improvement in CoQ10 synthesis in strains carrying mutations in the respiratory chain (section 3.3.2) or grown on alternative carbon sources (section 3.3.1), I continued the investigation into possible interactions between CoQ10 production and central metabolism, shifting my focus towards redox homeostasis. To assess the effect of NADH availability on CoQ10 production, carbon sources with different oxidation states were tested. Gluconate (oxidation state: +1) metabolism bypasses the reduction of one mole of NADH per mole of substrate consumed, compared to glucose (oxidation state: 0). Conversely, the catabolism of sorbitol (oxidation state: -1) leads to the reduction of one mole of NADH more than glucose per mole consumed (Figure 3.4A) (Lin et al., 2005). The production of CoQ10 by CC023 increased over two-fold when grown on sorbitol, compared to glucose and gluconate (Figure 3.4B). These results suggested that a high NADH/NAD^+ ratio favors CoQ10 production, and prompted me to revisit the effect of the Δ*cyoE* and Δ*nuoB* mutations in the context of sorbitol metabolism. As shown by Figure 3.4C, strains CC024 and CC025, carrying the Δ*cyoE*

and Δ*nuoB* mutations, respectively, produced equivalent amounts of CoQ10 as CC023 on sorbitol. No direct connection could thus be established between the activity of NADH-dehydrogenase I, cytochrome *bo'* oxidase and the effect of sorbitol on CoQ10 production.

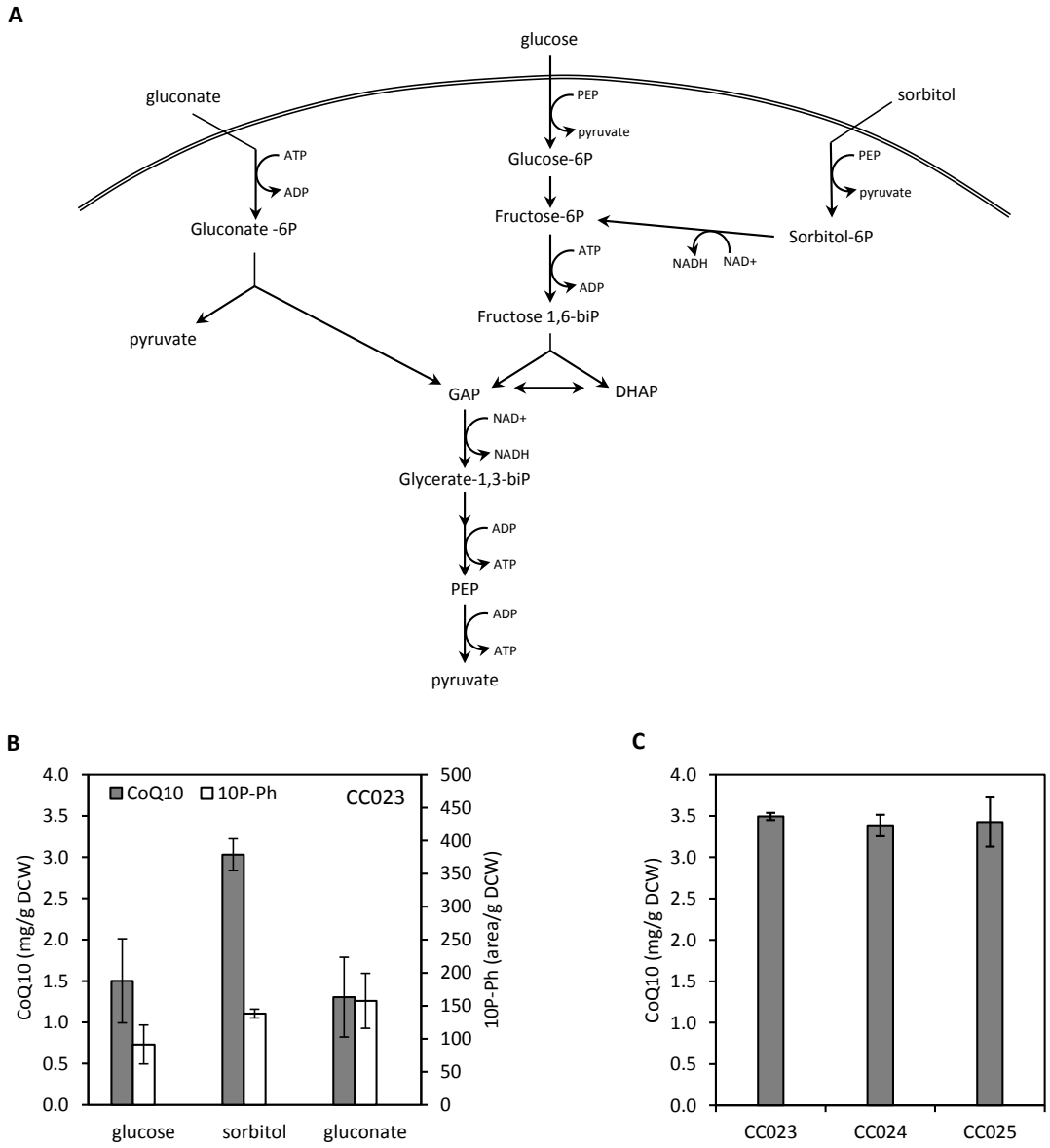

Figure 3.4 Effect of carbon substrates of different oxidation states on CoQ10 production

A) Catabolism of gluconate, glucose and sorbitol. Gluconate-6P, gluconate 6-phosphate; GAP, glyceraldehyde-3-phosphate; DHAP, dihydroxyacetone phosphate; glucose-6P, glucose 6-phosphate; fructose-6P, fructose 6-phosphate; fructose 1,6-biP, fructose-1,6-bisphosphate; glycerate-1,3-biP, glycerate 1,3-bisphosphate; PEP, phosphoenolpyruvate; sorbitol-6P, sorbitol 6-phosphate; ATP, adenosine triphosphate; ADP, adenosine diphosphate . **B**) CoQ10 (grey bars) and 10P-Ph (white bars) accumulation in strain CC023

following five days of aerobic flask fermentation on the indicated carbon substrate. **C**) CoQ10 production in strains CC023, CC024 and CC025 following five days of aerobic fermentation on sorbitol. Error bars represent the standard deviation of two (A) or three (B) biological replicates.

3.3.4 *CoQ10 production and metabolite excretion profile on sorbitol*

To investigate further the link between sorbitol metabolism and CoQ10 production, the accumulation of CoQ10 and of intermediate metabolites were followed over a time-course of five days. CC023 grew to slightly higher density on sorbitol (Figure 3.5B). Sorbitol was consumed at a lower rate, but over a longer period than glucose (Figure 3.5B). The production of CoQ10 in CC023 grown on sorbitol was sustained over 124 hours, whereas CC023 grown on glucose reached maximum CoQ10 content by 48 hours (Figure 3.5A). Strain CC023 produced over three-times more CoQ10 on sorbitol than on glucose, reaching 3.5 mg/g DCW of CoQ10. The accumulation pattern of PHB on glucose was characterized by the early excretion of 0.009 mM of PHB, of which 26% was consumed by 24 hours. On sorbitol, half of the secreted PHB was consumed between 24 and 51 hours, correlating with the two-fold increase in CoQ10 production observed during that period (Figure 3.5C). A drastic difference in acetate excretion was observed between the two conditions. Growth on glucose led to the accumulation of 80 mM acetic acid in the growth medium, while less than 10 mM of acetate was secreted during sorbitol fermentation, all of which consumed by 51 hours (Figure 3.5E). Minimum lactate was detected, under both conditions (Figure 3.5F). Up to 0.7 mM of pyruvate accumulated after 24 hours of growth on sorbitol, while only 0.4 mM was secreted by cells grown on glucose, after 100 hours of fermentation (Figure 3.5F). On both glucose and sorbitol, I observed the accumulation of an unidentified metabolite with strong absorption at 210 nm and 254 nm, named *Unknown 1*. Cells grown on sorbitol produced 2.4-fold more of

this compound compare to those grown on glucose, up to 51 hours. After this point, *Unknown 1* was consumed almost entirely by strain CC023 grown on sorbitol, while it remained stable in the glucose medium (Figure 3.5D). Analytical experiments using LC-MS were performed in order to identify *Unknown 1*, but were unsuccessful (Appendix, section A6).

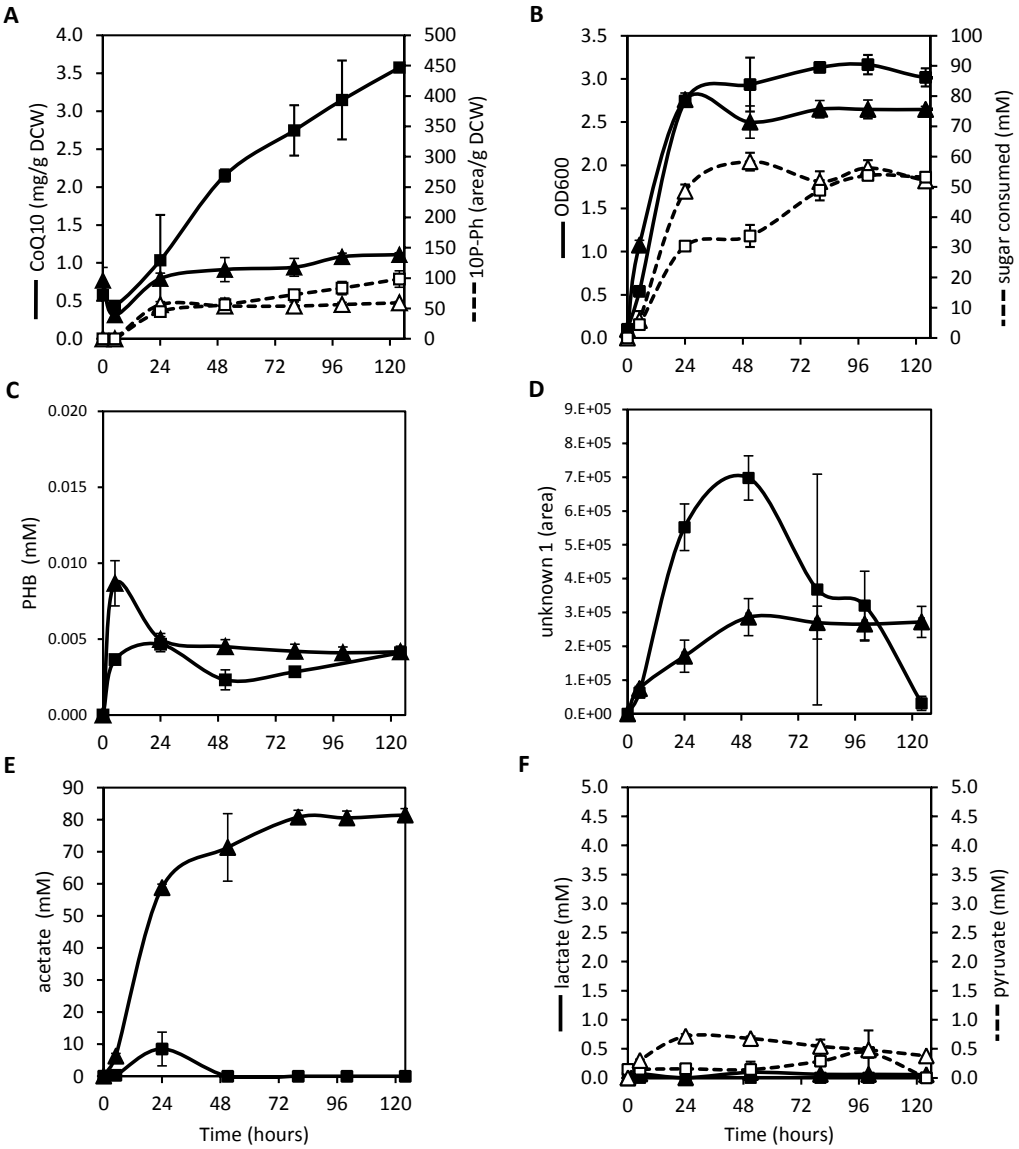

Figure 3.5 Time-course of CoQ10 production and metabolite secretion during aerobic flask fermentation on glucose and sorbitol (2012)
Strain CC023 was grown for five days on glucose (triangles) or sorbitol (squares), in August 2012. Samples were taken after 0, 5, 24, 51, 80, 100, and 124 hours to measure **A**) CoQ10 (filled shapes) and 10P-Ph (empty shapes) content **B**) optical density (filled shapes)

and sugar consumption (empty shapes) **C**) extracellular PHB **D**) extracellular *Unknown 1* **E**) extracellular acetate **F**) extracellular lactate (filled shapes) and pyruvate (empty shapes). Error bars show the standard deviation from three biological replicates.

3.3.5 *Elimination of acetate production pathways*

The most striking difference in metabolic profile between CC023 grown on sorbitol and glucose was the flux to acetate (Figure 3.5E). This prompted me to investigate the link between acetate production and CoQ10 accumulation. Two major biosynthetic pathways to acetate exist in *E. coli*: 1) the conversion of acetyl-CoA to acetyl phosphate by a phosphotransacetylase (encoded by *pta*) followed by the conversion of acetyl phosphate to acetate by an acetate kinase (*ackA*), yielding one adenosine triphosphate (ATP) and 2) the oxidation of pyruvate to acetate by pyruvate oxidase (*poxB*), with ubiquinone as an electron acceptor (Figure 3.1). The Pta-AckA pathway to acetate formation is mainly active during exponential phase, while *poxB* is up-regulated during late exponential and stationary phases (Dittrich et al., 2005). Two hypotheses drove my experimental design. First, as one mole of ATP is produced with each mole of acetate formed via the Pta-AckA route, the elimination of this pathway may lead cells to increase respiration to maintain ATP levels, indirectly triggering the up-regulation of the ubiquinone pathway. Alternatively, reducing acetate production, by eliminating both *ackA-pta* and *poxB*, may push more carbon towards CoQ10 intermediates. As fifteen moles of acetyl-CoA are required per mole of CoQ10 produced, I reasoned that a decrease in acetate production should translate in increased acetyl-CoA availability for the mevalonate pathway. To test these hypotheses, I introduced Δ*ackA-pta* alone or Δ*ackA-pta* Δ*poxB* in strain CC023, yielding CC026 and CC027, respectively (Table 3.1). These mutations had a slightly positive effect on biomass production in

CC027, compared to CC023 (Figure 3.6B). As expected, excreted acetate went down from 45 mM for CC023 to 15 and 7 mM for CC026 and CC027, respectively (Figure 3.6E). The downregulation of acetate biosynthetic pathways in CC026 and CC027 was compensated by an increase in lactate production, compared to CC023 (Figure 3.6F). Both CC026 and CC027 accumulated more pyruvate than CC023 (Figure 3.6G). The Δ*ackA-pta* mutation alone had no effect on CoQ10 production. However, CC023, carrying the mutations Δ*ackA-pta* Δ*poxB*, displayed a 1.5-fold increase in CoQ10 content. There was also a two-fold decrease in 10P-Ph accumulation in CC027 compared with CC023 (Figure 3.6A). Enhanced CoQ10 production in strain CC027 was correlated with a 3.2-fold increase in excretion of *Unknown 1*, compared to CC023 (Figure 3.6D). Overall, my results show that elimination of the ATP-yielding route (*ackA-pta*) to acetate production is not sufficient to improve CoQ10 content. Instead, both major acetate biosynthetic pathways must be deleted for CoQ10 production to go up.

Deleting the acetate biosynthetic pathways did not entirely mimic sorbitol metabolism, and the CoQ10 yields are not as high in CC027 as previously observed in CC023 on sorbitol (Figure 3.5A). No detectable PHB remained in the media by 24 hours, suggesting that it may have become limiting during fermentation (Figure 3.6C). *Unknown 1*, excreted and then consumed during growth on sorbitol (Figure 3.5D), remained at high concentration in the medium throughout fermentation of strain CC027 (Figure 3.6D). In addition, accumulation of lactate had not been observed in CC023 grown on sorbitol, and suggests that part of the carbon diverted from acetate excretion, instead of being channeled towards CoQ10 biosynthesis, is taking an alternative fermentation route (Figure 3.5F; Figure 3.6F).

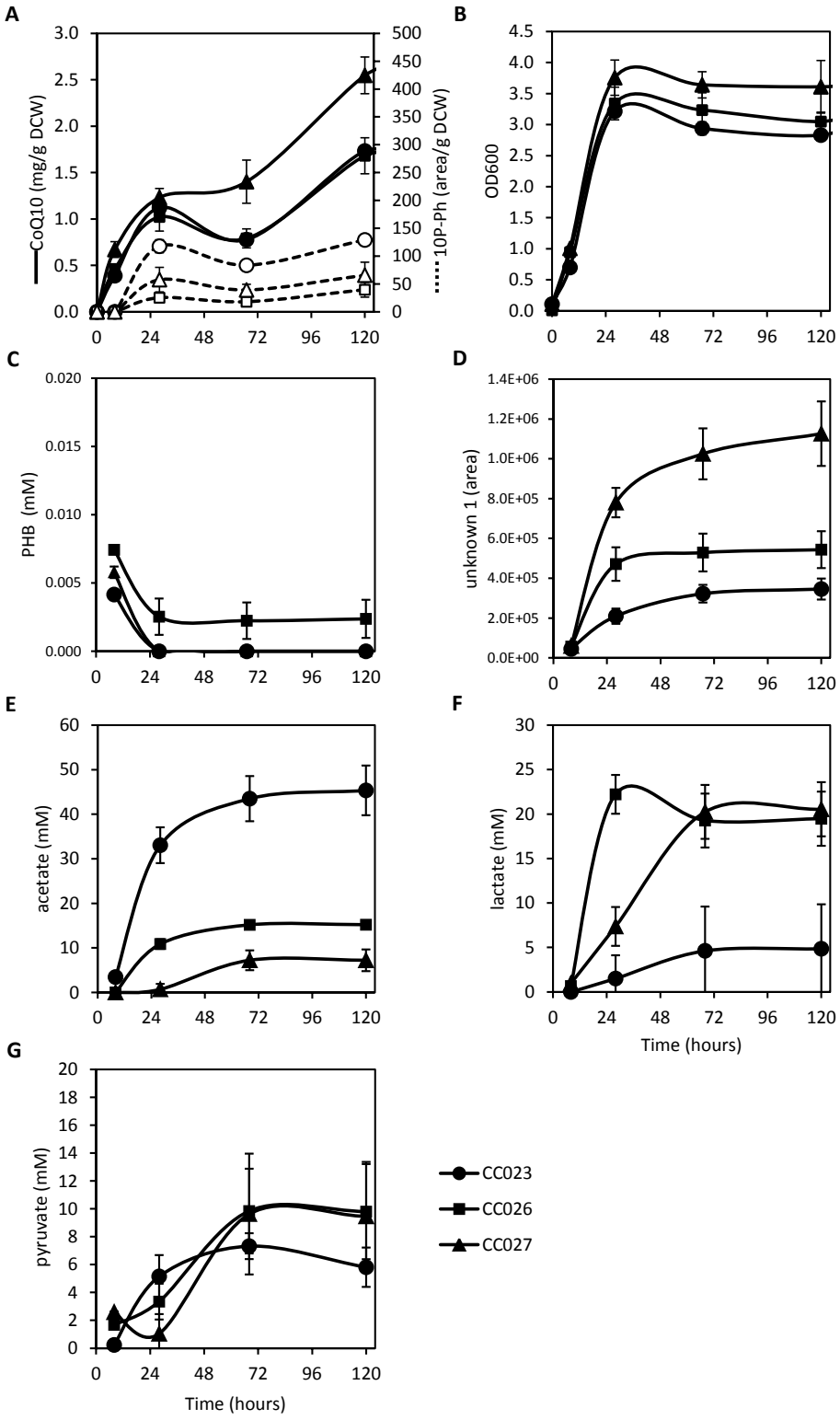

Figure 3.6 Time-course of CoQ10 production, growth, and metabolite accumulation following the deletion of acetate producing pathways

Strains CC023 (circles), CC026 (squares) and CC027 (triangles) were grown for five days on glucose. Samples were taken after 0, 8, 28, 68 and 120 hours to measure **A**) CoQ10 (filled shapes) and 10P-Ph (empty shapes) production **B**) optical density **C**) extracellular

PHB **D**) extracellular *Unknown 1* **E**) extracellular acetate **F**) extracellular lactate **G**) extracellular pyruvate. Error bars show the standard variation of three biological replicates.

As these experiments were carried out, a year after the experiments reported in sections 3.3.1 to 3.3.4, I started to observe increased variability between replicates, and sometimes significantly reduced accumulation of CoQ10 in my engineered strains. In particular, at this time, attempts to replicate experiments on sorbitol reported in sections 3.3.3 and 3.3.4 were unsuccessful, despite the reproducibility of the phenotype in initial experiments (see Appendix, section A3). The profile of excreted metabolites by the engineered strains also changed between 2012 and 2013. Notably, lactate and pyruvate excretion markedly increased in 2013 (Figure 3.4, Figure 3.5, Figure A 7).

3.3.6 *Elimination of lactate and acetate production pathways*

In an effort to direct carbon away from mixed-fermentation products and towards CoQ10 biosynthesis, the gene coding for lactate dehydrogenase, *ldhA*, was deleted and the mutation combined with the acetate biosynthesis mutations, yielding CC028 (Figure 3.1, Table 3.1). The *ldhA* knockout completely eliminated lactate production in strain CC028 (Figure 3.7G). However, this did not translate in increased CoQ10 production, compared to the inactivation of the acetate pathways alone, with both strain accumulating 2.5-3 mg/g DCW of CoQ10 (Figure 3.7A). In this experiment, I found one replicate of CC028 with significantly lower CoQ10 content, CC028c. As I had started to observe reduced reproducibility in my experiments using CoQ10 producing strains, the analysis of a culture with reduced CoQ10 production provided an opportunity to gain insight about this instability. Metabolite distribution was compared between the two tested strains and the CC028c outlier. The deletion of *ldhA* in CC028 resulted in higher

accumulation of pyruvate (Figure 3.7H). Pyruvate excretion reached 27 mM in CC028, and went up to 37 mM in CC028c, a 1.9-fold increase compared to CC027 (Figure 3.7F). The accumulation of pyruvate was inversely correlated with the glucose uptake, which reached 135 mM in CC027 but only 88 mM and 65 mM in CC028 and CC028c, respectively (Figure 3.7C). PHB production went up to 0.005-0.007 mM PHB, consumed within 53 hours by CC027 and CC028, but not by CC028c which only consumed one third the secreted PHB over the course of fermentation (Figure 3.7D). The levels of *Unknown 1* were also three times lower in CC028c compared to CC027 and CC028, correlating with lower CoQ10 production in CC028c (Figure 3.7B, E). Overall, my results show that the elimination of the lactate biosynthetic route, in a Δ*ackA-pta* Δ*poxB* background, introduces a bottleneck at the pyruvate node, restricting carbon flux towards CoQ10 production. This effect is exacerbated in CC028c, where even higher pyruvate secretion is associated with lower glucose uptake, reduced PHB consumption and inferior CoQ10 content.

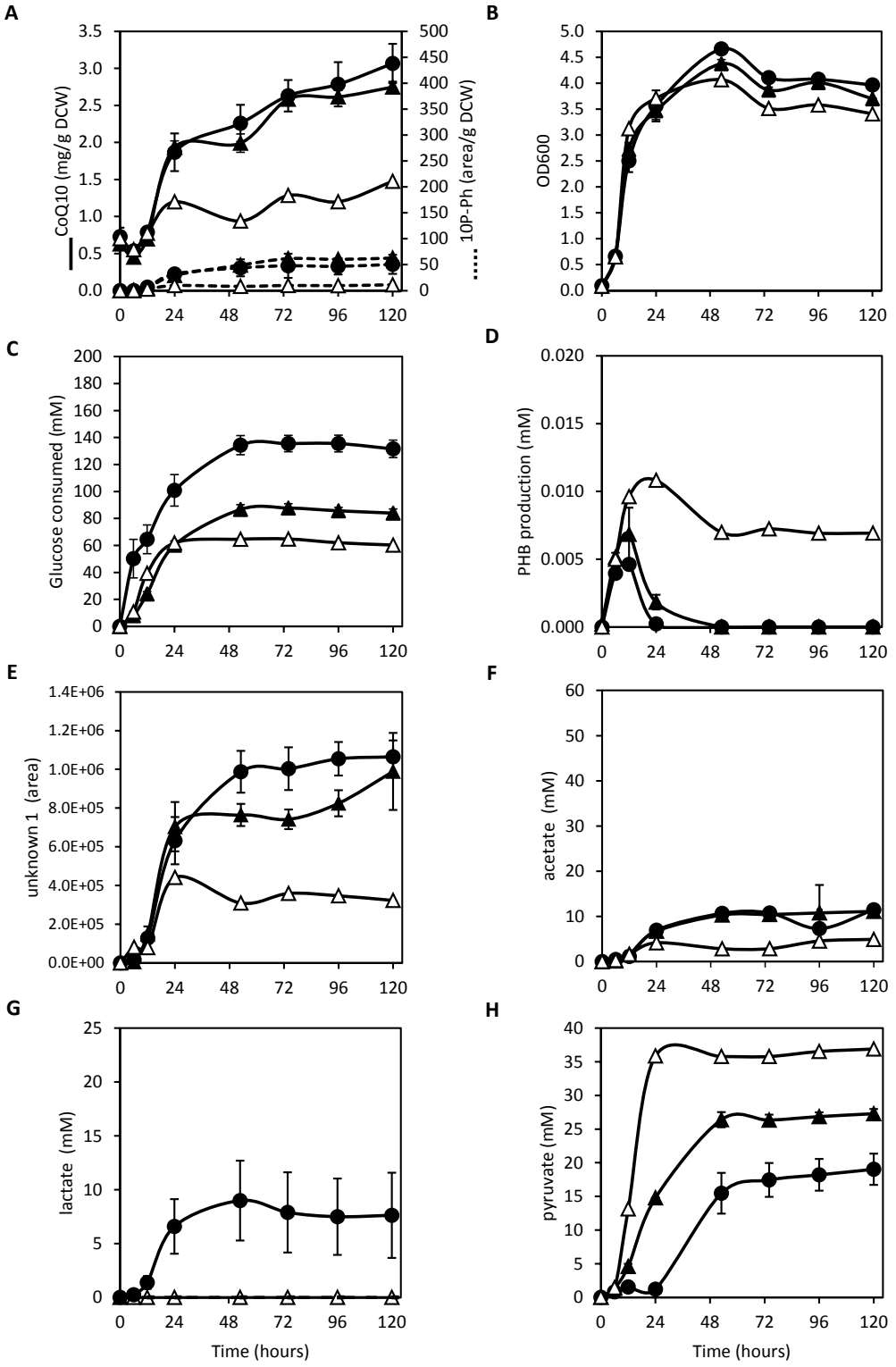

Figure 3.7 Time-course of CoQ10 production, growth, glucose uptake and metabolite secretion following the deletion of acetate and lactate production pathways
Strains CC027 (full circles) and CC028 (full triangles, empty triangles for CC028c) were grown for five days on glucose. Samples were taken after 0, 6, 12, 24, 53, 74, 96 and 120 hours to measure **A**) CoQ10 (full lines) and 10P-Ph (dashed lines) production **B**) optical

density **C**) glucose uptake **D**) extracellular PHB **E**) extracellular *Unknown 1* **F**) extracellular acetate **G**) extracellular lactate **H**) extracellular pyruvate. Error bars show the standard deviation of two or three biological replicates.

3.3.7 *Increasing the production of PHB*

In order to accommodate the expression of the plasmid pMtSa, I had chosen to transfer the recombinant top aromatic operon on *E. coli*'s chromosome (section 2.3.6). This had translated in a significant decrease in PHB production (Figure 3.5E), but the aromatic precursor remained in excess. Metabolite analyses presented in sections 3.3.5 and 3.3.6 show that while the amount of PHB excreted during exponential phase remained the same, the aromatic molecule was then entirely consumed from the fermentation medium by 24 hours, suggesting that PHB may become rate-limiting during the CoQ10 production phase, which typically extends up to 120 hours. In order to increase flux through the aromatic pathway, I inserted an additional copy of the upper aromatic operon on the plasmid pMtSa, yielding pMtSaLTAA. This plasmid was introduced in the CoQ10 production strain CC028, yielding CC029 (Table 3.1). Again, there was variability between replicates. CC028 produced less CoQ10 than previously reported, with only 1.5 mg/g DCW of CoQ10, similarly as CC028c in the experiment reported in section 3.3.6 (Figure 3.7A, Figure 3.8B). Despite a 2.9-fold increase in initial PHB production compared to CC028, strain CC029 had comparable CoQ10 content as CC028, except for one replicate, CC029b, which accumulated up to 2.7 mg/g DCW of CoQ10 (Figure 3.8B, C). Secretion of *Unknown 1* in CC028 and CC029 was similar to what I had observed before in strains accumulating lower levels of CoQ10, except for CC029b, which accumulated 2.4 times more of *Unknown 1* (Figure 3.8D). Similarly to what was reported for CC028 in section 3.3.6, all strains excreted more than 26 mM

pyruvate (Figure 3.7H, Figure 3.8E). In agreement with the genotype of the tested strains, no significant accumulation of acetate and lactate was observed in the growth medium (not shown).

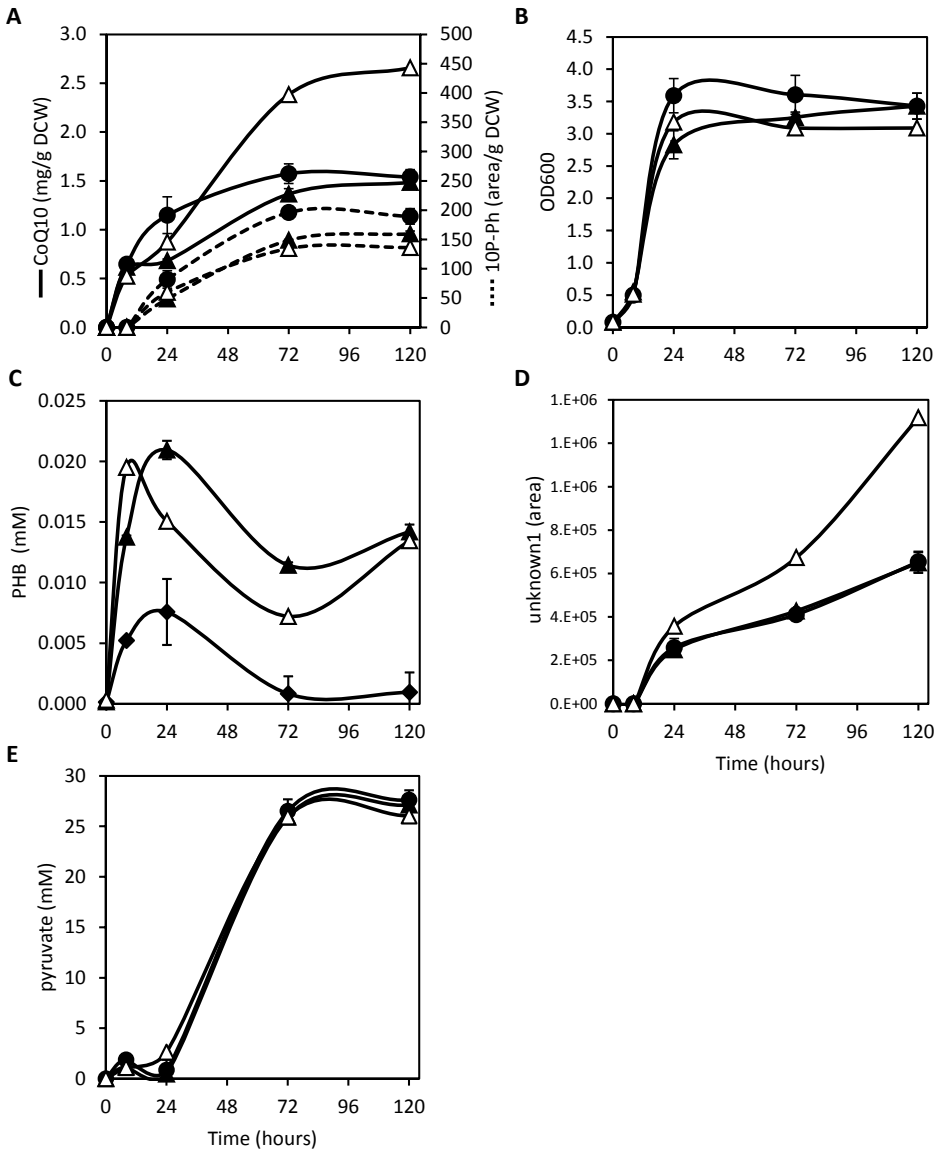

Figure 3.8 Time-course of CoQ10 production, growth and metabolite secretion following the expression of a plamid-localized copy of the upper aromatic operon
Strains CC028 (filled circles) and CC029 (filled triangles, empty triangles for CC029b) were grown for five days on M9-glucose medium. Samples were taken after 0, 24, 72, and 120 hours to measure **A**) CoQ10 (full lines) and 10P-Ph (dashed lines) production **B**) optical density **C**) extracellular PHB **D**) extracellular *Unknown 1* **E**) extracellular pyruvate. Error bars show the standard deviation of two or three biological replicates.

3.4 **Discussion**

In this chapter, I investigated how central metabolism may influence CoQ10 production, either directly by increasing fluxes through the engineered precursor

pathways, or indirectly by triggering upregulatory mechanisms for ubiquinone accumulation.

3.4.1 *Modulations in CoQ10 production using selected carbon sources*

The source of carbon available to *E. coli* is expected to result in variations of intracellular metabolic fluxes (Holms, 1996). In addition, transcriptional activity may be differentially modulated by alternative substrates, due to catabolite repression. My hypothesis was that carbon sources such as glycerol, pyruvate or succinate may enhance the production of CoQ10 in CC023, thereby shedding light on unknown control mechanisms limiting the production of CoQ10 in my engineered strain. None of the carbon source tested led to increased CoQ10 production in strain CC023. However, differences were observed in the growth rate and final biomass obtained on these substrates compared to glucose (Figure 3.2). As the engineered pathways consume increased amounts primary metabolites (PEP, E4P, acetyl-CoA), less energy-efficient carbon sources than glucose requiring the onset of gluconeogenesis reactions may difficultly sustain growth. Variations in CoQ10 production and growth between experiments may also reflect high selection pressure for mutations resulting in decreased flux to CoQ10, to either maintain pools of primary metabolites (PEP, E4P, acetyl-CoA) or to bypass the accumulation of toxic compounds (CoQ10 or intermediates) (see Appendix, section A2). Overall, these experiments provided the first clues that the dual pull on PEP and acetyl-CoA exerted by the engineered pathways, or the accumulation of CoQ10, create a burden on the primary metabolism of my engineered strains.

3.4.2 *Altering the electron transport chain for CoQ10 production*

The introduction of mutations in *nuoB* and *cyoE* intended to mimic restrictions in electron flux through the respiratory chain susceptible to trigger an upregulation of CoQ10 production. This hypothesis was based on reports that microaerobic conditions or treatment with respiration inhibitors stimulate CoQ10 production in microbes (Choi et al., 2005; Ha et al., 2007b; Seo and Kim, 2010). However, I did not observe differences in CoQ10 production in strains CC024 and CC025, bearing the Δ*cyoE* and Δ*nuoB* mutations, respectively, compared to CC023. As illustrated in Figure 3.1, the respiratory chain of *E. coli* is complex and redundant, with multiple NADH dehydrogenases and terminal oxidases, whose expressions vary depending on oxygen availability. A more systematic study including multiple combinations of mutations may be more appropriate to restrict electron flux through the respiratory chain in *E. coli*. An additional caveat in my hypothesis is that the positive effects of azide and microaerobic conditions on CoQ10 production were only observed in *R. radiobacter* and *R. sphaeroides*. These naturally high producers of CoQ10 use cytochrome *c*, in addition to ubiquinone, but unlike *E. coli* lack naphthoquinones. Such inherent differences may influence the cell's response to restricted flux in the electron transport chain. In addition, *E. coli* uses the redox state of its ubiquinone pool as a signal for the onset of aerobic/anaerobic metabolism (Georgellis et al., 2001). Promoter studies with different genes of the ubiquinone pathway have shown that the biosynthesis of ubiquinone is under the control of central transcriptional regulators including ArcA/B and FNR (Kwon et al., 2005; Soballe and Poole, 1997; Zhang and Javor, 2003). The accumulation of 10P-Ph, under conditions where the production of both PHB and isoprenoid precursors are deregulated, also points towards

an intrinsic regulation system that prevents the accumulation of high amounts of CoQ10 in engineered *E. coli*. The maximum CoQ10 content obtained in strain CC023, 3.5 mg/g (Figure 3.4C, Figure 3.5A), is comparable to what was previously reported in *E. coli* using different engineering strategies (Huang et al., 2011; Zahiri et al., 2006b). There may therefore be significant physiological restraints to maintain the ubiquinone pool within a given size range.

3.4.3 *Sorbitol and the production of increased levels of CoQ10*

The effect of sorbitol on CoQ10 production reported in sections 3.3.3 and 3.3.4 demonstrates that central metabolism can influence the synthesis of this antioxidant. Sorbitol has a lower oxidation state than glucose, and its catabolism produces more reducing equivalent, in the form of NADH. Under anaerobic conditions, to achieve redox balance, *E. coli* grown on sorbitol directs carbon flow towards the synthesis of more reduced products, typically ethanol and lactate, at the expense of acetate (Lin et al., 2005; San et al., 2002). Little is known about sorbitol metabolism under aerobic conditions. I observed a marked decrease in acetate production when CC023 was grown on sorbitol, but no ethanol was detected and I was not able to identify a more reduced product accumulating in the growth medium (Figure 3.5). It is possible that cells were able to achieve redox balance by increasing the activity of the aerobic respiratory chain. However, the Δ*nuoB* and Δ*cyoE* mutations did not alter fluxes to acetate (not shown). Therefore, it is unclear whether this mechanism is used to achieve redox homeostasis. Flux analysis of *E. coli* grown on fructose reveals a metabolic partition where no carbon goes to acetate, but acetyl-CoA is instead redirected to the TCA cycle (Holms, 1996).

Similarly, *E. coli* B strains secrete less acetate because of an upregulation of the glyoxylate bypass, resulting in more acetyl-CoA being pulled by the TCA cycle (van de Walle and Shiloach, 1998). Although I was not able to resolve TCA cycle intermediates with confidence in my analysis, I found that the secretion of molecules that may correspond to citrate, isocitrate α-ketoglutarate or oxaloacetate, displayed a different pattern on sorbitol compared to glucose (see Appendix, Figure A 8). It is possible that on sorbitol, CC023 maintained anaplerotic fluxes and TCA cycle activity after growth arrest, resulting in sustained glucose uptake, glycolysis and carbon flux towards CoQ10 biosynthesis throughout fermentation, and well beyond the stationary phase. It is also possible that increased CoQ10 production is solely linked to the higher availability of acetyl-CoA resulting from reduced flux to acetate. Enhanced CoQ10 production in a Δ*ackA-pta* Δ*poxB* mutant, CC027, supports this hypothesis (Figure 3.6). Alternatively, transcriptional upregulation of the ubiquinone pathway, in response to the altered redox status or to pH, may also play a role in enhancing CoQ10 biosynthesis. More precise analyses of intracellular metabolites, enzymatic activity, and transcriptional activity would be required in order to fully understand the link between sorbitol and CoQ10 production in CC023. My incapacity to observe the same phenotype on sorbitol in 2013 precluded such an investigation. On both glucose and sorbitol, metabolic activity in CC023 appeared changed between 2012 and 2013. On glucose, in 2013, less PHB was excreted into the medium, and more pyruvate and lactate were secreted, at the expense of acetate (Figure A 7). On sorbitol, more PHB was secreted in the medium early during fermentation compared to 2012, suggesting that the aromatic pathway was active, but that the PHB produced was not incorporated into CoQ10 (Figure A 7). My analysis is clearly

hindered by the lack of information about the production of isoprenoid precursors in CC023. A comparison of the accumulation pattern of FPP/DPP might not only have provided clues on the mechanism behind the positive effect of sorbitol on CoQ10 production, but also on the absence of this effect observed in 2013.

3.4.4 *Elimination of acetate and lactate production pathways to enhance CoQ10 production*

I was able to partially reproduce the phenotype first observed on sorbitol by deleting acetate production pathways, suggesting at least a coincidental link between CoQ10 and acetate secretion. However, there are differences in metabolic flux distribution between CC027 (Figure 3.6) and CC023 on sorbitol (Figure 3.5). In particular, the accumulation of pyruvate in CC027 was not observed on sorbitol. Secretion of pyruvate has been reported in strains carrying the Δ*pta* or Δ*ackA-pta* Δ*poxB* mutations, and has been proposed to result from the inhibition of pyruvate dehydrogenase (Dittrich et al., 2005; Kakuda et al., 1994). The accumulation of pyruvate was further enhanced by preventing lactate production (Δ*ldhA*), especially in CC028c, which correlated with decreased glucose uptake, and lower CoQ10 content (Figure 3.7A, C). As strain CC028 cannot recycle NADH to NAD^+ using lactate dehydrogenase, a high NADH/NAD^+ ratio may result in the inhibition of pyruvate dehydrogenase by NADH (Figure 3.1) (Schmincke-Ott and Bisswanger, 1981), leading to the observed accumulation of pyruvate. Supporting this hypothesis, I was able to decrease pyruvate secretion in CC027 using fed-batch fermentation, where oxidative respiration and NADH recycling to NAD^+ is favored by limiting the glucose supply (see Appendix, Figure A 10). The accumulation of pyruvate in aerobic flask fermentation reduces the

PEP/pyruvate ratio, which may lead to lower glucose uptake (Liao et al. 1996, Patnaik et al. 1992). The activity of pyruvate dehydrogenase also controls flux to acetyl-CoA, and to the mevalonate pathway. There might therefore be high selective pressure to downregulate flux to this foreign metabolic branch. I succeeded in increasing the production of CoQ10 by abrogating acetate biosynthesis, but it remains unclear whether this is due to a larger pool of acetyl-CoA being pulled by the mevalonate pathway, or by indirect effects on the activity of the ubiquinone pathway. As previously mentioned, an analysis of isoprenoid accumulations patterns should provide clues to answer that question.

3.4.5 *Availability of PHB for CoQ10 production*

The five-days flask fermentations were often characterized by the secretion of PHB during the first 24 hours, followed by its complete consumption between 48 and 120 hours (Figure 3.6C, Figure 3.7D, Figure A 7C). This suggests that the aromatic precursor may have become limiting to CoQ10 production in these experiments. Extracellular PHB was notably lower than what was previously reported on M9 medium supplemented with yeast extract, and reported in Chapter 2. The use of minimal medium for CoQ10 production thus appears to restrain flux through the aromatic pathway, perhaps due to increased demand for aromatic amino acids. In previous experiments, extracellular PHB concentration also remained more or less stable between 24 and 120 hours of fermentation, despite a concomitant increase in CoQ10 content (Figure 3.5, Figure 2.9). It is possible that in later experiments, PHB production was sustained throughout fermentation and channeled directly to the ubiquinone pathway, bypassing the excretion

of this organic acid. The complete consumption of PHB, observed only in experiments performed in 2013, may reflect mutations resulting in lower PHB production during the stationary phase. As mentioned before, there might be high selective pressure to decrease flux of PEP through the engineered aromatic pathway. In order to enhance the activity of the shikimate pathway, I added a copy of the top aromatic operon into pMtSa, and expressed the resulting plasmid in strain CC029. The fermentation of strains CC028 and CC029, except CC029b, was characterized by delays in the accumulation pattern of *Unknown 1* and CoQ10 compared to previous experiments, which again may be the result of unknown mutations (Figure 3.8). The increased PHB production in strain CC029, even in CC029b, did not concur with enhanced CoQ10 contents, compared to those previously observed (Figure 3.8A). This suggests that the availability of PHB is not limiting CoQ10 production in my engineered strains.

3.4.6 *Reproducibility and strain stability*

Early in this investigation, I observed that my production strains did not display reproducible patterns of growth, metabolite accumulation and CoQ10 production. High fluxes towards the aromatic pathway and the foreign mevalonate pathway are certainly creating a burden on *E. coli*'s metabolism. Both PEP and acetyl-CoA, the primary substrates of the aromatic and mevalonate pathways, respectively, play pivotal roles in central metabolism. PEP is required for the uptake of several carbon substrates, and flux partitioning of PEP between pyruvate and oxaloacetate defines the balance between biomass production, TCA cycle activity and acetate secretion (Figure 3.1) (Liao et al., 1994). Acetyl-CoA plays an equally crucial role, at the branchpoint between glycolysis,

respiration (via the TCA cycle) and fermentation (via acetate production). The faith of these two metabolites is also interdependent: flux of acetyl-CoA to the TCA cycle requires the concomitant conversion of PEP to oxaloacetate, and accordingly, acetyl-CoA activates PEP carboxylase (Chang et al., 1999; Liao et al., 1994). The pull on these two metabolites exerted by the synthetic mevalonate and aromatic pathways in strain CC023 and its derivatives may lead to stochastic metabolic responses. There might also be high selective pressure to restrict fluxes to these deregulated pathways. In order to simplify my interpretation of metabolite accumulation, I had chosen to carry all experiments in minimal media. By doing so, cells had to use the chosen substrate for all biosynthetic reactions as well as for energy production, which may have exacerbated the selective pressure to divert carbon away from the engineered pathways. In Chapter 2, I had demonstrated that expression of the synthetic operons did not require the addition of IPTG, even when grown on glucose (section 2.3.8). It is possible that the burden exerted by fluxes towards mevalonate and PHB would have been curtailed by more stringent transcriptional control of expression. By inducing their expression late in exponential phase, or in stationary phase, the selective pressure to divert carbon flux away from these secondary pathways could have been minimized. There might also be plasmid instabilities in the engineered strains expressing the three recombinant plasmids, pTUbiA$_e$DPS$_o$, pMBIS and pMtSa. Decreased plasmid retention, especially in fermentation lasting several days, has been reported when plasmids derived from the same vector backbones as those used in this study were co-expressed (Anthony et al., 2009). Individual plasmid stability should therefore be assessed in the CoQ10 production strains, in order to ensure their compatibility and sustained expression.

Finally, the secretion pattern of *Unknown 1* shows that this unidentified metabolite is produced concurrently to CoQ10 (Figure 3.6D, Figure 3.7E, Figure 3.8D). A notable exception to this was observed on sorbitol, were *Unknown 1* accumulated for up to 51 hours, and was thereafter consumed from the growth media (Figure 3.5D). This led me to hypothesize that *Unknown 1* was a ubiquinone intermediate, but my inability to extract this compound using hexane does not support such a model (Appendix, section A6). Alternatively, *Unknown 1* may share precursors with CoQ10, and accumulate by pulling intermediates formed via the engineered pathways. The absorption of *Unknown 1* at 254 nm suggests that it could be an aromatic molecule, but I was unable to identify the compound by mass spectrometry (see Appendix Figure A 11). Future identification of *Unknown 1* may clarify the link between sorbitol metabolism, acetate biosynthesis and CoQ10 production. It may also shed light on an imbalance within the synthetic pathways, allowing potential improvements of the engineering strategy.

The premise of this Chapter was that the "base strain", CC023, could be used to develop novel strategies to increase CoQ10 production, by harnessing endogenous control mechanisms of carbon fluxes and ubiquinone biosynthesis. However, inherent engineering problems in this production strain, leading to instabilities and precursor imbalance, have added too many layers of complexity to the results to obtain a clear picture of the interplay between *E. coli*'s central metabolism and CoQ10 production. Nevertheless, these experiments have opened several avenues of investigation regarding a link between sorbitol catabolism, flux to acetate, and CoQ10 biosynthesis, which should be pursued following the optimization of the production strains.

Chapter 4. Conclusion and future directions

The central hypothesis of this thesis was that the identification and upregulation of rate-limiting steps in CoQ10 biosynthesis had the potential to result in unprecedented accumulation of this molecule in *E. coli*. Moreover, by investigating metabolic or physiological factors influencing the synthesis of CoQ10 in *E. coli*, I hoped to gain insight for the design of novel engineering strategies to maximize carbon flux towards CoQ10 biosynthesis. Several original findings were obtained throughout this project, opening opportunities for future research to optimize *E. coli* as a production platform for CoQ10.

I was able to significantly enhance the production of CoQ10 by increasing the supply of aromatic and isoprenoid precursors in *E. coli*, and by overexpressing UbiA, the enzyme responsible for the prenylation PHB. However, specific CoQ10 contents in the engineered strains remained relatively low considering that PHB was produced in molar excess and that the efficiency of the mevalonate pathway (expressed via pMtSa and pMBIS) to produce isoprenoids is well documented (Ma et al., 2011). This strongly suggests that a portion of the carbon flux directed towards CoQ10 biosynthesis was in fact diverted to by-products. The accumulation of *Unknown 1*, reported in Chapter 3, supports this hypothesis. In order to better characterize flux through the engineered pathways, it will be primordial to conduct experiments where both aromatic and isoprenoid intermediates are quantified. In particular, the complete turnover of FPP/IPP into DPP by the heterologous DPS_o needs to be ensured. To this end, analytical methods have to be developed for the quantification of DPP *in vivo*. In addition, visualizing

detailed carbon partitioning using metabolic flux analysis could reveal the existence of competing reactions or of additional bottlenecks in the engineered pathways. Further optimization of gene expression or enzyme activity may henceforth be necessary.

The deregulated production of aromatic and isoprenoid precursors led to the accumulation of 10P-Ph, shedding light on a previously unknown bottleneck in the ubiquinone pathway. As discussed in Chapter 2, enzymes of the ubiquinone pathway form a putative complex and inadequate activity of several members of this complex may lead to an accumulation of 10P-Ph. My results show that increasing PHB prenyltransferase (UbiA) activity restrains the accumulation of 10P-Ph. However, increasing the activity of the putative monooxygenase UbiI has no effect on 10P-Ph production. To abrogate 10P-Ph accumulation altogether, an extensive investigation of interactions between enzymes of the ubiquinone pathway will be required. In addition, the overexpression of different combinations of Ubi genes in an engineered *E. coli* strain where the production of aromatic and isoprenoid precursors is deregulated may lead to the identification of a group of enzymes required to channel 10P-Ph towards CoQ10.

By investigating the interplay between central metabolism and CoQ10 biosynthesis in my engineered strains, I found a link between sorbitol catabolism and the production of CoQ10. My results suggest that this link is articulated, directly or indirectly, around the marked reduction in acetate excretion observed during growth on sorbitol. Supporting this hypothesis, higher CoQ10 contents were also observed following the deletion of the two main acetate production pathways. In order to understand the biology behind these observations, it will be necessary to test the impact sorbitol catabolism, as well as of a Δ*ackA-pta* Δ*poxB* background, on fluxes towards PHB

or towards mevalonate, in engineered strains expressing these synthetic pathways independently. Comparative analyses of transcriptional and metabolic activity in these conditions may also shed light on indirect effects of reduced acetate production or altered redox status on the expression of genes of the ubiquinone pathway.

Importantly, these future experiments entail the development of stable engineered strains. As documented in Chapter 3, the engineered strains expressing both the deregulated aromatic pathway and the complete mevalonate pathway appeared to be prone to instabilities and mutations, perhaps because of the dual pull on PEP and acetyl-CoA. To my knowledge, it is the first instance where two major intermediates of central carbon metabolism are simultaneously diverted towards foreign or deregulated pathways. The pressure exerted by these abnormal fluxes may lead to the selection of mutations in the engineered strains. Metabolic flux analyses would certainly provide insight regarding the source of these instabilities and the nature of the selected mutations. Once understood, deleterious effects could be circumvented by modulating the intensity and the timing of expression the engineered genes.

Despite the development of rational engineering strategies, the strains developed for this thesis were able to accumulate up to 3.5 mg/g CoQ10, which falls in the same range as the specific contents reported in other studies (Huang et al., 2011; Zahiri et al., 2006b). These yields fall below those obtained with *R. radiobacter* and other natural producers of the molecule. It follows that there may be unknown intrinsic factors specific to *E. coli* that prevent the accumulation of high amounts of ubiquinone. Such factors may include the ability to spatially accommodate excess ubiquinone in the inner membrane, unique regulatory mechanisms to maintain ubiquinone concentrations within a precise

range, and native properties of the respiratory chain. The strains of *R. radiobacter* and *R. sphaeroides* that have been isolated for their high CoQ10 content may provide the key to unraveling the underlying mechanisms that favor the production of CoQ10 in microbes. Comparative genomic and metabolomic investigations of the ubiquinone pathway and of the respiratory chain in these species may elucidate the inherent abilities of these organisms to accumulate CoQ10 in their membrane. Lessons learned from these high producers may then be applied to inverse engineering industrially-suitable hosts such as *E. coli*. Overall, a better understanding of the limiting factors in the accumulation of ubiquinone in *E. coli* will be essential for this organism to become a suitable platform for the industrial production of CoQ10.

Appendix

This appendix contains a selection of experimental data that was judged incomplete, non-reproducible, non-conclusive or hampered by technical difficulties. It is included here to support certain arguments articulated in Chapters 2 and 3, as well as in an effort to leave a clear and complete record of the work accomplished as part of this thesis.

A1. *Protein purification of $DPS_{S.bae}$*

I had originally intended to characterize the enzymatic activity of $DPS_{S.bae}$ *in vitro*, and have, to this end, purified $DPS_{S.bae}$ proteins from *E. coli* cultures. This part of the project was not pursued because of the relatively low impact of this type of study, and because the complementation of Δ*ispB* by DPS_o (section 2.3.1) provided proof of the functionality of the isolated gene.

The $dps_{S.bae}$ gene retrieved by inverse PCR from the genomic DNA of *S. baekryungensis* had two putative start codons, and no recognizable ribosome-binding site, which originally prompted me to clone two versions of $dps_{S.bae}$: *dps-L* and *dps-S*. These two open-reading frames were cloned into the vector pET19b (Novagen) using 5' *Nde*I and 3' *Bam*HI restriction sites, yielding pET-DPS-S and pET-DPS-L. I then overexpressed and purified both proteins. Colonies of *E. coli* BL21(DE3) expressing pET-DPS-L, pET-DPS-S or pET19b (empty vector control) were inoculated into 4 mL LB broth and incubated with shaking for four hours at 37ºC, to an OD_{600} of 1.8. One mL from these starting cultures was then transferred to 100 mL LB and incubated at 30ºC for

an additional four hours, to an OD_{600} of 0.9. The temperature of the cultures was rapidly brought down to 20ºC on ice, at which point cultures were induced with 0.4 mM IPTG. The cultures were then incubated overnight at 20ºC. The following day, cells were pelleted by centrifugation and suspended in 10 mL 50 mM Tris pH=7.5 and 1 mM phenylmethylsulfonyl fluoride and sonicated using a Sonic Dismembrator (Fisher Scientific) at an amplitude of 3, for 1 minute and 40 seconds (pulsar ON for 5 seconds, pulsar OFF for 15 seconds). The soluble and insoluble fractions were isolated by centrifugation at 16100 x g using a microcentrifuge. Aliquots (35 µL) of the soluble and insoluble fractions in sample loading buffer (50 mM Tris-HCl pH=6.8, 10% glycerol, 2% SDS, 0.001% bromophenol blue, 100 mM DTT) were ran on a 12% SDS-PAGE gel. His-DPS-L was detected in the soluble fraction and had the expected size of ~39.6KDa, as determined by the ExPASy Compute PI/MW tool (http://ca.expasy.org/tools/pi_tool.html). His-DPS-S was detected in the insoluble fraction, at the expected size of ~36.6 kDa (Figure A 1A).

His-DPS-L, expressed in a soluble form, was further purified by immobilized metal affinity chromatography. The remaining soluble fraction of pET-DPS-L (~5ml) was prepared for purification by addition of 500 µL 10X lysis buffer (500 mM NaH_2PO_4, 3M NaCl, 100 mM imidazole). The lysate was added to a column containing 10 mL of Ni-sepharose slurry. The column was then washed eight times with 5 mL washing buffer (50 mM NaH_2PO_4, 300 mM NaCl, 20 mM imidazole). The protein was eluted with 5 mL elution buffer (50 mM NaH_2PO_4, 300 mM NaCl, 250 mM imidazole), and 25 one-mL fractions were collected. Thirty-five µL of each fraction was run on a 12% SDS-PAGE gel. Fractions 10 and 11 contained most of His-DPS-L (Figure A 1B).

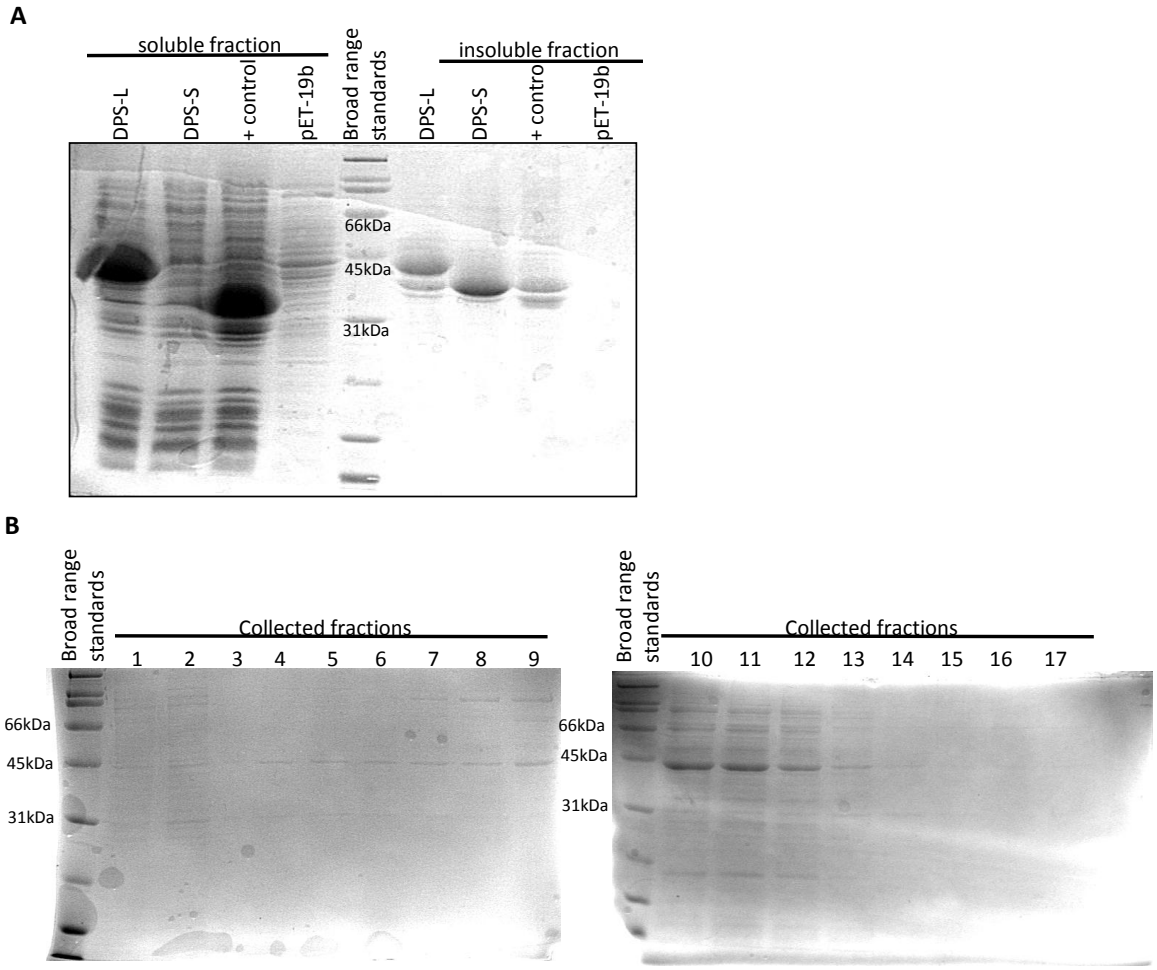

Figure A 1 Protein purification of DPS*S.bae*
A) SDS-PAGE analysis of BL21(DE3) crude protein extracts following His-DPS-L and His-DPS-S expression **B)** Elution fractions analysis by SDS-PAGE following metal-affinity purification of His-DPS-L.

A2. *Effect of selected carbon sources on growth and CoQ10 production*

As mentioned in section 3.3.1, several attempts have been made to compare CoQ10 production between CC023 cultures grown on different carbon substrates. In addition to the experiment presented in section 3.3.1 (Figure 3.2), the following experiments were also documented, and are included here to illustrate the challenges encountered. These experiments were conducted in fermentation medium (Tsuruta et al.,

2009), as described in section A4, in order to facilitate eventual comparisons between flask fermentations and fed-batch fermentations in bench-top fermentors. It was later realized that the use of fermentation medium in flask experiments was undesirable because of its poor buffering capacity, which resulted in high variability between replicate experiments. Fermentation medium was therefore replaced by M9 medium in experiments presented in the main body of this thesis.

The experiment shown in Figure A 2 was done in fermentation medium, supplemented with 0.06 % casamino acids and 150 mM of the selected carbon source.

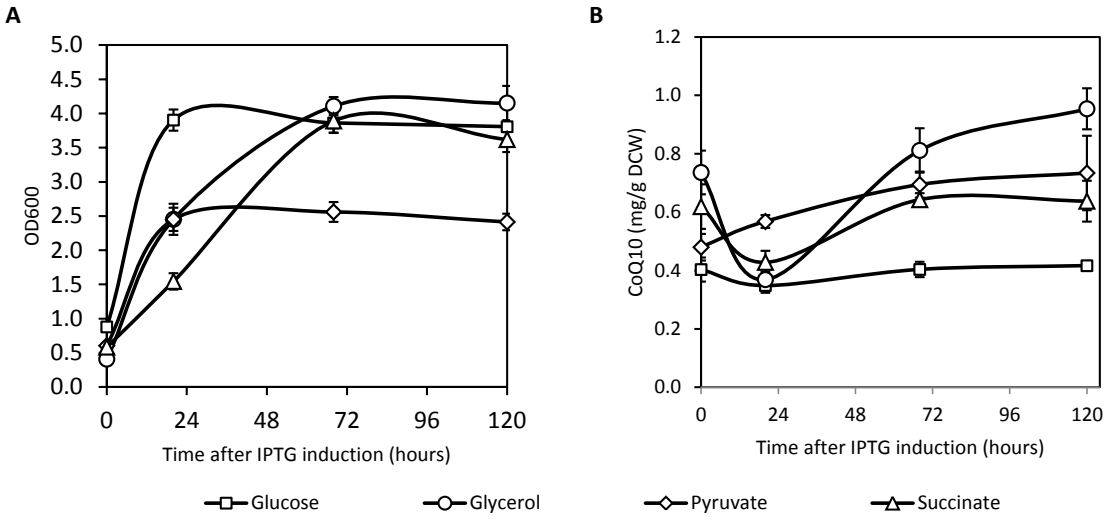

Figure A 2 Growth and CoQ10 production on fermentation medium supplemented with casamino acids and selected carbon sources
Strain CC023 was grown for five days with 150 mM of either glucose (squares), glycerol (circles), pyruvate (diamonds) or succinate (triangles). Cultures were induced with 0.5 mM IPTG during early exponential phase. Aliquots were taken after 0, 20, 72 and 120 hours to measure **A)** optical density and **B)** CoQ10 content. Error bars show the standard variation of three biological replicates.

The experiment presented in Figure A 3 was done using fermentation medium, but only the pre-cultures were supplemented with 0.3% casamino acids. The concentrations of carbon substrate were adjusted to result in equivalent carbon units for

each tested condition: 17 mM glucose, 33mM glycerol, 33 mM pyruvate and 25 mM succinate. Because of an experimental error, only the glycerol and succinate cultures were induced, which should not have a significant impact on CoQ10 production based on my findings presented in section 2.3.8.

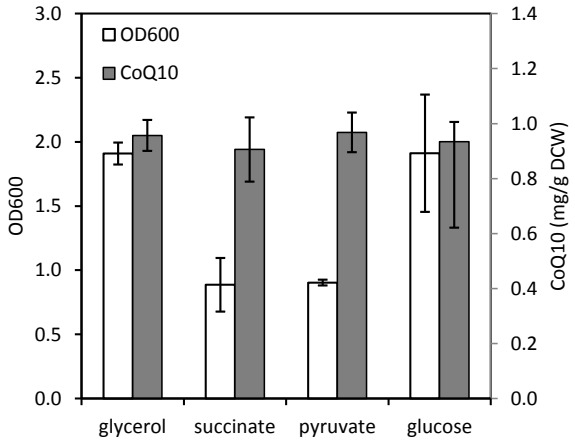

Figure A 3 Growth and CoQ10 production on fermentation medium supplemented with selected carbon sources
Strain CC023 was grown for five days with either 33 mM glycerol (circles), 25 mM succinate, 33 mM pyruvate or 17 mM glucose,. Glycerol and succinate cultures were induced with 1 mM IPTG during early exponential phase. After five days, optical density and CoQ10 content were measured. Error bars show the standard variation of three biological replicates.

In order to test whether different concentrations of substrate may influence growth and CoQ10 production in strain CC023, I then tested a range of concentrations (0.1%, 1% and 10%) of glucose, glycerol, pyruvate and succinate. Because the addition of casamino acid complicated the interpretation of carbon fluxes and appeared to negatively affect CoQ10 production, it was omitted from the fermentation medium.

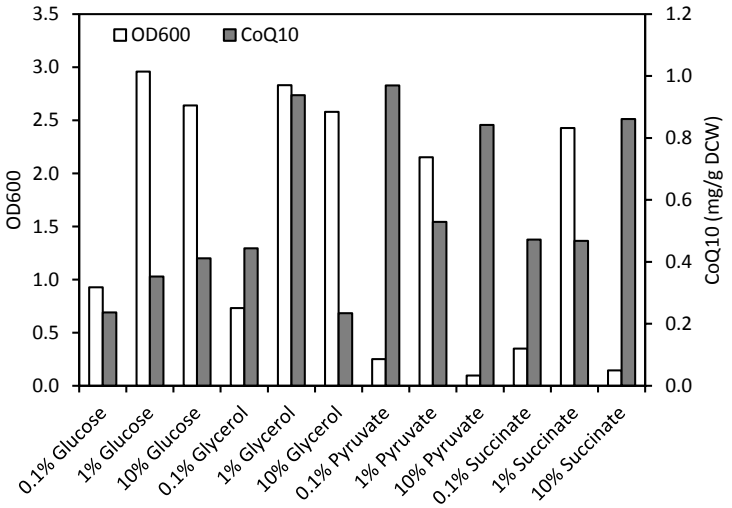

Figure A 4 Growth and CoQ10 production on fermentation medium supplemented with different concentrations of selected carbon sources
Strain CC023 was grown for five days with 0.1%, 1% or 10% glucose, glycerol, pyruvate or succinate. Glycerol and succinate cultures were induced with 1 mM IPTG during early exponential phase. After five days, optical density and CoQ10 content were measured.

The next experiments, performed in 96-well plates, were conducted in order to characterize the growth pattern of strain CC023 on the different carbon sources.

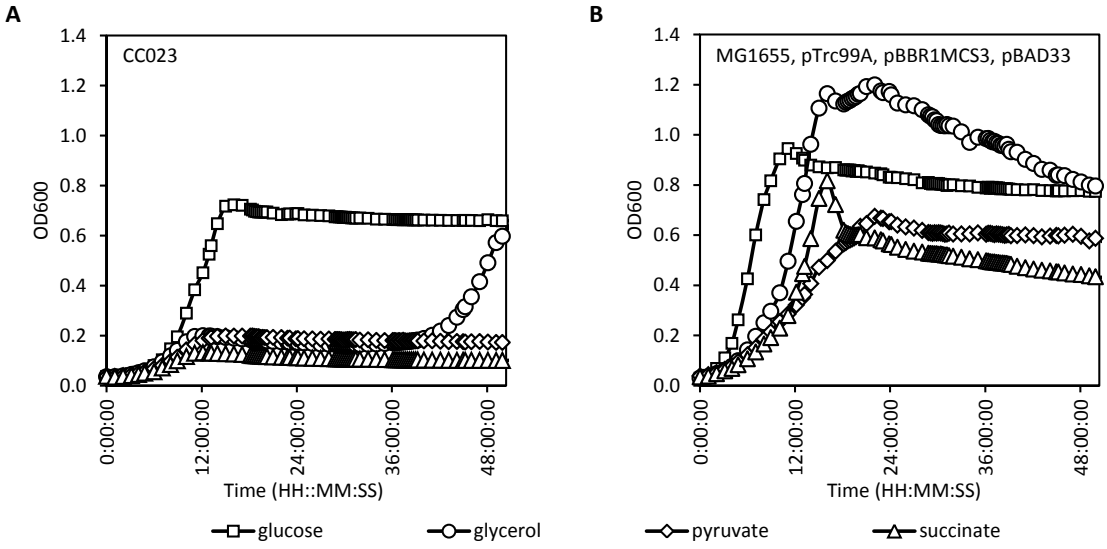

Figure A 5 Influence of selected carbon substrates on growth of CoQ10 producing and control strains
A) Strain CC023 and **B)** a control strain (MG1655, pTrc99A, pBBR1MCS3, pBAD33) were grown in triplicate in a 96-well plate incubated in a microtiter plate reader with continuous shaking, in fermentation medium supplemented with 16.7 mM glucose (squares), 33.3 mM glycerol (circles), 33.3 mM pyruvate (diamonds) or 25 mM succinate

(triangles). Once they reached exponential phase, cultures were induced with 0.5 mM IPTG. Optical densities were measured automatically by the plate reader.

Figure A 5 demonstrates that the severe growth reduction observed on pyruvate and succinate is attenuate in a control strain carrying empty vectors, compared to strain CC023. This suggests that these carbon substrates are poorly able to sustain biomass production when the mevalonate and aromatic pathways are overexpressed, presumably because acetyl-CoA and PEP become rate-limiting (Figure 3.1). I then attempted to demonstrate the link between overexpression of these two pathways and growth reduction. To do so, I created two additional strains: CC023noARO (MG1655, Δ*ispB*, pTUbiA$_e$DPS$_o$, pMBIS, pMtSa), which does not contain the integrated aromatic operons, and CC023noISO (MG1655, Δ*ispB*, *aroB::*LTAA, *ubiC::*LLACC, pTUbiA$_e$DPS$_o$, pMBIS), which does not carry the upper mevalonate pathway. Figure A 6 shows the growth pattern of these two strains on glucose, pyruvate, succinate, and on medium containing both pyruvate and succinate, compared to that of strain CC023, and of a control strain (MG1655, pTrc99A, pBBR1MCS3, pBAD33). The interpretation of this experiment was complicated by the strong growth inhibition observed following the IPTG induction of the cultures. Cell densities of CC023 on pyruvate and succinate reached higher levels in this experiment (Figure A 6A) than it previously did (Figure A 5A) while those of the control strain were lower (Figure A 6D) than before (Figure A 5B). In addition, strain CC023 displayed an extended lag phase on glucose (Figure A 6A), which had previously been observed in the experiment summarized by Figure A 4. The strain was therefore re-built by transforming strain MG1655 Δ*ispB aroB*::LTAA *ubiC*::LLACC + pTUbiA$_e$DPS$_o$ with plasmids pMBIS and pMtSA for subsequent experiments.

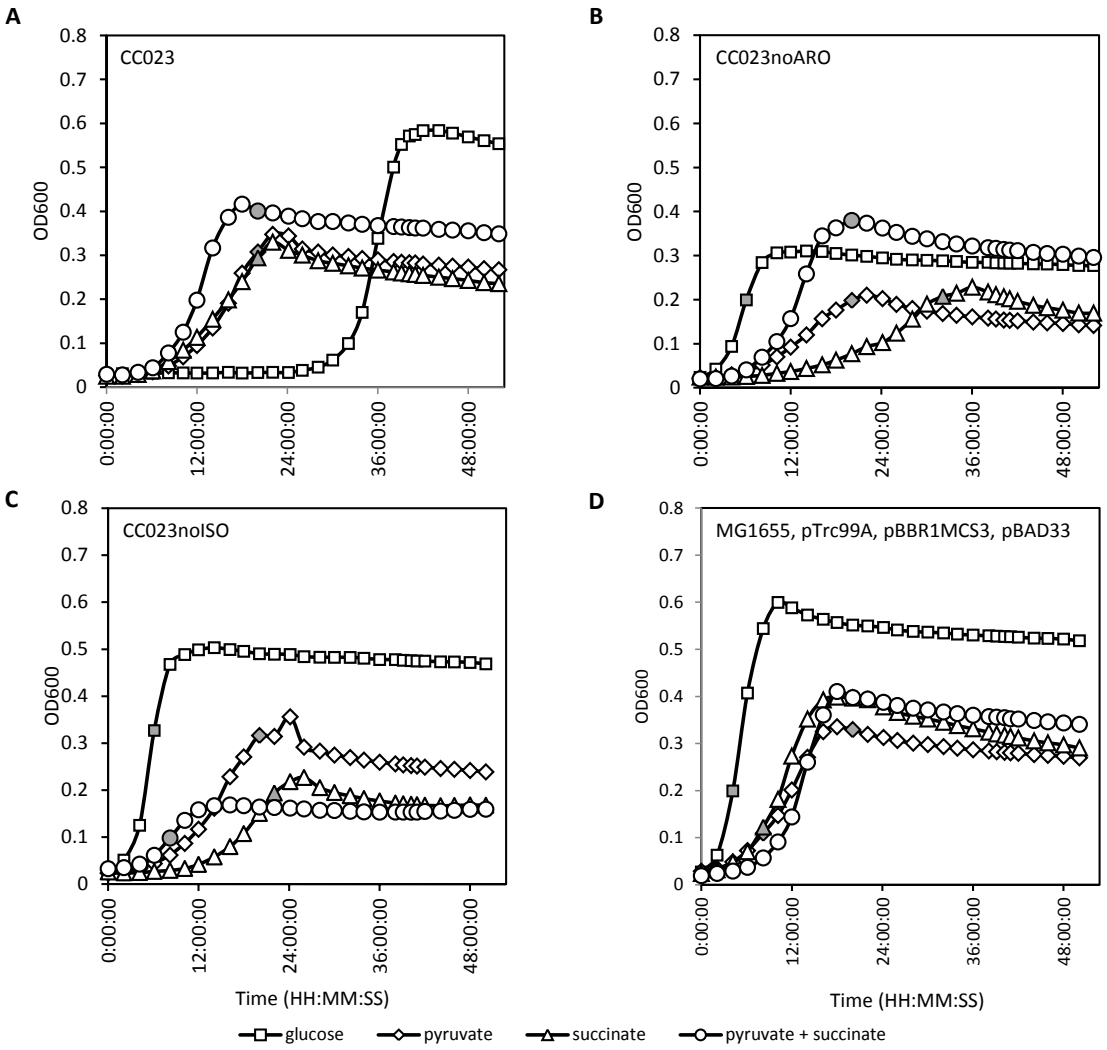

Figure A 6 Effect of the mevalonate and aromatic operons during growth of *E. coli* on selected carbon substrates

Strains CC023, CC023noARO (MG1655, Δ*ispB*, pTUbiA$_e$DPS$_o$, pMBIS, pMtSa), CC023noISO (MG1655, Δ*ispB*, *aroB::*LTAA, *ubiC::*LLACC, pTUbiA$_e$DPS$_o$, pMBIS) and a control strain (MG1655, pTrc99A, pBBR1MCS3, pBAD33) were grown in triplicate in a 96-well plate incubated in a microtiter plate reader with continuous shaking, in fermentation medium supplemented with 16.7 mM glucose (squares), 33.3 mM pyruvate (diamonds), 25 mM succinate (triangles) or a mix of 15 mM pyruvate and 13 mM succinate (circles). Grey symbols show when cultures were induced with 0.5 mM IPTG. Optical densities were measured automatically by the plate reader.

Overall, these experiments illustrate the reproducibility and strain stability issues observed when characterizing growth and CoQ10 production of strain CC023 on selected carbon substrates.

A3. *CoQ10 production on sorbitol, as reported from 2013 experiments*

The positive effect of sorbitol on CoQ10 production in strain CC023 was observed in at least three independent experiments, each performed in three biological replicates, in July and August 2012. Upon return from maternity leave in May 2013, similar experiments done in identical conditions failed to yield the same results. CoQ10 production was henceforth reduced on sorbitol compared to glucose. In addition, the profile of secreted metabolites was different from what had been previously documented, on both glucose and sorbitol. These changes were observed in repeated experiments, and previous results could not be reproduced by reintroducing plasmids and mutations in strain CC023. The accumulation of PHB was lower on glucose that what had previously been observed, with the excretion of only 0.004 mM PHB and no detectable PHB remaining in the medium by 28 hours (Figure 3.5C, Figure A 7C). When grown on sorbitol, strain CC023 accumulated three times more PHB than it previously did in similar conditions, with up to 0.015 mM of PHB accumulating in the growth medium (Figure 3.5C, Figure A 7C). Enhanced excretion of PHB correlated with reduced accumulation of CoQ10 and of *Unknown 1* by cells grown on sorbitol, compared to cells grown on glucose, and compared to 2012 experiments (Figure 3.5A, C; Figure A 7A, C). Strain CC023 grown on glucose secreted less acetate that previously observed, but produced more lactate and pyruvate (Figure 3.5E, F; Figure A 7E, F). Cells grown on sorbitol produced no acetate, as previously observed (Figure 3.5A, C; Figure A 7A, C).

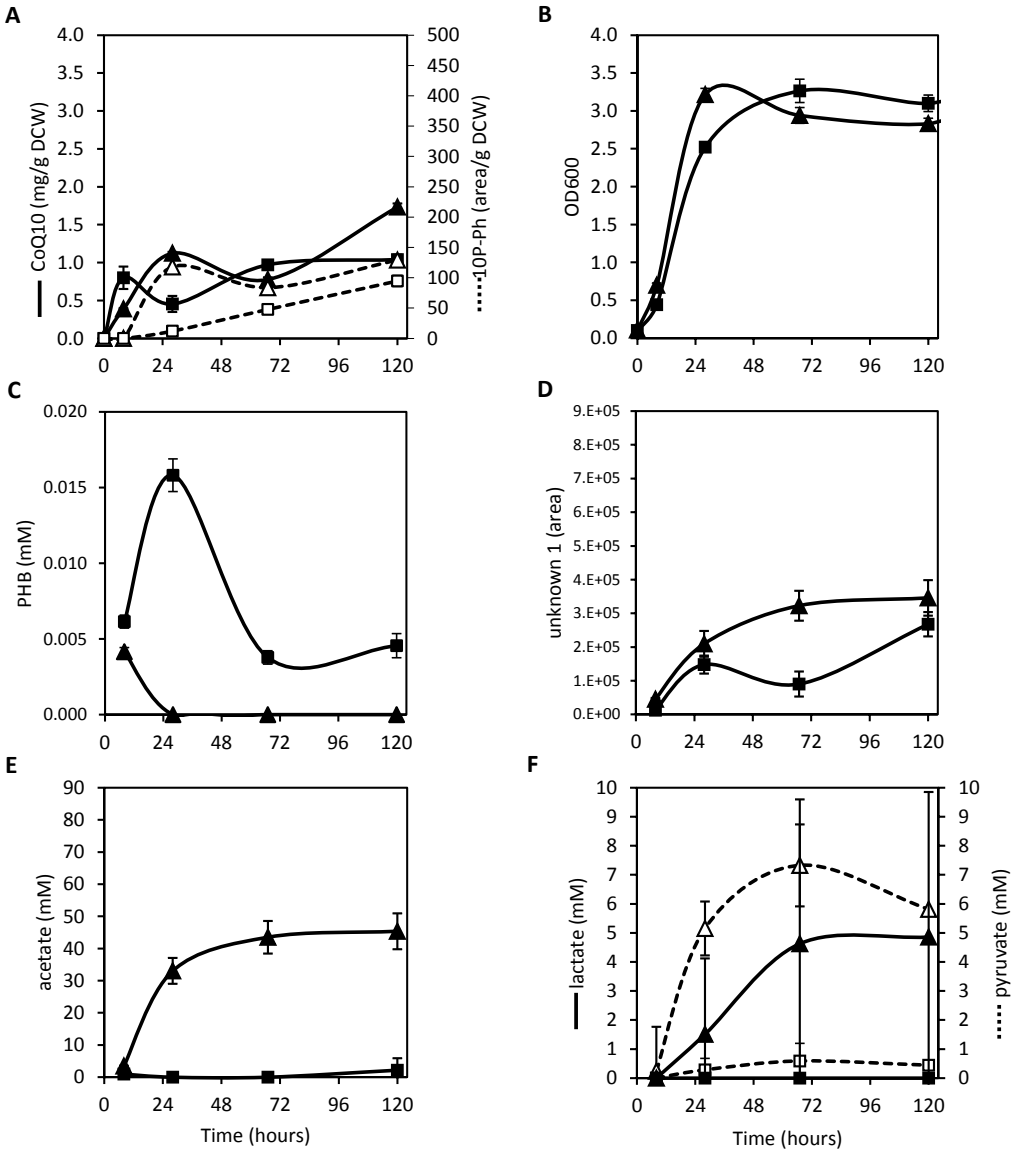

Figure A 7 Time-course of CoQ10 production and metabolite secretion during aerobic flask fermentation on glucose and sorbitol (2013)
Strain CC023 was grown for five days on glucose (triangles) or sorbitol (squares), in June 2013. Samples were taken after 0, 8, 28, 68, and 120 hours to measure **A)** CoQ10 (filled shapes) and 10P-Ph (empty shapes) content **B)** optical density **C)** extracellular PHB **D)** extracellular *Unknown 1* **E)** extracellular acetate **F)** extracellular lactate (filled shapes) and pyruvate (empty shapes). Error bars show the standard deviation of three biological replicates.

A4. *Accumulation of putative TCA cycle intermediates*

This section reports the accumulation pattern of an extracellular metabolite first identified as citrate in strains tested as part of the experiments reported in Figure 3.5

(Time-course of CoQ10 production and metabolite secretion during aerobic flask fermentation on glucose and sorbitol (2012)) and Figure 3.6 (Time-course of CoQ10 production, growth, and metabolite accumulation following the deletion of acetate producing pathways). As other TCA cycle intermediates including oxaloacetate, isocitrate and α-ketoglutarate co-elute with citrate under my analytical conditions, I could not attest with confidence of the identity of this metabolite, and therefore chose to exclude it from the body of the thesis. The secretion of this putative TCA cycle intermediate is enhanced during growth on sorbitol and in strain CC027, in which genes controlling acetate production are deleted (Figure A 8, Figure A 9). Differences in accumulation pattern of this putative TCA intermediate between the strains/conditions tested provides hints regarding the fluxes directing carbon flow and CoQ10 production.

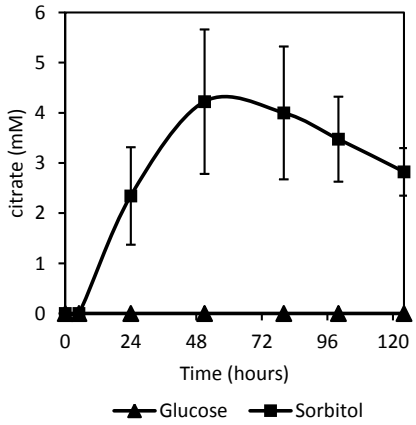

Figure A 8 Time-course of citrate (or other TCA intermediates) secretion during aerobic flask fermentation on glucose and sorbitol
A metabolite corresponding to citrate, oxaloacetate, isocitrate and/or α-ketoglutarate accumulated in the growth medium following growth on glucose (triangles) or sorbitol (squares). Samples were taken as part of the experiment reported in *Figure 3.5 Time-course of CoQ10 production and metabolite secretion during aerobic flask fermentation on glucose and sorbitol (2012)*. Error bars show the standard deviation of three biological replicates.

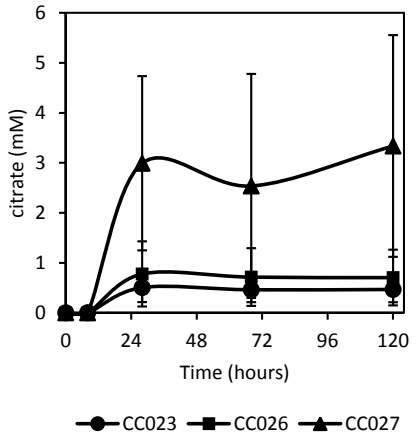

Figure A 9 Time-course of citrate (or other TCA intermediates) secretion during aerobic flask fermentation following the deletion of acetate producing pathways
A metabolite corresponding to citrate, oxaloacetate, isocitrate and/or α-ketoglutarate accumulated in the growth medium following growth of strains CC023 (circles), CC026 (squares) and CC027 (triangles) on glucose. Samples were taken as part of the experiment reported in *Figure 3.6 Time-course of CoQ10 production, growth, and metabolite accumulation following the deletion of acetate producing pathways*. Error bars show the standard deviation of three biological replicates.

A5. *CoQ10 production in fed-batch fermentation*

The flask experiments presented so far were done in condition where carbon is in excess. Growth in excess glucose may lead to the depletion of TCA cycle intermediates, and halt of respiratory chain, resulting in an accumulation of NADH (Wolfe, 2005). The accumulation of pyruvate in strain CC028 led to the hypothesis that pyruvate dehydrogenase had decreased activity. This enzyme complex, which converts pyruvate to acetyl-CoA, is inhibited by NADH (Schmincke-Ott and Bisswanger, 1981). Fed-batch fermentation has the advantage of maintaining glucose levels limiting, thereby minimizing mixed-acid fermentation and maximizing aerobic respiration. I tested the production of CoQ10 by CC028 under these conditions. To ensure that the rate of supplied glucose did not exceed the growth rate, and that carbon was not metabolized into mixed-fermentation products, a pH-stat controlled the feed pump by switching the latter off when pH went down below a set value.

A pH-stat fed-batch fermentation was done based on the process described by Tsuruta *et al.* (2009). Strain CC028 was streaked on M9 solid medium supplemented with 2% glucose and grown for two days. Several colonies were used to inoculate 5 mL pre-cultures in M9 medium supplemented with 3 % glucose and appropriate antibiotics. Following 48 hours of growth, pre-cultures were spun down and adjusted to an OD_{600} of 1, and used to inoculate 100 mL of M9 (3% glucose) medium in a 1L-baffled flask. This seed culture was grown for 6 hours, and then used to inoculate a 2L bioreactor (Applikon). The initial fermentation medium consisted of 1.3 L containing 5.46 g KH_2PO_4, 20.41 g K_2HPO_4, 2.6 g $(NH_4)_2SO_4$ and 2.21 g citric acid prepared and sterilized in the fermentor vessel. Post sterile additions, prepared as filter-sterilized concentrated

stocks, consisted of 1.5% glucose, 1.2 g $MgSO_4 \cdot 7H_2O$, 4.5 mg thiamine·HCl, 8.4 mg EDTA, and 10 mL of batch trace metal solution containing (per liter) 0.136 g $CoCl_2$, 1.5 g $MnCl_2 \cdot 4H_2O$, 0.12 g $CuCl_2$, 0.3 g H_3BO_4, 0.25 g $Na_2MoO_4 \cdot 2H_20$, 1.3 g $Zn(CH_3COO)_2 \cdot 2H_20$, and 10 g Fe(III) citrate hydrate (Tsuruta et al., 2009). Antibiotics were also added for plasmid retention. Fermentation was carried out at 37°C, and the pH maintained at 7 using automated addition of 0.25% v/v NH_4OH or 1M HCl. The initial agitation rate was set to 700 rpm, and the air flow to 1.5 air volume/vessel volume/minute. Dissolved oxygen was maintained above 40% of air saturation by an agitation cascade from 700 to 1000 rpm, followed by the addition of pure oxygen by a mass flow controller. A 25% v/v solution of Antifoam A (Sigma-Aldrich) was used to control foam. Following the exhaustion of the initial glucose, a sharp rise in dissolved oxygen above 60% triggered the onset of an exponential feed. The following equation was used by the fermentor software (BioXpert) to control feed rate: $m_s(t) = S_o \mu e^{\mu(t-t0)}$, where S_o is the initial glucose concentration (15 g/L), μ is the specific growth rate ($0.12h^{-1}$) and t_o is the time of glucose depletion from the batch medium. Once the feed rate reached 31 g glucose/h, it was reduced to 11.7 g/h and held constant for the remainder of fermentation. The feed rate was additionally controlled by a pH-stat, turning feed off when pH dropped below 6.96. The culture was induced with 0.1 mM IPTG after the onset of the fed-batch phase.

After an extended lag phase, the strain grew to high density, reaching an OD_{600} of 44 (Figure A 10B). Initial glucose was entirely consumed after 20 hours, and the resulting rise of dissolved oxygen triggered the onset of the fed-batch phase (Figure A 10B). During exponential phase and up to 32 hours, dissolved oxygen oscillated around 40%,

after which it went up to 80%, suggesting decreased respiration. After 72 hours, the filter of the air outlet of the fermentor became obstructed by water and bacteria, causing a sharp rise of pressure in the fermentor vessel, which stopped the fermentation. This problem was encountered multiple times during experiments using this fermentor, and has hampered my attempts to perform sustained fermentations. Secretion of PHB remained undetectable during the initial batch phase, and reached 0.16 mM by 64 hours (Figure A 10C). Similarly, *Unknown 1* accumulated only during the fed-batch phase (Figure A 10D). Considering the cell densities reached during this experiment, the secretion of *Unknown 1* appeared to be increased by ten-fold compared to previous flask experiments. Pyruvate accumulation reached approximately 40 mM by the end of the fermentation, which is lower than what was secreted by strain CC028 in flask experiments, when normalizing to cell mass (Figure 3.7H, Figure A 10E). This supports the initial hypothesis that pyruvate secretion by strain CC028 is linked to the inhibition of pyruvate dehydrogenase by high NADH concentrations. Nevertheless, CoQ10 contents stayed low throughout the fermentation, reaching only 0.3 mg/g DCW (Figure A 10A). The accumulation pattern of PHB suggests that the expression of the engineered pathways is mainly active when respiratory rates are lower, during the fed-batch phase. Similarly to flask fermentations where the CoQ10 production phase extends for several days into the stationary phase, it is possible that CoQ10 might have continued to accumulate if fed-batch fermentation could had been sustained for more than 72 hours. However, I also suspect that the extended lag phase favored the apparition of point-mutants which out-competed strain CC028 during the exponential phase. This would be consistent with the high variability observed between replicates during flask fermentation

experiments. Further optimization of my engineered strain and of the fermentation process will be required before fed-batch fermentation can be used a tool to increase CoQ10 production.

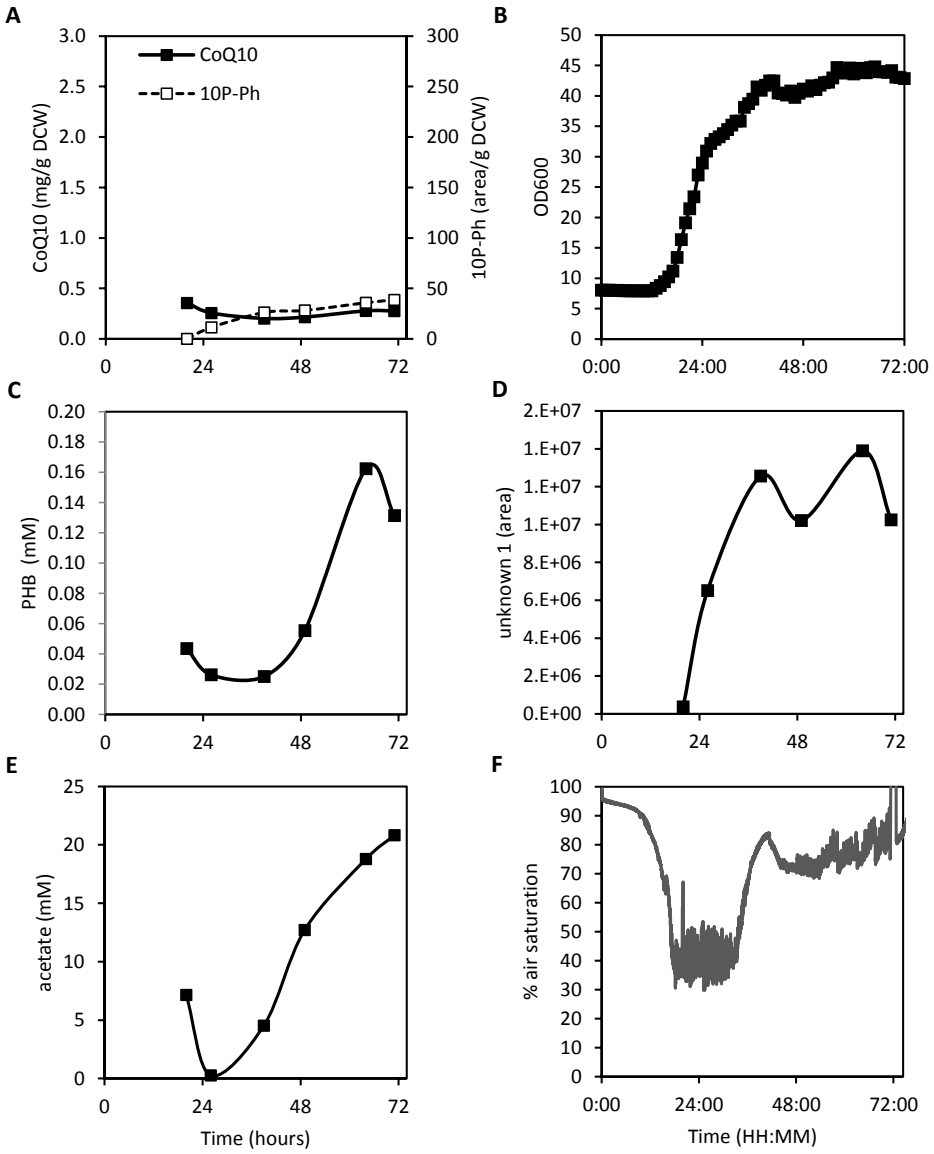

Figure A 10 Fed-batch fermentation for CoQ10 production
Strain CC027 was grown for 72 hours in a bench-top fermentor. Following the exhaustion of initial glucose, fed-batch fermentation was initiated and controlled by a pH-stat. Samples were taken after 20, 26, 39, 49, 64 and 72 hours to measure **A**) CoQ10 content **C**) secreted PHB **D**) secreted *Unknown 1* **E**) secreted acetate. **B**) Optical density was measured every minute using a Bug Eye. **F**) Dissolved oxygen was recorded every minute using BioExpert.

A6. *Identification of Unknown 1*

Unknown 1 is an unidentified metabolite secreted by engineered strains of *E. coli*, with an accumulation pattern closely correlated to that of CoQ10 (Figure 3.5D, Figure 3.6D, Figure 3.7E, Figure 3.8D, Figure A 10D). Attempts were made to identify

Unknown 1 by mass spectrometry. To this end, samples (20 µL) previously established as containing high concentrations of *Unknown 1* were resolved by HPLC, using an Aminex HPX-87H column (Bio-Rad) heated at 65°C, and a mixture of 85% H_2SO_4 and 15% acetonitrile as the mobile phase, at 0.6 mL/minute. *Unknown 1* eluted after 13.7 minutes, and was detected by a PDA detector at 254 nm and 210 nm. The eluent from the PDA detector was collected in a 1.5 mL tube. Different attempts were made to identify *Unknown 1* from the collected fraction.

In a first attempt, *Unknown 1* was collected from the supernatant fraction of a sample taken after 72 hours of fed-batch fermentation of strain CC028 (section A5). In this sample, *Unknown 1* eluted 0.4 minutes after an undetermined amount of mevalonate, which absorbs at 210 nm but not at 254 nm. The collected fraction was evaporated in a speed vacuum concentrator and suspended in 0.1% formic acid. A 10 µL aliquot of this suspension was analyzed by LC-MS, using a Fast Acid Analysis column (Bio-Rad) heated at 65°C, using 0.1% formic acid and 15 % acetonitrile as the mobile phase. Resolved molecules were channeled to a Fourier Transform Ion Cyclotron Resonance Mass Spectrometer (FTMS), scanning between m/z=50 and m/z=350, at r=100,000 @ m/z=400.

Consistently with the co-elution of mevalonate with *Unknown 1* in the collected sample, mevalonolactone was identified by FTMS (Figure A 11). The additional ions detected by LC-FTMS could not be associated with known metabolites of *E. coli*.

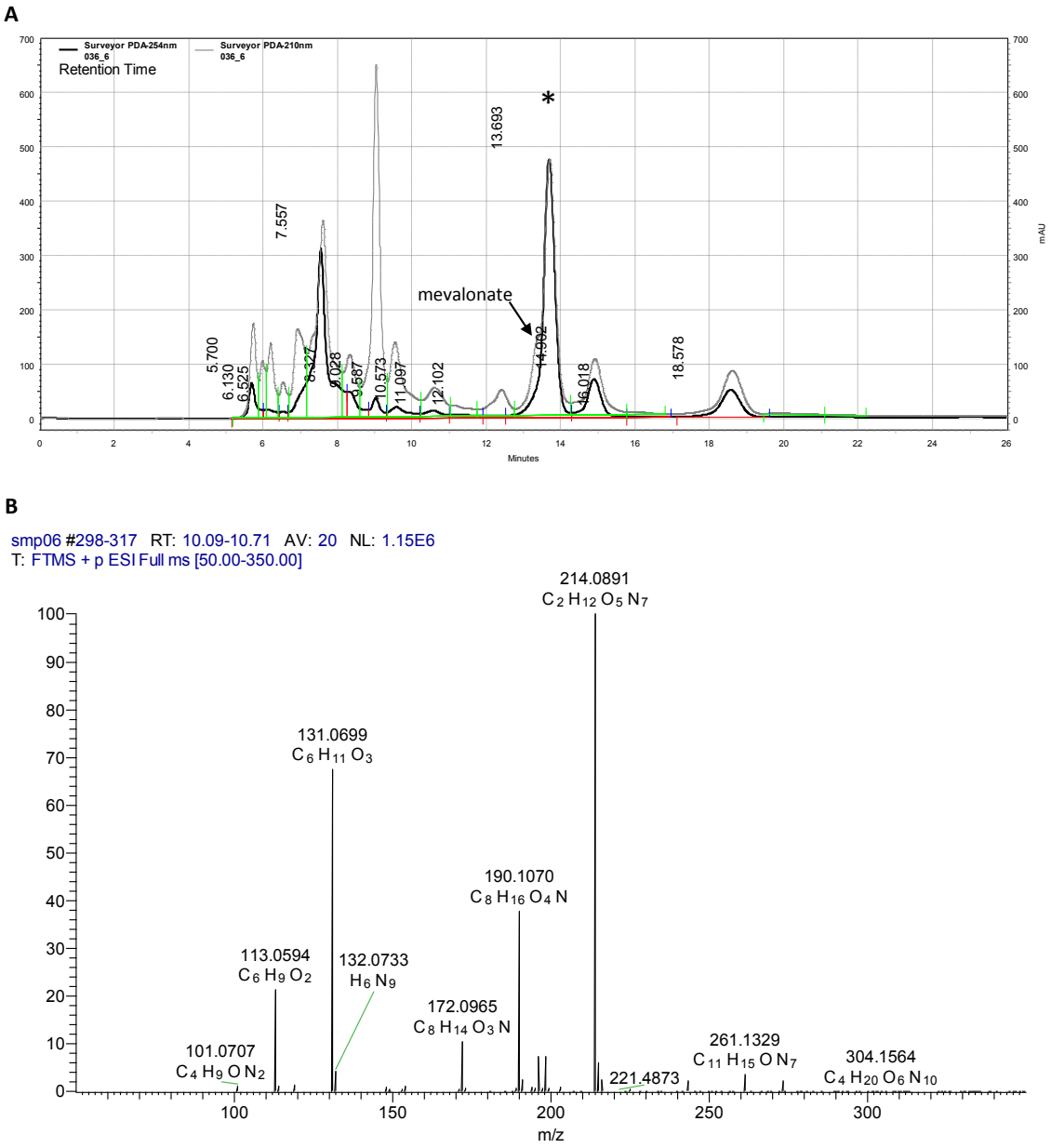

Figure A 11 Identification of *Unknown 1* from the supernatant fraction of a culture of strain CC028 after 72 hours of fed-batch fermentation

A) *Unknown 1* was detected at 210 nm and 254 nm after 13.693 minutes of HPLC analysis, and is marked by a star on the chromatogram. **B)** Spectra of detected ions following LC-FTMS analysis of a collected fraction of *Unknown 1*. The protonated ion labeled as $C_6H_{11}O_3$ $[M+H]^+$=131.0699 corresponds to mevalonolactone (exact mass = 130.0630). The protonated ion labeled as $C_2H_{12}O_5N_7$ $[M+H]^+$=214.0891 corresponds to a contaminant present throughout the analysis. The protonated ions m/z=113.0594, m/z=172.0965 and m/z=190.1070 could not be associated with known *E. coli* metabolites.

In a second attempt, *Unknown 1* was collected from the supernatant fraction of a sample taken after 120 hours of flask fermentation of strain CC023. A Control sample was collected between 18.1 and 18.4 minutes of analysis, as no detectable peaks at 254 nm were visible during this time window. The *Unknown 1* and Control fractions were each spiked with 5 µg/ml of CoQ10, as an internal control. A 100 µL sample from each collected fraction (500 µL) was saved for analysis. The remaining 400 µL of each sample was extracted with one volume of hexane, in order to extract putative quinone intermediates. The hexane fraction of each sample was evaporated in a nitrogen stream and suspended in acetone. The aqueous fraction of each fraction was also analyzed. All fractions were analyzed by RP-HPLC using the quinone analysis method described in section 2.2.11, and were detected at 254 nm. No absorption peak was detected from the *Unknown 1* and Control fractions, except for the CoQ10 internal standard. Samples were then analyzed by LC-FTMS, using the quinone analysis method previously described, and scanning by FTMS between m/z=50 and m/z=1500, at r=100,000. No ions were detected in the *Unknown 1* fractions that were absent from corresponding Control fractions (not shown). This suggests that *Unknown 1* is not retained by reverse-phase chromatography (ZORBAX Eclipse XDB-C18 4.6 x 150 mm, 5 µm), and that it is not a quinone intermediate or derivative.

In conclusion, my attempts to identify *Unknown 1* remained unfruitful. Additional work will be required to ensure that the isolation of *Unknown 1* from biological samples is effective, and that appropriate analytical methods are developed.

Bibliography

Alexander, K., Young, I. G., 1978. Alternative hydroxylases for the aerobic and anaerobic biosynthesis of ubiquinone in *Escherichia coli*. Biochemistry. 17**,** 4750-5.

Anthony, J. R., et al., 2009. Optimization of the mevalonate-based isoprenoid biosynthetic pathway in Escherichia coli for production of the anti-malarial drug precursor amorpha-4,11-diene. Metab Eng. 11**,** 13-9.

Anthony, L. C., et al., 2004. Tightly regulated vectors for the cloning and expression of toxic genes. J Microbiol Methods. 58**,** 243-50.

Baba, S. W., et al., 2004. Yeast Coq5 C-methyltransferase is required for stability of other polypeptides involved in coenzyme Q biosynthesis. J Biol Chem. 279**,** 10052-9.

Baba, T., et al., 2006. Construction of Escherichia coli K-12 in-frame, single-gene knockout mutants: the Keio collection. Mol Syst Biol. 2**,** 2006 0008.

Bader, M. W., et al., 2000. Disulfide bonds are generated by quinone reduction. J Biol Chem. 275**,** 26082-8.

Barker, J. L., Frost, J. W., 2001. Microbial synthesis of p-hydroxybenzoic acid from glucose. Biotechnol Bioeng. 76**,** 376-90.

Bekker, M., et al., 2009. Respiration of Escherichia coli can be fully uncoupled via the nonelectrogenic terminal cytochrome bd-II oxidase. J Bacteriol. 191**,** 5510-7.

Bekker, M., et al., 2007. Changes in the redox state and composition of the quinone pool of Escherichia coli during aerobic batch-culture growth. Microbiology. 153**,** 1974-1980.

Bhasin, M., et al., 2005. PSLpred: prediction of subcellular localization of bacterial proteins. Bioinformatics. 21**,** 2522-4.

Chang, D. E., et al., 1999. Acetate metabolism in a pta mutant of Escherichia coli W3110: importance of maintaining acetyl coenzyme A flux for growth and survival. J Bacteriol. 181**,** 6656-63.

Choi, G.-S., et al., 2005. Restricted electron flux increases coenzyme Q10 production in *Agrobacterium tumefaciens* ATCC4452. Process Biochemistry. 40**,** 3225-3229.

Choi, J. H., et al., 2009. Synergistic effects of chromosomal ispB deletion and dxs overexpression on coenzyme Q(10) production in recombinant Escherichia coli expressing Agrobacterium tumefaciens dps gene. J Biotechnol. 144**,** 64-9.

Claros, M. G., von Heijne, G., 1994. TopPred II: an improved software for membrane protein structure predictions. Comput Appl Biosci. 10**,** 685-6.

Collins, M. D., Jones, D., 1981. Distribution of isoprenoid quinone structural types in bacteria and their taxonomic implication. Microbiol Rev. 45**,** 316-54.

Cox, G. B., et al., 1969. Biosynthesis of ubiquinone in *Escherichia coli* K-12: location of genes affecting the metabolism of 3-octaprenyl-4-hydroxybenzoic acid and 2-octaprenylphenol. J Bacteriol. 99**,** 450-8.

Datsenko, K. A., Wanner, B. L., 2000. One-step inactivation of chromosomal genes in Escherichia coli K-12 using PCR products. Proc Natl Acad Sci U S A. 97**,** 6640-5.

Davis, B. D., 1951. Inhibition of *Escherichia coli* by p-aminobenzoic acid and its reversal by p-hydroxybenzoic acid. The Journal of Experimental Medicine. 94**,** 243-254.

Dittrich, C. R., et al., 2005. Characterization of the acetate-producing pathways in Escherichia coli. Biotechnol Prog. 21**,** 1062-7.

Dixson, D. D., et al., 2011. Reinvestigation of coenzyme Q10 isolation from Sporidiobolus johnsonii. Chem Biodivers. 8**,** 1033-51.

Erhardt, H., et al., 2012. Disruption of individual nuo-genes leads to the formation of partially assembled NADH:ubiquinone oxidoreductase (complex I) in Escherichia coli. Biochim Biophys Acta. 1817**,** 863-71.

Farmer, W. R., Liao, J. C., 2001. Precursor balancing for metabolic engineering of lycopene production in *Escherichia coli*. Biotechnol. Prog. 17**,** 57-61.

Farr, S. B., Kogoma, T., 1991. Oxidative stress responses in Escherichia coli and Salmonella typhimurium. Microbiol Rev. 55**,** 561-85.

Georgellis, D., et al., 2001. Quinones as the redox signal for the arc two-component system of bacteria. Science. 292**,** 2314-6.

Geu-Flores, F., et al., 2007. USER fusion: a rapid and efficient method for simultaneous fusion and cloning of multiple PCR products. Nucleic Acids Res. 35**,** e55.

Gibert, I., et al., 1988. Regulation of *ubiG* gene expression in *Escherichia coli*. J Bacteriol. 170**,** 1346-9.

Gibson, D. G., et al., 2009. Enzymatic assembly of DNA molecules up to several hundred kilobases. Nat Methods. 6**,** 343-5.

Gin, P., Clarke, C. F., 2005. Genetic evidence for a multi-subunit complex in coenzyme Q biosynthesis in yeast and the role of the Coq1 hexaprenyl diphosphate synthase. J Biol Chem. 280**,** 2676-81.

Gulmezian, M., et al., 2007. The role of UbiX in Escherichia coli coenzyme Q biosynthesis. Arch Biochem Biophys. 467**,** 144-53.

Gutowski, S. J., Rosenberg, H., 1975. Succinate uptake and related proton movements in Escherichia coli K12. Biochem J. 152**,** 647-54.

Ha, S. J., et al., 2009. Ca2+ increases the specific coenzyme Q10 content in Agrobacterium tumefaciens. Bioprocess Biosyst Eng. 32**,** 697-700.

Ha, S. J., et al., 2007a. Controlling the sucrose concentration increases Coenzyme Q10 production in fed-batch culture of Agrobacterium tumefaciens. Appl Microbiol Biotechnol. 76**,** 109-16.

Ha, S. J., et al., 2007b. Optimization of culture conditions and scale-up to pilot and plant scales for coenzyme Q(10) production by *Agrobacterium tumefaciens*. Appl Microbiol Biotechnol. 74**,** 974-80.

Hajj Chehade, M., et al., 2013. ubiI, a new gene in Escherichia coli coenzyme Q biosynthesis, is involved in aerobic C5-hydroxylation. J Biol Chem. 288**,** 20085-92.

Hamilton, J. A., Cox, G. B., 1971. Ubiquinone biosynthesis in Escherichia coli K-12. Accumulation of an octaprenol, farnesylfarnesylgeraniol, by a multiple aromatic auxotroph. Biochem J. 123**,** 435-43.

Harker, M., Bramley, P. M., 1999. Expression of prokaryotic 1-deoxy-D-xylulose-5-phosphatases in *Escherichia coli* increases carotenoid and ubiquinone biosynthesis. FEBS Lett. 448**,** 115-9.

Hodgson, J. M., et al., 2002. Coenzyme Q10 improves blood pressure and glycaemic control: a controlled trial in subjects with type 2 diabetes. Eur J Clin Nutr. 56**,** 1137-42.

Holms, H., 1996. Flux analysis and control of the central metabolic pathways in Escherichia coli. FEMS Microbiol Rev. 19**,** 85-116.

Hsu, A. Y., et al., 2000. Genetic evidence for a multi-subunit complex in the O-methyltransferase steps of coenzyme Q biosynthesis. Biochim Biophys Acta. 1484**,** 287-97.

Hsu, A. Y., et al., 1996. Complementation of *coq3* mutant yeast by mitochondrial targeting of the *Escherichia coli* UbiG polypeptide: evidence that UbiG catalyzes both O-methylation steps in ubiquinone biosynthesis. Biochemistry. 35**,** 9797-806.

Huang, M., et al., 2011. Multiple Strategies for Metabolic Engineering of Escherichia coli for Efficient Production of Coenzyme Q10. Chinese Journal of Chemical Engineering. 19**,** 316-326.

Ingledew, W. J., Poole, R. K., 1984. The respiratory chains of *Escherichia coli*. Microbiol Rev. 48**,** 222-71.

Inui, M., et al., 2008. Mechanisms of inhibitory effects of CoQ10 on UVB-induced wrinkle formation in vitro and in vivo. Biofactors. 32**,** 237-43.

Kakuda, H., et al., 1994. Construction of Pta-Ack pathway deletion mutants of Escherichia coli and characteristic growth profiles of the mutants in a rich medium. Biosci Biotechnol Biochem. 58**,** 2232-5.

Kien, N. B., et al., 2010. Coenzyme Q10 production in a 150-l reactor by a mutant strain of Rhodobacter sphaeroides. J Ind Microbiol Biotechnol. 37**,** 521-9.

Kim, S. J., et al., 2006. Amplification of 1-deoxy-D-xyluose 5-phosphate (DXP) synthase level increases coenzyme Q10 production in recombinant *Escherichia coli*. Appl Microbiol Biotechnol. 72**,** 982-5.

Kim, S. W., Keasling, J. D., 2001. Metabolic engineering of the nonmevalonate isopentenyl diphosphate synthesis pathway in *Escherichia coli* enhances lycopene production. Biotechnol Bioeng. 72**,** 408-15.

Knoell, H. E., 1979. Isolation of a soluble enzyme complex comprising the ubiquinone-8 synthesis apparatus from the cytoplasmic membrane of *Escherichia coli*. Biochem Biophys Res Commun. 91**,** 919-25.

Knoell, H. E., 1981. Stand-by position of the dioxygen-dependent ubiquinone-8 synthesis apparatus in anaerobically grown *Escherichia coli* K-12. FEMS Microbiol Lett. 10**,** 59-62.

Koo, B. S., et al., 2010. Improvement of coenzyme Q(10) production by increasing the NADH/NAD(+) ratio in Agrobacterium tumefaciens. Biosci Biotechnol Biochem. 74**,** 895-8.

Kovach, M. E., et al., 1995. Four new derivatives of the broad-host-range cloning vector pBBR1MCS, carrying different antibiotic-resistance cassettes. Gene. 166**,** 175-6.

Kroger, A., Klingenberg, M., 1973. Further evidence for the pool function of ubiquinone as derived from the inhibition of the electron transport by antimycin. Eur J Biochem. 39**,** 313-23.

Kwon, O., et al., 2005. Regulation of the ubiquinone (coenzyme Q) biosynthetic genes *ubiCA* in *Escherichia coli*. Curr Microbiol. 50**,** 180-9.

Lang, V. J., et al., 1987. Characterization of the specific pyruvate transport system in Escherichia coli K-12. J Bacteriol. 169**,** 380-5.

Lass, A., Sohal, R. S., 1998. Electron transport-linked ubiquinone-dependent recycling of alpha-tocopherol inhibits autooxidation of mitochondrial membranes. Arch Biochem Biophys. 352**,** 229-36.

Lawrence, J., et al., 1974. Biosynthesis of ubiquinone in Escherichia coli K-12: biochemical and genetic characterization of a mutant unable to convert chorismate into 4-hydroxybenzoate. J Bacteriol. 118**,** 41-5.

Lee, J. K., et al., 2004. Cloning and functional expression of the *dps* gene encoding decaprenyl diphosphate synthase from *Agrobacterium tumefaciens*. Biotechnol Prog. 20**,** 51-6.

Lee, J. K., et al., 2007. Cloning and characterization of the *dxs* gene, encoding 1-deoxy-d-xylulose 5-phosphate synthase from *Agrobacterium tumefaciens*, and its overexpression in *Agrobacterium tumefaciens*. J Biotechnol. 128**,** 555-66.

Lee, P. T., et al., 1997. A C-methyltransferase involved in both ubiquinone and menaquinone biosynthesis: isolation and identification of the *Escherichia coli ubiE* gene. J Bacteriol. 179**,** 1748-54.

Leppik, R. A., et al., 1976a. Membrane-associated reactions in ubiquinone biosynthesis. 2-Octaprenyl-3-methyl-5-hydroxy-6-methoxy-1,4-benzoquinone methyltransferase. Biochim Biophys Acta. 428**,** 146-56.

Leppik, R. A., et al., 1976b. Membrane-associated reactions in ubiquinone biosynthesis in *Escherichia coli*. 3-Octaprenyl-4-hydroxybenzoate carboxy-lyase. Biochim Biophys Acta. 436**,** 800-10.

Liao, J. C., et al., 1994. Alteration of the biochemical valves in the central metabolism of Escherichia coli. Ann N Y Acad Sci. 745**,** 21-34.

Lin, H., et al., 2005. Effect of carbon sources differing in oxidation state and transport route on succinate production in metabolically engineered Escherichia coli. J Ind Microbiol Biotechnol. 32**,** 87-93.

Lipshutz, B. H., et al., 2005. An improved synthesis of the "miracle nutrient" coenzyme Q10. Org Lett. 7**,** 4095-7.

Ma, S. M., et al., 2011. Optimization of a heterologous mevalonate pathway through the use of variant HMG-CoA reductases. Metab Eng. 13**,** 588-97.

Malpica, R., et al., 2004. Identification of a quinone-sensitive redox switch in the ArcB sensor kinase. Proc Natl Acad Sci U S A. 101**,** 13318-23.

Mancini, A., Balercia, G., 2011. Coenzyme Q(10) in male infertility: physiopathology and therapy. Biofactors. 37**,** 374-80.

Marbois, B., et al., 2005. Coq3 and Coq4 define a polypeptide complex in yeast mitochondria for the biosynthesis of coenzyme Q. J Biol Chem. 280**,** 20231-8.

Marbois, B., et al., 2010. para-Aminobenzoic acid is a precursor in coenzyme Q6 biosynthesis in Saccharomyces cerevisiae. J Biol Chem. 285**,** 27827-38.

Martin-Montalvo, A., et al., 2011. Respiratory-induced coenzyme Q biosynthesis is regulated by a phosphorylation cycle of Cat5p/Coq7p. Biochem J. 440**,** 107-14.

Martin, S. F., et al., 2007. Coenzyme Q and protein/lipid oxidation in a BSE-infected transgenic mouse model. Free Radic Biol Med. 42**,** 1723-9.

Martin, V. J., et al., 2003. Engineering a mevalonate pathway in *Escherichia coli* for production of terpenoids. Nat Biotechnol. 21**,** 796-802.

Martinez-Morales, F., et al., 1999. Chromosomal integration of heterologous DNA in Escherichia coli with precise removal of markers and replicons used during construction. J Bacteriol. 181**,** 7143-8.

Martinez, I., et al., 2008. Replacing Escherichia coli NAD-dependent glyceraldehyde 3-phosphate dehydrogenase (GAPDH) with a NADP-dependent enzyme from Clostridium acetobutylicum facilitates NADPH dependent pathways. Metab Eng. 10**,** 352-9.

Matsumura, M., et al., 1983. Anaerobic production of ubiquinone-10 by *Paracoccus denitrificans*. Applied Microbiology and Biotechnology. 17**,** 85-89.

Myers, C. E., et al., 1987. 5-Iminodaunomycin. An anthracycline with unique properties. J Biol Chem. 262**,** 11571-7.

Negishi, E., et al., 2002. A novel, highly selective, and general methodology for the synthesis of 1,5-diene-containing oligoisoprenoids of all possible geometrical

combinations exemplified by an iterative and convergent synthesis of coenzyme Q(10). Org Lett. 4**,** 261-4.

Nikel, P. I., et al., 2010. Redox driven metabolic tuning: carbon source and aeration affect synthesis of poly(3-hydroxybutyrate) in Escherichia coli. Bioeng Bugs. 1**,** 291-5.

Norholm, M. H., et al., 2012. Manipulating the genetic code for membrane protein production: what have we learnt so far? Biochim Biophys Acta. 1818**,** 1091-6.

Okada, K., et al., 1998. Molecular cloning and mutational analysis of the *ddsA* gene encoding decaprenyl diphosphate synthase from *Gluconobacter suboxydans*. Eur J Biochem. 255**,** 52-9.

Okada, K., et al., 1997a. Cloning of the *sdsA* gene encoding solanesyl diphosphate synthase from *Rhodobacter capsulatus* and its functional expression in *Escherichia coli* and *Saccharomyces cerevisiae*. J Bacteriol. 179**,** 5992-8.

Okada, K., et al., 1997b. The ispB gene encoding octaprenyl diphosphate synthase is essential for growth of Escherichia coli. J Bacteriol. 179**,** 3058-60.

Okada, K., et al., 1996. Polyprenyl diphosphate synthase essentially defines the length of the side chain of ubiquinone. Biochim Biophys Acta. 1302**,** 217-23.

Padilla, S., et al., 2009. Hydroxylation of demethoxy-Q6 constitutes a control point in yeast coenzyme Q6 biosynthesis. Cell Mol Life Sci. 66**,** 173-86.

Park, Y. C., et al., 2005. Batch and fed-batch production of coenzyme Q10 in recombinant *Escherichia coli* containing the decaprenyl diphosphate synthase gene from *Gluconobacter suboxydans*. Appl Microbiol Biotechnol. 67**,** 192-6.

Patnaik, R., Liao, J. C., 1994. Engineering of Escherichia coli central metabolism for aromatic metabolite production with near theoretical yield. Appl Environ Microbiol. 60**,** 3903-8.

Peterson, J., Phillips, G. J., 2008. New pSC101-derivative cloning vectors with elevated copy numbers. Plasmid. 59**,** 193-201.

Pitera, D. J., et al., 2007. Balancing a heterologous mevalonate pathway for improved isoprenoid production in Escherichia coli. Metab Eng. 9**,** 193-207.

Poon, W. W., et al., 2000. Identification of *Escherichia coli ubiB*, a gene required for the first monooxygenase step in ubiquinone biosynthesis. J Bacteriol. 182**,** 5139-46.

Ringquist, S., et al., 1992. Translation initiation in Escherichia coli: sequences within the ribosome-binding site. Mol Microbiol. 6**,** 1219-29.

Saiki, K., et al., 1992. Heme O biosynthesis in Escherichia coli: the cyoE gene in the cytochrome bo operon encodes a protoheme IX farnesyltransferase. Biochem Biophys Res Commun. 189**,** 1491-7.

Sakato, K., et al., 1992. Agitation-aeration studies on coenzyme Q10 production using *Rhodopseudomonas spheroides*. Biotechnol Appl Biochem. 16**,** 19-22.

Sambrook, J., et al., 1989. Molecular Cloning: A Laboratory Manual. Cold Spring Harbor Laboratory Press, New York, NY.

San, K. Y., et al., 2002. Metabolic engineering through cofactor manipulation and its effects on metabolic flux redistribution in Escherichia coli. Metab Eng. 4**,** 182-92.

Schaars, C. F., Stalenhoef, A. F., 2008. Effects of ubiquinone (coenzyme Q10) on myopathy in statin users. Curr Opin Lipidol. 19**,** 553-7.

Schmelzer, C., et al., 2007. Functional connections and pathways of coenzyme Q10-inducible genes: an in-silico study. IUBMB Life. 59**,** 628-633.

Schmelzer, C., et al., 2010. The reduced form of coenzyme Q10 mediates distinct effects on cholesterol metabolism at the transcriptional and metabolite level in SAMP1 mice. IUBMB Life. 62**,** 812-8.

Schmincke-Ott, E., Bisswanger, H., 1981. Dihydrolipoamide Dehydrogenase Component of the Pyruvate Dehydrogenase Complex from Escherichia coli K12. European Journal of Biochemistry. 114**,** 413-420.

Seo, M. J., Kim, S. O., 2010. Effect of limited oxygen supply on coenzyme Q(10) production and its relation to limited electron transfer and oxidative stress in Rhizobium radiobacter T6102. J Microbiol Biotechnol. 20**,** 346-9.

Shestopalov, A. I., et al., 1997. Aeration-dependent changes in composition of the quinone pool in *Escherichia coli*. Evidence of post-transcriptional regulation of the quinone biosynthesis. FEBS Lett. 404**,** 272-4.

Shults, C. W., et al., 2002. Effects of coenzyme Q10 in early Parkinson disease: evidence of slowing of the functional decline. Arch Neurol. 59**,** 1541-50.

Singh, R. B., et al., 1998. Randomized, double-blind placebo-controlled trial of coenzyme Q10 in patients with acute myocardial infarction. Cardiovasc Drugs Ther. 12**,** 347-53.

Soballe, B., Poole, R. K., 1997. Aerobic and anaerobic regulation of the *ubiCA* operon, encoding enzymes for the first two committed steps of ubiquinone biosynthesis in *Escherichia coli*. FEBS Lett. 414**,** 373-6.

Sourris, K. C., et al., 2012. Ubiquinone (coenzyme Q10) prevents renal mitochondrial dysfunction in an experimental model of type 2 diabetes. Free Radic Biol Med. 52**,** 716-23.

Stroobant, P., et al., 1972. Mutants of *Escherichia coli* K-12 blocked in the final reaction of ubiquinone biosynthesis: characterization and genetic analysis. J Bacteriol. 109**,** 134-9.

Takahashi, S., et al., 2003. Isolation and expression of *Paracoccus denitrificans* decaprenyl diphosphate synthase gene for production of ubiquinone-10 in *Escherichia coli*. Biochemical Engineering Journal. 16**,** 183-190.

Thomason, L. C., et al., 2007. E. coli genome manipulation by P1 transduction. Curr Protoc Mol Biol. Chapter 1**,** Unit 1 17.

Tsuruta, H., et al., 2009. High-level production of amorpha-4,11-diene, a precursor of the antimalarial agent artemisinin, in Escherichia coli. PLoS One. 4**,** e4489.

Urakami, T., Hori-Okubo, M., 1988. Production of isoprenoid compounds in the facultative methylotroph *Protomonas extorquens.* J. Ferment. Technol. 66**,** 323-332.

van de Walle, M., Shiloach, J., 1998. Proposed mechanism of acetate accumulation in two recombinant Escherichia coli strains during high density fermentation. Biotechnol Bioeng. 57**,** 71-8.

Vermeglio, A., Joliot, P., 1999. The photosynthetic apparatus of Rhodobacter sphaeroides. Trends in Microbiology. 7**,** 435-440.

Voegele, R. T., et al., 1993. Glycerol kinase of Escherichia coli is activated by interaction with the glycerol facilitator. J Bacteriol. 175**,** 1087-94.

Wang, K. C., Ohnuma, S., 2000. Isoprenyl diphosphate synthases. Biochim Biophys Acta. 1529**,** 33-48.

Weaver, L. M., Herrmann, K. M., 1990. Cloning of an aroF allele encoding a tyrosine-insensitive 3-deoxy-D-arabino-heptulosonate 7-phosphate synthase. J Bacteriol. 172**,** 6581-4.

Wolfe, A. J., 2005. The acetate switch. Microbiol Mol Biol Rev. 69**,** 12-50.

Wu, Z., et al., 2003. Effects of dissolved oxygen concentration and DO-stat feeding strategy on CoQ10 production with Rhizobium radiobacter. World Journal of Microbiology and Biotechnology. 19**,** 925-928.

Yang, X., et al., 2010. Coenzyme Q10 reduces beta-amyloid plaque in an APP/PS1 transgenic mouse model of Alzheimer's disease. J Mol Neurosci. 41**,** 110-3.

Yen, H. W., Chiu, C. H., 2007. The influences of aerobic-dark and anaerobic-light cultivation on CoQ(10) production by Rhodobacter sphaeroides in the submerged fermenter. Enzyme and Microbial Technology. 41**,** 600-604.

Yen, H. W., et al., 2010. Cultivation of Rhodobacter sphaeroides in the stirred bioreactor with different feeding strategies for CoQ(10) production. Appl Biochem Biotechnol. 160**,** 1441-9.

Yen, H. W., Shih, T. Y., 2009. Coenzyme Q10 production by Rhodobacter sphaeroides in stirred tank and in airlift bioreactor. Bioprocess Biosyst Eng. 32**,** 711-6.

Yoshida, H., et al., 1998. Production of ubiquinone-10 using bacteria. J Gen Appl Microbiol. 44**,** 19-26.

Yoshida, Y., et al., 2006. Evaluation of the dietary effects of coenzyme Q in vivo by the oxidative stress marker, hydroxyoctadecadienoic acid and its stereoisomer ratio. Biochim Biophys Acta. 1760**,** 1558-68.

Young, I. G., et al., 1972. Biochemical and genetic studies on ubiquinone biosynthesis in *Escherichia coli* K-12:4-hydroxybenzoate octaprenyltransferase. J Bacteriol. 110**,** 18-25.

Young, I. G., et al., 1971. Characterization and genetic analysis of mutant strains of *Escherichia coli* K-12 accumulating the ubiquinone precursors 2-octaprenyl-6-

methoxy-1,4-benzoquinone and 2-octaprenyl-3-methyl-6-methoxy-1,4-benzoquinone. J Bacteriol. 105**,** 769-78.

Young, I. G., et al., 1973. Pathway for ubiquinone biosynthesis in *Escherichia coli* K-12: gene-enzyme relationships and intermediates. J Bacteriol. 114**,** 42-52.

Zahiri, H. S., et al., 2006a. Biochemical characterization of the decaprenyl diphosphate synthase of *Rhodobacter sphaeroides* for coenzyme Q(10) production. Appl Microbiol Biotechnol.

Zahiri, H. S., et al., 2006b. Coenzyme Q10 production in recombinant *Escherichia coli* strains engineered with a heterologous decaprenyl diphosphate synthase gene and foreign mevalonate pathway. Metab Eng. 8**,** 406-16.

Zhang, D., et al., 2007. Ubiquinone-10 production using *Agrobacterium tumefaciens dps* gene in *Escherichia coli* by coexpression system. Mol Biotechnol. 35**,** 1-14.

Zhang, H., Javor, G. T., 2003. Regulation of the isofunctional genes *ubiD* and *ubiX* of the ubiquinone biosynthetic pathway of *Escherichia coli*. FEMS Microbiol Lett. 223**,** 67-72.

Zhu, X., et al., 1995. Production of ubiquinone in *Escherichia coli* by expression of various genes responsible for ubiquinone biosynthesis. Journal of Bioscience and Bioengineering. 79**,** 493-495.